THE ASTROPHYSICAL JOURNAL, 398:319–349, 1992 October 10

WHY ALL STARS SHOULD POSSESS CIRCUMSTELLAR TEMPERATURE INVERSIONS

JACK D. SCUDDER
Laboratory for Extraterrestrial Physics, Mail Code 692, NASA Goddard Space Flight Center, Greenbelt, MD 20771
Received 1990 July 12; accepted 1992 April 20

ABSTRACT

The consequences are presented of a postulated nonthermal distribution at the point in a stellar atmosphere where the plasma is nearly fully ionized and optically thin. The most immediate consequences are (1) that the temperature and quasi-neutral plasma density become anticorrelated with increasing radius in a thin transition region, leaving the temperature profile inverted in excess of 10^6 K up into a corona *without* depositing wave or magnetic field energy into the gas above the base of the transition region as suggested to be possible in the previous paper (Scudder 1992a, hereafter Paper I); (2) that the temperature inversion process is essentially independent of magnetic topology working only slightly more efficiently on "closed" than on "open" flux tubes; (3) that the inversion temperature scale height can be extremely short for stars on the main sequence; (4) that there is an alternative suprathermal interpretation for the excess or "turbulent" Doppler widths by generalizing the Voigt-Hjerting line profile; (5) that the observed temperature dependence of the excess UV Doppler widths can be derived; (6) that a determination of a measure, κ_+^{-1}, of the ion nonthermal tail strength in the solar transition region of $\kappa_+ = 2.2 \pm 0.8$ implies a transition region temperature scale height of $\simeq$400 km, consistent with observations (for reference $\kappa = \infty$ is a Gaussian); (7) that a transition region/low coronal temperature profile from the inferred value of κ simply produces solar coronal temperatures as a direct generalization of the exponential atmosphere; (8) that there is more than enough energy flux to sustain the solar corona against its known losses for $2.49 < \kappa < 6.25$; (9) that various correlations of heating with magnetic orientation and altitude in loops and sunspots follow as ready corollaries of this postulate; (10) that inversion temperatures in excess of 10^6 K for representative ZAMS stars are obtained, suggesting that they are capable of thermal X-ray emission as observed; (11) that the Parker critical point location in stellar radii is proportional to κ and always above the stellar surface; (12) that the asymptotic wind speeds scale as $U_\infty \simeq O(1)V_{esc}/\kappa^{1/2}$; (13) that U_∞(1 AU) at Earth is estimated to be between 300 and 600 km s^{-1}, consistent with κ-values in the range 2.4–7.1; (14) that values of κ determined for different groups of stars based on the scaling of item (12) determine credible maximum inversion temperatures for these groups, including an explanation of why some classes of stars usually are not X-ray emitters; and (15) that a mechanism exists for "heating" solar wind minor ions proportionally to their mass.

Subject headings: solar wind — stars: atmospheres — stars: coronae — stars: mass loss

1. INTRODUCTION

1.1. *Background*

For over a half-century solar physicists have been trying to establish a viable scenario that produces and maintains the solar corona at a few million degrees while the visible and underlying photospheric/chromospheric "surface" of the star is only $\sim 5500 \pm 1000$ K (cf. Ulmschneider, Rosner, & Priest 1991 for a review). The recent detection all over the H-R diagram of hot, X-ray–producing circumstellar envelopes ($T > 10^6$ K) has established that this type of inversion is commonplace for a wide variety of stars with bound atmospheres (Rosner, Golub, & Vaiana 1985; Parker 1990). Inklings that there was a high-temperature gas near the solar surface date from 1931 (Grotrian 1931a, b, 1939). Somewhere between Bowen & Edlen's 1939 paper identifying mysterious coronal emission lines with transitions in highly ionized ions and Waldemeier's 1945 paper, a consensus was reached that the outer envelope of our star was hotter than its surface. That the "observed" temperature profile was not a monotonic function of distance from the presumed nuclear furnace in the interior of the star prompted a series of theoretical papers (Alfvén 1947; Biermann 1948; Schatzmann 1949) which sought to identify the dispersal of mechanical energy in the motions of the subphotospheric hydrogen convection zone (HCZ) as the cause for the heating of the entire coronal envelope. These papers showed that there was adequate mechanical energy available in the HCZ; the stumbling block then, as now (cf. Narain & Ulmschneider 1990), was to develop a convincing scenario for the maintenance of the distended temperature inversion above the chromosphere into the sparse corona, where the temperature continues to rise, maximizing somewhere between 2 and 8 $R_\odot$ (Munro & Jackson 1977; Lallement, Holzer, & Munro 1986; Withbroe et al 1985).

Although the HCZ is undoubtedly the ultimate energy source of the coronal heating, theoretical and observational work have not unambiguously identified a viable mechanism(s) to explain the observed temperature profile. Such a mechanism must convey (and deposit!) suitable portions of this energy reservoir past the chromosphere into the transition region and up into the lower corona. The sharp scale and the thermodynamically counterintuitive temperature inversion of the transition region has attracted considerable theoretical attention. Because the energy density requirement for raising the sparse coronal gas to such high temperatures is small compared with that required for the maintenance of the chromosphere and the radiation that emanates from it, the requisite energy budget is even larger than that necessary to sustain the gas at these

elevated temperatures. Estimates suggest that an energy flux of between 10^5 and 10^7 ergs cm^{-2} s^{-1} is required to sustain the corona against its known and perceived losses. An obstacle for such theories is the tendency for dispersive waves to steepen, shock, and deposit their mechanical energy rather abruptly at the top of the chromosphere or the bottom of the adjoining transition region in the vicinity of 2090 km above the $\tau = 1$ photosphere (cf. Narain & Ulmschneider 1990 for a review). In this location the temperature rise has already begun ($T \sim 5000$ K), but the transition region (TR) to the coronal values of (2–3) $\times$ 10^6 K is rather strongly suggested to be *external* to the region where this mechanical energy flux is severely reflected and/or attenuated. Mechanisms that have been investigated for communicating this energy up into the transition region and low corona are those of (1) Osterbrock (1960), who worked on scenarios of the various magnetohydrodynamic (MHD) modes and how they would be channeled through the structured granulation cells; (2) Ionson (1982). Hollweg (1984, 1986), and Davila (1986), who have examined the MHD-like mode propagation on the interfaces of different closed field line structures within topologically closed magnetic loops to obtain resonance damping of hydromagnetic power in the low corona; and (3) Parker (1972, 1981a, b, 1983a, b, 1990), who has championed the dissipation of twisted bundles of magnetic flux driven by the random walk of magnetic field lines anchored on both ends in the photosphere.

These approaches to the maintenance of the corona have appeal, since "[the] Second Law of thermodynamics does not permit us to heat the chromosphere [and above] with the thermal [*sic*] energy of the cooler photosphere. But, if nonthermal [*sic*] energy is present in the photosphere, it might somehow be focused on the tiny amount of material above so as to heat it. Non-thermal energy is available in the photosphere in the form of magnetic fields and [*sic*] convective motion" (Zirin 1988). Thus, all of the preceding attempts at explaining the corona attempt to convect the energy content of reservoirs represented by bulk fluid velocity fluctuations ($\boldsymbol{V}$) or by the enormous energy density in the magnetic field ($\boldsymbol{B}$) out of the hydrogen convection zone (HCZ); each mechanism then is suggested to convert this convected energy into local temperature enhancements at some other locale. In Zirin's inventory these two nonthermal energy reservoirs are the only "nonthermal" ones available. These would be the only reservoirs if even linear nonequilibrium thermodynamics (deGroot & Mazur 1984) were a sufficiently general description for the system under consideration. As if it were not enough to cause the temperature to rise abruptly, these same theories must accomplish this feat while heat flows ($\boldsymbol{q} = -\kappa \nabla T$) back down the same temperature gradient into the lower transition region!

The present paper, building on the "velocity filtration" process developed in the previous article in this issue (Scudder 1992a, hereafter Paper I), suggests a new way to *let* the corona and transition region become "hotter" than the underlying chromosphere. It exploits the nonequilibrium energy content of postulated suprathermal tails at the sites where the HCZ energy is converted to nondirected motion. Consistent with Zirin's summary, a natural but previously unconsidered form of nonthermal energy is used to explain the remarkable temperature inversions of the outer envelopes of most main-sequence stars that have outer convection zones or other abrupt terminations of energy transport from the stellar interior. This process will take place with or without the presence of magnetic fields and is almost as effective on "open" field lines as "closed" ones. This reservoir resides in the suprathermal high-velocity tail of the velocity distribution function which is postulated to be unimportant in the usual truncations of the fluid moment hierarchy. In much the same way as the exponential atmosphere retains its temperature, the evolution of a boundary distribution with a super-Maxwellian hyperpressure moment evolves with altitude into a hotter temperature gas *without* the bulk viscous or Joule deposition of energy in the locale where the plasma is hotter.

The energy density in the suprathermal tails at the base of the transition region is supplied by the ultimate power source of the HCZ. The main advantage of the present approach is to tap the HCZ power directly into the tails in the same locale where this power is observed to be dissipated. The subsequent velocity filtration caused by gravity proceeds without further intervention to produce the temperature inversion of both electrons and ions in the overlying layers. By contrast, previous models explain the coronal inversion by (1) transporting some severely attenuated fluid consequence of the HCZ (δB or δV) to a higher level above the TR, (2) converting this transported energy into heat at or near the maximum in the temperature profile, and (3) regarding kinetic effects, such as heat flow, as "sinks," in competition with the "process" making the inversion, per se.

While it has been widely recognized that the radiation and the gas are not in equilibrium in the transition region and corona, insufficient attention has been paid to the possibility that the gas itself might not be well approximated by a local Maxwellian distribution (cf., however, Scudder & Olbert 1979a, b; Roussel-Dupré 1980; Shoub 1982, 1983; Ljepojevic & MacNeice 1988, 1989). Two related issues in this connection are the strong speed dependence of the collision frequency and the driven character of the equilibrium.

The usual argument for a Maxwellian distribution in the low TR starts with the high collision frequency there; however, the usual Spitzer formula exaggerates by orders of magnitude the collision frequency of the particles that carry the energy flux and those with sufficient energy to reach the middle and higher TR and coronal altitudes. This, in turn, implies that the likelihood of a local Maxwellian $f(\boldsymbol{v})$ cannot be surmised based solely on the Spitzer-based Knudsen number which contrasts the Spitzer free path with the shortest scale length of the macroscopic variables. The relaxation rates of initial distributions toward the Maxwellian form are angle- and speed-dependent, and then only straightforward when no spatial gradients, forces, or heat fluxes are present in the equilibrium final state. The rates of approach toward a local Maxwellian are strongly speed-dependent, the lower energies responding faster than the higher ones. Without an isothermal enclosure for a boundary condition there can be no H-theorem; then there is no requirement that the equilibrium speed distribution be Maxwellian or even quasi-Maxwellian. The low-energy portion of the distribution is probably more Maxwellian than the higher energy portion, but the precise accommodation of the equilibrium $f(\boldsymbol{v})$ to these forces cannot be presaged. Without an isothermal enclosure the equilibrium fully ionized plasma (FIP) distribution function will have significant departures from a Maxwellian shape ($[f(\boldsymbol{v}) - f_M(\boldsymbol{v})]/f_M \gg 1$) for v's that control the third moment of the distribution (Scudder & Olbert 1979a, b). The statistical mechanics, the conventional heat laws, and the usual *form* of the second law of thermodynamics built on perturbations to local Maxwellians are without

foundation in this circumstance (deGroot & Mazur 1984). It is even possible in strong gradient regimes that heat flows from colder to hotter temperatures (cf. Scudder & Olbert 1983).

The textbook estimates of the collision times (e.g., Spitzer 1962; Rossi & Olbert 1970) for equipartition and self-Maxwellization refer to spatially uniform, force-free systems *relaxing* from an "initial" condition *without* further constraints. To be specific, such time scales identify the time τ_m for transients at speeds less than the root mean square speed $w_T \equiv (3kT/m)^{1/2}$ to damp out of equations like the homogeneous force-free Boltzmann equation

$$\frac{1}{\tau_M} \simeq \frac{\partial \ln f_0}{\partial t} = \frac{1}{f_0}\frac{\delta f_0}{\delta t} .$$

Thus, the traditional estimates of the small Coulomb Knudsen number based on Spitzer's free path only suggest that $f(v)$, $v < w_T$, is safely assumed to be nearly Maxwellian. This, too, must be qualified. When mechanical energy is being "absorbed," or in the presence of a DC finite temperature gradient, or the microstate is forced, the Spitzer times for "self-Maxwellization" do not comment directly on the "driven" *equilibrium* distribution (even for $v < w_T$) that should be expected in such inhomogeneous locales, viz.,

$$\frac{D \ln f_0}{Dt} = \frac{1}{f}\frac{\delta f_0}{\delta t} ,$$

$$\frac{1}{\tau_{\rm driven}} = \frac{\partial \ln f_0}{\partial t} = \frac{1}{f_0}\frac{\delta f_0}{\delta t} - \frac{\boldsymbol{a}}{f_0}\cdot\frac{\partial f_0}{\partial \boldsymbol{v}} - \frac{\boldsymbol{v}}{f_0}\cdot\frac{\partial f_0}{\partial \boldsymbol{x}}$$

$$= \frac{1}{\tau_M} \pm \text{corrections [forces, gradients } (\boldsymbol{x}, \boldsymbol{v})] .$$

The collisional time scale for Coulomb collisions varies approximately as $\tau_{\rm Spitzer} = \tau_m(v/w_T)^3$, so that $\tau_{\rm driven}$ above may be dominated by local small-angle scattering at low energies, but by global forces and gradients at higher energies. The equilibrium boundary distribution $f(\boldsymbol{x}_0, \boldsymbol{v})$ will almost surely have significant transport modifications, easily possessing a prominent fore-aft skew above $w' \equiv 2.6w_c$ (the global/local boundary discussed by Scudder & Olbert 1979a, b), as well as a suprathermal tail. These features are not erased by collisions at *low energy* ($v \leq w'$), because they are driven by the dissipation mechanism ($\partial/\partial t \neq 0$) of the HCZ power to be skewed to transport energy from where it is absorbed to another location; this situation is complicated by the macroscopic mechanical equilibrium ($a \neq 0$) of the star that requires this transport to take place in strong gradient regimes ($\partial/\partial x \neq 0$). Higher energy particles experience relatively little scattering while being accelerated, becoming the important signatures of energization (cf. Parker 1958b; Dreicer 1959). Additional causes of nonthermal tails are inductive electric fields associated with the waves below the TR; in this class of phenomena are the consequences of reconnection, possibly in the form of nanoflares or other nonstationary processes to be defined. *It is the strong speed dependence of the collisions in a FIP that makes it so difficult to ensure that $f(v)$ is a Maxwellian for $v' > w'$ in an astrophysical plasma.*

This paper questions the long-held belief that additional energy supplies (as in the form of the three classes of mechanisms summarized above) are needed to explain the coronal temperature inversion; estimates are made to support this position and refute arguments, such as that of a skeptic of this work, that the present paper's proposal fails on grounds of inadequate energy flux. So that the issues are clearly framed, a form of the skeptic's calculation for the energy flux is presented in § 1.1.1 and contrasted with the same quantity *based on the premises of this paper* in § 1.1.2. The skeptic's suggestion that the present approach fails on energy flux grounds is quantitatively refuted in § 1.1.2.

1.1.1. *The Skeptic's Energy Budget*

The skeptic asserted that below a location $|\boldsymbol{v}| = v^*$ (specified by him) in velocity space, $f(\boldsymbol{v})$ should be a Maxwellian distribution; in the positive-r hemisphere of velocity space the skeptic suggested that phase-space densities in excess of Maxwellian were not prohibited by the collisionality of the gas, including consideration of its speed dependence. Thus, an inverse power law in speed was considered consistent with the known facts (cf. Fig. 1*b*, *solid curve*).

The skeptic has thus allowed for the ultimate transport in the form of quasi-ballistic suprathermal tail for $v > v^*$. At the same time he has presupposed that the war between ballistic/transport effects and scattering has been decisively won below v^* by scattering. All signatures of non-Maxwellian transport are thus suppressed even though the collision frequency is a smooth function of particle speed! The value of v^* set by the skeptic was that implicit speed where the speed-dependent Coulomb free path, $\lambda(v^*)$, divided by the density scale height is unity, viz.,

$$\frac{\lambda(v^*)}{L_D} = 1 . \tag{1}$$

The Coulomb free path for suprathermal speeds is related to the free path of the root mean square particle, $\lambda_{\rm mfp}$, and the usual Knudsen number, $K \equiv \lambda_{\rm mfp}/L_D$, and v^* of equation (1) by the following explicit relationship:

$$\frac{v^*}{w_{\rm th}} = \left(\frac{9}{4K}\right)^{1/4} . \tag{2}$$

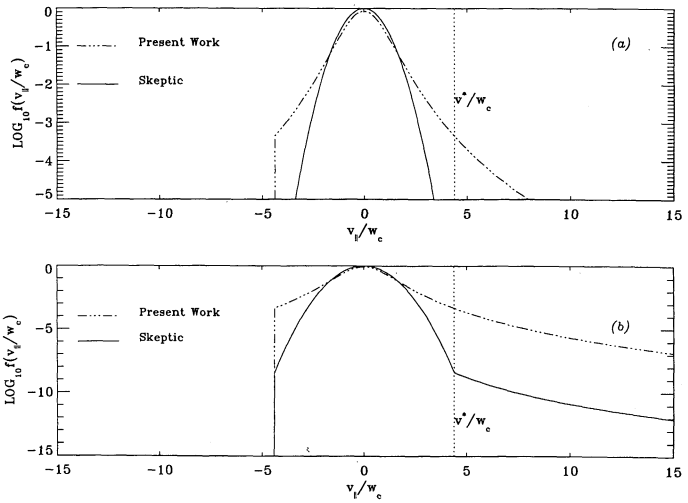

FIG. 1.—Nonthermal distribution vs. Maxwellian + tails added. Contrast of skeptic's view of velocity distribution function along the magnetic field in the TR (*solid curve*) as a truncated Maxwellian distribution within v^* with power-law tail appended, and that supposed in the present paper (*dashed curve*), which is a truncated version of a kappa distribution function defined in Paper I, (eq. 7a). Panel *a* is a magnification of the upper portion of panel *b*.

If the power-law tail postulated above v^* varies inversely as the $(2\kappa + 2)$ power of the speed, as does the kappa function considered below in § 1.1.2, and if the distribution function remains strictly Maxwellian and, hence, symmetric below $|v| = v^*$, then the energy flux, ϵ_M^T, moving upward from the surface due to this asymmetric tail above v^* is

$$\epsilon_M^T = \frac{nmw_c^3}{2\pi^{1/2}} \exp\left(-\frac{3}{2K^{1/2}}\right) \times \frac{\kappa^2}{(\kappa-2)(\kappa-1)}\left[2 + \frac{3}{K^{1/2}} + \frac{9}{4K}\left(\frac{\kappa-1}{\kappa}\right)\right] \times \left(1 + \frac{3}{2\kappa K^{1/2}}\right). \quad (3a)$$

The exponential factor in equation (3a) reflects the skeptic's assumption of a Maxwellian model *at* the speed where the power-law tail is allowed to commence. For small Knudsen numbers the exponential factor of equation (3a) overpowers all other K dependence, so that ϵ_M is controlled by the value of the distribution function at the threshold of the allowed asymmetry, $f(v^*)$. Assuming that the density in the low transition region is $n = 3 \times 10^{10}$ cm^{-3}, that the temperature is 1.4×10^4 K, and the Knudsen number is $K = 6 \times 10^{-3}$ (Fontenla, Avrett, & Loeser 1990, hereafter FAL), the skeptic's energy flux $\epsilon_M^T(v > v^*)$ at the base of the TR is

$$\epsilon_M^T = \sim 61/(\kappa - 2) \text{ ergs cm}^{-2} \text{ s}^{-1}. \quad (3b)$$

The Maxwellian premise is enforced at $v^* = 4.4w_c$, where the suprathermal tail is "attached"; the exponential factor there is 4×10^{-9} of its value at zero kinetic energy! Alternatively, the skeptic is assuming, a priori that f_B is a Maxwellian for over 9 powers of 10 dynamic range and that in this part of velocity space there are *no* imprints of the equilibrium forces or inhomogeneity! Equation (3) is suggested by the skeptic to be an upper bound for the available energy flux, because it does not contain the heat conduction "known" to fall back down through the TR from the hotter corona. (Note that ϵ_M^T can increase without limit as $\kappa \to 2$ from above; the skeptic used $\kappa \simeq 3$.) The canonically required energy flux to sustain the corona against radiation and solar wind losses is 10^5–10^7 cgs units. Because the estimate of equation (3b) with $\kappa \simeq 3$ is argued to be an *upper bound and is well below that necessary to support the heating and losses from the corona, the skeptic has summarily rejected the relevance of the velocity filtration effects described below for explaining the temperature inversion of the corona without bulk heating.*

1.1.2. *The Energy Budget of a Suprathermal Distribution*

The present paper challenges the necessity of additional heating above the base of the TR, (1) by reviewing the skeptic's rationale for $f(v < v^*)$ being a Maxwellian in the TR and (2) by showing that *a more reasonable suprathermal distribution in the TR does have adequate energy flux and can explain the temperature inversion of the corona.* The skeptic's conclusions derive from the *assumption* that the phase-space density *up to and at* v^* is transport-free at a Maxwellian level set by the density and thermal speed of the TR. This assumption rests on an argument about the self-Maxwellization time; such an argument ignores (1) the speed dependence of this time scale and (2) the driven and inhomogeneous character of the kinetic equilibrium in the low TR which will cause transport distortions in the distribution function at any speed v where $K(v)$ is not zero. On the basis of previous solar wind calculations which *include* the convolutions over the speed-dependent scattering (Scudder & Olbert 1979a, b) the generic transport signatures (departures from the Maxwellian equilibrium distribution function) are suggested to be present in fully ionized plasmas at strongly inhomogeneous locations like the TR at *all* speeds above the generic Coulomb "window" at $v > v' \equiv 2.6w_c$ (Scudder & Olbert 1979b). For the locale at hand ($v^* = 4.4w_c > v'$) these transport signatures will be present in the equilibrium f at $v < v^*$. These distortions come at the slight expense of the phase-space density at low random speeds. In systems with strong temperature profiles the local distribution function is oversupplied phase-space density relative to a Maxwellian *both* by transport from inhomogeneity and by any particle accelerations caused by the HCZ mechanical energy deposited there or nearby. To allow for this transport/driven distribution function, a nonthermal distribution function with substantial corrections above those of a Maxwellian above v' and *inside* of v^* is suggested to be appropriate for that location in the TR where the plasma is fully ionized (approximately $H \sim 2090$ km according to FAL); an example of such a distribution is illustrated by the dashed curve in Figure 1 and is contrasted with the skeptic's, depicted with the solid curve. (It should be noted here, too, that transport-modified distributions of the type theoretically motivated here in the inaccessible TR region are commonplace in all astrophysical plasmas that have been sampled with *in situ* instrumentation [cf. Paper I]; previous work has suggested the same theoretical cause for these distributions as is suggested here in the TR.) Figures 1*a* and 1*b* truncate the logarithmic ordinate of the same two distributions at different levels. The absolute size of the presently suggested nonthermal distribution function at v^* is still small, less than 10^{-4} of the central peak, but approximately 10^5 times larger than that of the skeptic! Optical measurements currently can only "see" down about two orders of magnitude from the peak of the velocity distribution when the wing of lines are resolved. Thus optical measurements cannot currently comment directly on the two hypotheses of Figure 1*b*; possibly future work could, however. Current optical measurements do, however, contain widespread suggestions that lines are broader than projected from Doppler broadening of an exact Maxwellian gas of emitters. To assess the viability of the suprathermal postulate of the present paper, numerous predictions and cross-checks concerning already known phenomena in solar physics and astronomy are organized below in §§ 4–6.

Immediately, however, the skeptic's computation is redone for a low TR distribution *appropriate for the nonthermal premises of this paper*, chosen to be a member of the kappa distribution function class (defined in eq. [7a] of Paper I) which typifies empirically sampled plasmas. This calculation illustrates the *radically enhanced and adequate* energy fluxes provided by a range of suprathermal inner boundary conditions. Values of κ *in this same range* are independently suggested below to explain "excess" widths of Doppler spectra, to explain the magnitude of the corona temperature inversion itself, the observed range of solar wind speeds, and to suggest the scale length of the transition region's temperature profile.

Assuming that the suprathermal power-law tail exponent is the same in the present scenario as in the skeptic's Gaussian + power-law assessment of § 1.1.1 above (cf. Fig. 1*b*), the available energy flux, ϵ_κ^T above the *same* v^*, is given by the

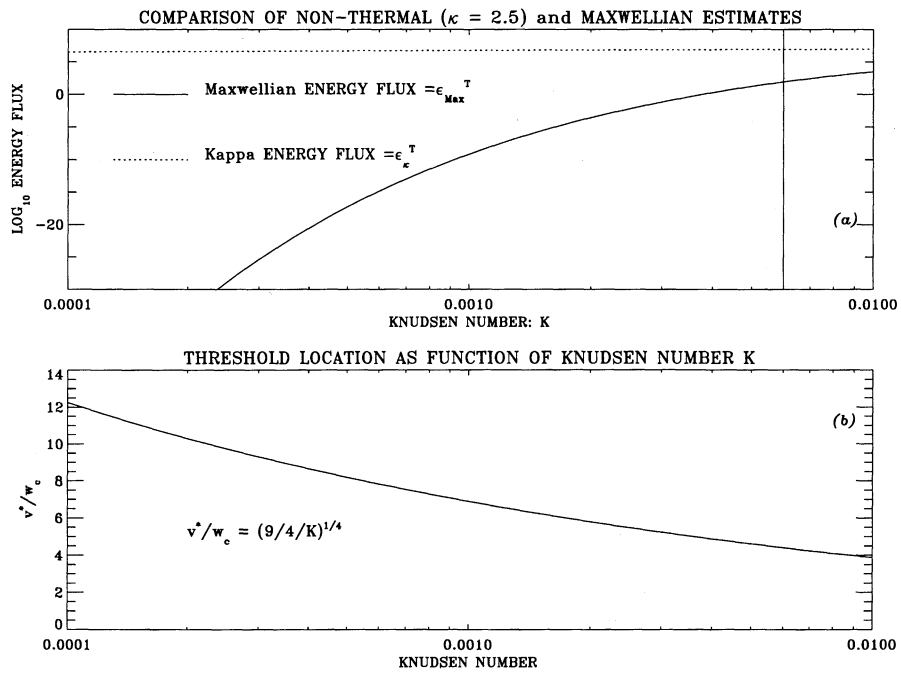

FIG. 2.—(*a*) Comparison of available energy flux, ϵ_M^T, at 2090 km in the TR for skeptic's distribution function of Fig. 1 (*solid curve*) vs. that (ϵ_κ^T) for the present paper's postulated transport-modified distribution function (*dotted line*) of Fig. 1; (*b*) Illustrates variation of v^* as Knudsen number changes.

expression

$$\epsilon_\kappa^T = \frac{A_\kappa n m w_c^3}{2\pi^{1/2}} \left(\frac{\kappa 2K^{1/2}}{\kappa 2K^{1/2}+3}\right)^\kappa \frac{\kappa^2}{(\kappa-1)(\kappa-2)} \times \left[\left(\frac{9}{4K}\right)^{1/2}\left(\frac{\kappa-1}{\kappa}\right)+\frac{3}{K^{1/2}}+2\right]. \quad (4a)$$

A_κ is an $O(1)$ constant that adjusts the overall normalization to account for the dispersal of some of the particles into the suprathermal wings (cf. Fig. 1*a*, where this constant lowers the dashed curve relative to the solid curve near $v = 0$). Using the same numbers as the skeptic for density (3×10^{10}), temperature (1.4×10^4), and Knudsen number (6×10^{-3}), the energy flux available from a $\kappa = 2.2$ (consistent with Doppler widths below in § 5) suprathermal distribution function is

$$\epsilon_{\kappa=2.5}^T = 3 \times 10^7 \text{ ergs cm}^{-2} \text{ s}^{-1}. \quad (4b)$$

This value is much larger than the skeptic's upper-bound Maxwellian + tail value (for the same κ*)* of $\epsilon_M^T = \sim 300$ ergs $\text{cm}^{-2}\ \text{s}^{-1}$ based on equation (3a). The consistently *large difference in the common logarithms* of skeptic/Maxwellian versus kappa energy fluxes of equations (3a) and (4a) is illustrated in Figure 2*a* at fixed κ, as a function of Knudsen number, by the solid and dashed curves, respectively. In this $\kappa = 2.5$ regime the ϵ_κ^T flux (*dashed curve*) is relatively insensitive to the Knudsen number variations (cf. eq. [4a]), while the ϵ_M^T curve of the skeptic (*solid curve*) is uniformly smaller and strongly dependent on the Knudsen number. This enormous relative sensitivity reflects the large ratio of phase-space density of the suprathermal model and the skeptic's Maxwellian model *at* the presumed onset of the power-law tail at $v^*(\kappa)$ when $v^*(\kappa) \gg w_c$. The issue becomes how strong the skeptic's argument is that $f(v^*)$ is a Maxwellian, at and below v^*.

The absolute size of ϵ_κ^T *from equation (4) using realistic parameters gives an energy supply that is midway in the* 10^5–10^7 cgs *regime thought to be required for supporting the corona*! Specializing our attention to the Knudsen and density regime referred to above (FAL), the variation of the energy flux, $\epsilon_\kappa^T(K = 6 \times 10^{-3})$, as a function of the unknown κ suprathermal tail strength, is illustrated with the solid curve in Figure 3. This graph suggests that values of κ in the interval [2.49, 6.25] *can* provide the necessary energy fluxes thought necessary to maintain the corona indicated by the horizontal dash-dot lines at 10^5 and 10^7 cgs.

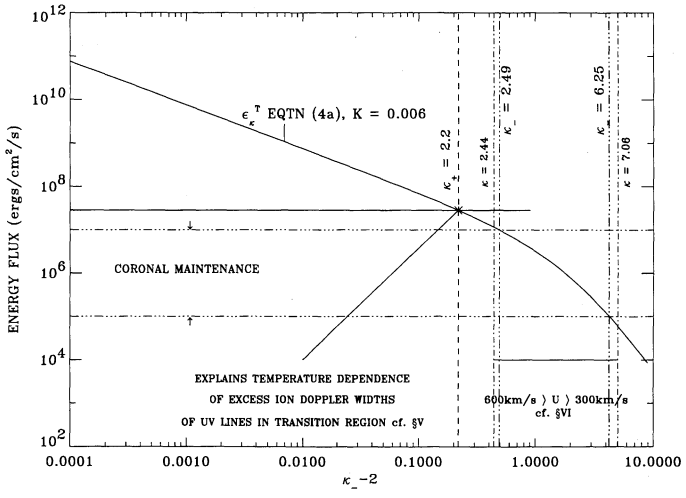

FIG. 3.—Kappa requirements at 2093 km in transition region. Variation of $\epsilon_\kappa^T(K = 6.0 \times 10^{-3}, \kappa)$ vs. κ. Horizontal lines indicate the range of ϵ required to support the corona. Values of κ_- in the interval [2.49, 6.25] are required to have sufficient ϵ, with smaller κ's required for higher ϵ's. Parameters assumed for this location of 2090 km are $N = 3 \times 10^{10}$ cm^{-3}, $T = 1.4 \times 10^4$ K; κ_+ required for nonthermal lines in § 5 is also indicated, as is the interval [2.44, 7.06] in $\kappa_+ = \kappa_-$ found necessary in § 6 for 300 km s^{-1} < U < 600 km s^{-1}, the most frequently occurring range of the bulk speed in the solar wind.

1.1.3. *Energy Fluxes from Skews at Speeds below v**

Finally, the above estimates of the energy flux in both the Maxwellian and the kappa form assumes that the distribution function at speeds below v^* are perfectly symmetric and do not contribute ($\pm$) to the skew moment for the energy flux. For precisely the same reason that the suprathermal function is skewed and relevant in determining $f(v^*)$, there *will* be asymmetries in the fore and aft portions of f below v^*. For the small Knudsen numbers under consideration the velocity space below v^* is still well above the local thermal velocity (cf. Fig. 2*b*), so that any asymmetries in this range will strongly influence the heat moment. Because the energy flux is proportional to the density, these asymmetries of the $f(\boldsymbol{v})$ could be very small but still supply significant energy flux beyond the tail estimates above. Without solving this difficult problem to obtain these additional contributions, it is clear that there might be some contribution here. With a transport-modified suprathermal distribution as an inner boundary condition, the energetics are potentially modified from that indicated in Figure 1 because of the heat carried by the lower energy particles below v^*.

To show the sensitivity of the energy flux to the symmetry of the distribution where most of the particles are located, consider the following estimate of its possible contribution. Assume that the upward-moving portion of the velocity space inside of $|\boldsymbol{v}| = v^*$ is given by a kappa distribution of density n_+ and most probable speed w_+; also assume that the downward-flowing portion of this speed shell is occupied with a kappa distribution with the same value of κ *but* different values for the density, n_-, and most probable speed, w_-. While these free numbers are nearly the same, by the fact that they are different, a simple estimate can be made of the contributions to the skew of the distribution that is possible by such a slight asymmetry. In order that this newly introduced freedom does not cause the gas to have a velocity, $n_+ w_+ = n_- w_-$ is required. In the regime where $v^*/w_c \gg 1$, the approximate heat flux from this skewed distribution is given by

$$Q_\kappa \lesssim \frac{A_\kappa n_+ m_e w_+^3 (1 - T_-/T_+)}{4\pi^{1/2}} \frac{\kappa^2}{(\kappa - 1)(\kappa - 2)}$$

$$= 4.4 \times 10^5 \left(1 - \frac{T_-}{T_+}\right) \frac{\kappa^2}{(\kappa - 1)(\kappa - 2)} \text{ cgs} . \quad (5a)$$

Because collisions are more vigorous at lower energies, gross asymmetries in the distribution below v^* are unlikely. Assuming $T_-/T_+ = 0.95$ and $\kappa = 2.5$, results in

$$Q_\kappa(\kappa = 2.5,\ n = 3 \times 10^{10},\ T_\pm = 1.4 \times 10^4,\ T_-/T_+ = 0.95)$$
$$\simeq 1.8 \times 10^5 \text{ cgs} , \quad (5b)$$

which is only 0.6% of the suprathermal tail contribution to ϵ_κ^T estimated in equation (4b). Assuming that the asymmetry at low energies opposed the suprathermal tail contribution, ϵ_κ^T, there would not be a significant correction to the above conclusion. The skeptic's Maxwellian + tail estimate of equation (3) *also* neglected the contributions of the type just estimated in equation (5b); taking the limit at $\kappa \to \infty$ of equation (5b), a similar type of estimate yields $Q_M \simeq 4.4 \times 10^5$ cgs, far in excess of the Maxwellian-anchored unbalanced tail's contribution of equation (3), but well below and possibly of the opposite sign to the 10^5–10^7 cgs usually thought to be required to sustain the corona.

1.1.4. *Paper Plan*

It is on the basis of equation (5b) and (4b) that an exploration of the implications of a suprathermal distribution function at 2090 km altitude is suggested to be energetically consistent with being the *sole* supporter of the corona, and the study of its further consequences warranted. The long-standing view (rephrased by the skeptic) that additional energy flux (beyond that present in the time-independent velocity distribution function at the base of the TR) is self-evidently required to maintain the corona is thus demonstrated to be ripe for serious revision.

With this premise the thermal particle at coronal altitudes ($1.03\ R_\odot$) is best associated with previously being an *extremely* suprathermal particle in the high chromosphere ($h \simeq 2100$ km); as a result, the phase-space density above 1.5 thermal speeds at coronal altitudes is almost solely determined by nearly ballistic trajectories from the transition region. Although the thermal particles in the low transition region experience significant Coulomb scattering, this does not prevent the more energetic particles that can overcome the potential barrier from communicating farther up into the transition region and corona without significant Coulomb impediment. This type of problem is appropriate for the FIPH transport approach outlined in Paper I, which permits an initial, but incomplete, kinetic discussion of the expected behavior of the spatial profile when both collisional and collisionless populations are present; the FIPH approach is more flexible than that predicated on Chapman-Enskog (Chapman 1916; Enskog 1917) or Spitzer-Braginskii (Spitzer & Härm 1953; Braginskii 1965) expansions.

From the outset it cannot be overemphasized that all the effects described below follow simply from conservation of energy, from a kinetic calculation of the equilibrium profile of gravitationally confined gas. The temperature inversion reflects the spatial profile of a time-stationary velocity distribution function that has a suprathermal excess interacting with an attractive potential force field. The theory discussed here reveals how the temperature inversion arises without postulating some entropy-producing device at work in these regimes, and represents the generalization of the "exponential atmosphere."

The essential ingredients of the present, *coherent* process which explains the coronal temperature inversion require the examination of seven interrelated issues that affect the kinetic description of the plasma within and above the transition region, which will be briefly discussed in turn: (1) the kinetic generalization of temperature; (2) the nature of the equilibrium forces above the photosphere; (3) the degree of ionization at and above the transition region; (4) the energy dependence of the Coulomb free path, λ_{fp}, in a plasma; (5) the essential role of spatial inhomogeneity in the transition region and in astrophysics; (6) the variation of λ_{mpf}/L_{scale} at the transition region and above; and (7) the Knudsen regime fluid closure approximations. The predictions of this understanding of the coronal temperature inversion are also contrasted with the current state of solar and stellar observations.

1.2. *Temperature and Thermodynamics in Strong Gradients*

Strictly speaking, temperature, T, is defined only for "equilibrium" systems enclosed in an infinite-capacity heat bath. For such systems T is uniformly the same as that of the bath, even in the presence of forces derivable from a potential. It is quite clear that the asymmetrically heated and incompletely enclosed systems of astrophysics are not in

"equilibrium" in the thermodynamic sense: thermal gradients are expected. In such systems there are many ways to discuss the nondirected energy content of the gas, but kinetic theory clearly identifies the quantity τ given below,

$$\tau = \frac{\frac{2}{3}\,\mathrm{Tr}\,\mathbf{P}}{nk_B} = \frac{\frac{2}{3}\,\mathrm{Tr}\,\langle \frac{1}{2} mww \rangle}{\langle 1 \rangle}, \tag{6}$$

as the suitable spatially dependent generalization of temperature for the situation when the probability distribution is non-Maxwellian. (In this equation $\mathbf{P}$ is the pressure tensor in the fluid frame, Tr stands for the trace of the tensor that follows, $\langle a \rangle$ stands for the velocity distribution weighted average of the quantity a, and $\boldsymbol{w}$ is a particle velocity relative to the bulk velocity.) Since most diagnostics that infer astrophysical "temperatures" invert a signature that depends on the velocity dispersion of radiators or absorbers, the quantity τ is a useful quantity for the theory to predict.

Perhaps Zirin's (1988) synopsis explains the research approaches previously taken for seeking mechanisms to support the coronal temperature inversion (which is a τ profile), but his summary also reflects the narrow scope of what forms of "nonthermal" energy reservoirs might be available. At the truncated lowest magnetofluid level, the state of the gas is summarized in terms of the truncated set of moment variables of density, velocity, temperature, and magnetic field: $\{n, \boldsymbol{V}, T, \boldsymbol{B}\}$; if the effect is "not thermal," it is natural to seek the energy from the other reservoirs: magnetic fields, $[\boldsymbol{B}]$, or convective fluid motions, $[\boldsymbol{V}]$. In this sense Zirin's accurate summary of previous researchers' lines of reasoning exposes a premise common to all prior approaches to explaining the corona: because a temperature (τ) profile is nonmonotonic, a thermodynamically viable mechanism is one that dissipates some form of mechanical or magnetic energy as "viscous" or "Joule" heat *where* the plasma is hot. This premise is often "justified" by appealing to linear nonequilibrium thermodynamic arguments associated with the second law of thermodynamics. From a broader point of view, "nonthermal" should also include any departures from local thermodynamic equilibrium, which would show up in "nonthermal" features on the velocity distribution function in the form of a heat flux and/or suprathermal tails or any other of the infinity of moments necessary to have a full kinetic reconstruction of the distribution function.

The Clausius form of the second law is usually phrased for closed systems which can only exchange heat via photons, but not via particles or organized bulk flows with its surroundings (cf. e.g., Fermi 1936, pp. 30–31). When it applies, this law reduces for collision-dominated systems with weak (infinitesimal) gradients of $\{n, \boldsymbol{V}, T, \boldsymbol{B}\}$ to the empirical synthesis that the observed direction of heat flow is from the locally hotter region to the nearby cooler one (cf. Fermi 1936, p. 30).

The form of the second law in the context of continuum systems which are open in the above sense and/or spatially nonuniform requires further care as discussed by de Groot & Mazur (1984, p. 20). In general, the direction of heat flow *cannot* be presaged in low-density fully ionized plasmas in the presence of finite gradients. Whether random energy density reservoirs in the photosphere/chromosphere can support the inverted temperature profile above the chromosphere cannot be discounted by an appeal to the *ab initio* "higher ground" of the second law of thermodynamics whose mathematical structure for such systems is unknown (Landau & Lifshitz 1960). In the original open, continuum, weak gradient formulation, the second law takes the form that the entropy "source term," σ, must be greater than or equal to zero and is only a function of plasma state variables but not of their gradients. DeGroot & Mazur (1984, p. 183) show that when Enskog's (1917) first-order corrections to the distribution function are sufficiently accurate, the structure of the "source term" σ is identical to its form in closed systems; the only difference is that now the expression must be evaluated with the local transport-modified moment parameters such as $T \to \tau$ (p. 183). Enskog's first-order corrections, or, equivalently, those of Spitzer & Härm (1953) and Braginskii (1965) for a plasma, are those for weak temperature gradients, for systems slightly removed from thermodynamical equilibrium and hence from global, not local, spatial homogeneity of the temperature; it is in this approximation that kinetic theory recovers the familiar and oft-quoted Fourier's linear law ($\boldsymbol{q} = -\kappa \nabla T$) between the heat flow and the temperature gradient which is the mathematical restatement of Clausius's law. Hence, if in an astrophysical system where Enskog's (Spitzer's) first-order method does *not* provide a sufficiently accurate prediction of the distribution function, and hence the thermodynamic fluxes such as the heat flow, then the structure of the entropy source term in terms of local macroscopic variables (like τ for T) is no longer guaranteed to be of the traditional form, becoming a functional of the macroscopic gradients (deGroot & Mazur 1984, p. 183). Statistical mechanical calculations of this type are typical for outlining nonequilibrium (inhomogeneous) systems where the "closed" system behavior and the "open" ones should have similar functional dependences.

Accordingly, if it is the case that the statistical mechanics of the expanding plasma is not amenable to the Enskog-Spitzer approximation scheme (cf. Scudder & Olbert 1979a, b; Olbert 1983; Scudder & Olbert 1983; Shoub 1983, 1989) as empirically motivated by the omnipresent suprathermal tails of *in situ* observations, then there is no reason to expect that the usual form of the Clausius statement of the second law constrains the mechanism by which the corona is maintained. If the heat law is not known to be representable in terms of first-order gradients in the macroscopic observables by a defensible application of the Chapman-Enskog linearization approach, one may reliably conclude neither that heat flows from the corona down into the chromosphere nor that generalized transport supply of the hot, sparse material above the photosphere is precluded by the second law of thermodynamics (deGroot & Mazur 1984, p. 180). Finally, the fact that appeal can be made to statistical mechanics to ascertain when the thermodynamics of equilibria is binding for inhomogeneous (nonequilibrium) situations implies that the results of statistical mechanics take precedence in cases of conflict between the two disciplines (deGroot & Mazur 1984; cf. Landau & Lifshitz 1960).

The stunning practical successes of (linear) nonequilibrium thermodynamics as in the form of Onsager's (1931a, b) relations testifies more to the ubiquity in our experience of weak thermal gradient physics than to the generality of the (linear) nonequilibrium theory. The controlling role of gravity renders astrophysics the locale of strong gradients; the plasmas of astrophysics emanate from the "edges" of stars, themselves strong spatial inhomogeneities. It is thus by no means obvious in astrophysics that the pervasive weak-gradient physics of human experience is maintained in all locales, especially at the surfaces of stars, and especially when mechanical power is being abruptly terminated there like waves on a beach! In fact

the last 30 years of *in situ* plasma measurements illustrate the omnipresent nonthermal distributions, the strong departures of distributions from the Enskog-Spitzer-Braginskii perturbative form (Montgomery 1972), the concurrent importance of system and short scale variations (Scudder & Olbert, 1979a, b), and the global, yet simultaneously local, character of dilute astrophysical plasmas.

In this paper the thesis is advanced that the high chromosphere above $H \sim 2090$ km, as well as the transition region and corona above, are regimes where Enskog's linearization fails to describe the velocity distribution at the relevant suprathermal speeds which control the long-distance communication and transport in the plasma. Accordingly, there is the possibility, without mechanical or magnetic energy deposition, that transport of the type modeled on that developed in the previous paper (Paper I), which is more general than that provided by Chapman-Enskog–Spitzer-Braginskii's formulation, can actually "filter" the distribution of random speeds so that the temperature ($\tau \equiv \frac{2}{3}$ Tr $\mathbf{P}/nk$) is radically hotter above the high chromosphere than its source, even though its energy density, or pressure, decreases monotonically.

In Paper I it was suggested that the *velocity filtration* process caused by an attractive potential induces a macroscopic closure relation such that temperature and density are anticorrelated; for isomagnetic flux tubes this relationship for a modeled nonthermal kappa distribution simplifies further to be a polytrope relation with exponent $\gamma < 1$. In Figure 4 the results of two theory/data analysis efforts in the low corona (Withbroe 1988) and transition region (FAL) have been replotted on log-log paper to illustrate that in the transition region there is room for an equivalent polytrope of the type suggested in Paper I. Theories and inversions of observations are incomplete at some level, and the uncertainty bands have been constructed about the curves to indicate estimates of the uncertainties in the various regions. Within these errors, the least-squares slope gives an effective polytrope $\gamma = 0.19$ and an effective suprathermal tail index $\kappa \simeq 1.7$ upon using equation (31c) in Paper I.

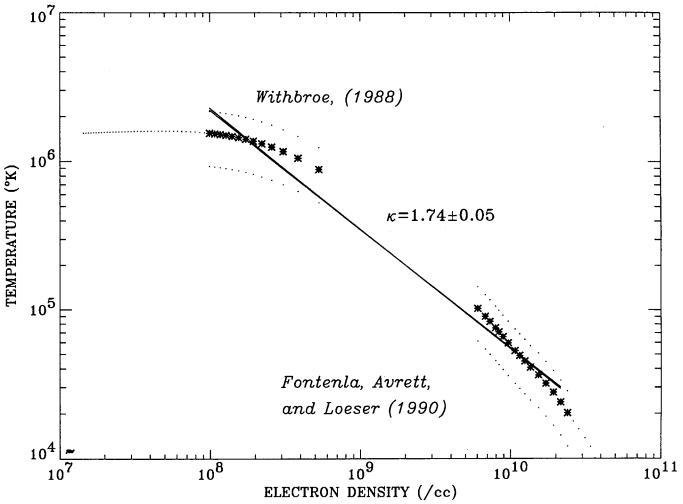

FIG. 4.—Summary of low coronal and transition region models in T vs. n space to illustrate polytrope possibility with $\gamma < 1$. Coronal data/model from Withbroe (1988); transition region data/model adapted from a figure in Fontenla, Avrett, & Loeser (1990).

1.3. *Degree of Ionization*

It is of course well known by now that the gas of the Sun is almost completely ionized in the high chromosphere (above $H \sim 2090$ km; cf. Gibson 1973), becoming increasingly fully ionized with height by the UV radiation bath, the reduced rate of recombination, and the increasing mean energy of the electrons and impact ionization. The crucial observational fact is that a significant portion of the transition region and essentially all of the coronal plasma regime can be thought of as a plasma with its dominant constituents ionized at least once and in many cases ionized many times. When the anion H^- is disrupted, the emissivity of the chromosphere drops markedly, leaving the overlying areas optically thin to the light, and with each kilometer in altitude the gas is increasingly uncoupled from the radiation field. As soon as the combined effects of the UV radiation and the impact ionization disrupt the anion H^-, which accounts for most of the opacity, the gas is well on its way to being ionized at least once, and through the transition region gradually even helium is completely stripped en route to the corona.

1.4. *Speed Dependence of the Free Path in a Plasma*

In Paper I in this series the free path of a singly charged particle in a fully ionized plasma was illustrated (Fig. 1) as a function of its relative speed w with respect to its target, and contrasted with that of neutral hard sphere scattering. The reader's attention is drawn to the w^4 asymptotic speed dependence of the Coulomb free path and the fact that it is unbounded until limited near the speed of light by relativistic Čerenkov effects (Tidman, Guernsey, & Montgomery 1964); this strong speed dependence implies that *the free path of a particle in a fully ionized plasma (FIP) can easily be orders of magnitude different from that of the most probably speed particle.* It has been demonstrated previously (Scudder & Olbert 1979a, b) that above $w = 2.16 w_T$ [$w_T = (3kT_c/m)^{1/2}$] there is a very high probability that the particle will not be significantly scattered in one thermal mean free path, $\lambda_{\rm mfp}$, and thus has a significantly larger ballistic range than that of the root mean square speed particle. Above $w = 2.16 w_T$ local scattering is increasingly ineffective at forestalling the formation of nonlocal transport phase-space signatures; there will be a transport signature in this regime unless the plasma system to which the local situation is connected by lines of magnetic force is isothermal.

Because the high chromosphere has such a cool mean energy ($kT_* \simeq 0.5$ eV) and is at the bottom of such a large effective potential well ($\simeq$995 eV), the particles that can energetically make it to higher levels in the atmosphere must be significantly suprathermal particles. To gain energetic access to infinity, particles in the high chromosphere require speeds in excess of 30 local thermal speeds w_T. Without energization by an external agent, the low kinetic energy population at *any* height must have started with an energy above the potential energy stored upon gaining access to that height; thus, the one-thermal-speed particles in the $T = 100$ eV corona at 1.1 $R_\odot$ would, for example, have had a kinetic energy of approximately 199.5 eV in the high chromosphere, which is nearly 20 thermal speeds in the 0.5 eV chromospheric distribution. Since the free path scales as $(w/w_T)^4$, the uphill character of the equivalent potential implies that the collisionality of the particles that can energetically communicate across the transition region is significantly reduced from that of the typical particle at the altitude in question. Hence the initial free path of the $\sim$200 eV

particle at the base of the transition region r_0, $\lambda_{fp}(200\text{ eV}, r_0)$, is 160,000 times that of the rms speed particle at the same height at $T = 0.5$ eV, $\lambda_{mfp}(T = 0.5\text{ eV}, r_0)$! In order to forestall ballistic effects from being important in the transition region and above, the *mean* free path over scale lengths in this plasma must be much smaller than 6×10^{-6} at the base of the transition region; notice that this is even a stronger condition than what is required for getting the local heat moment to converge (cf. Scudder & Olbert 1983). This more stringent condition results from trying to understand what level of collisionality will forestall the communication of suprathermal tails at one altitude into temperature at another in a specific potential; in the jargon of moment expansions, such a calculation suggests when the "hyperpressure" moment and "hyperheat fluxes" are no longer important, which is an even more severe requirement than getting the heat flux to be locally determined. As shown quantitatively below in § 3, the distribution function at 1.03 $R_\odot$ in the heat-carrying interval between 1 and 5 thermal speeds (cf. Table 1) is almost completely determined by the assumed suprathermal boundary distribution in the high chromosphere!

Recent modeling of the transition region by FAL has provided a semiempirical assessment of the electron mean free path over the scale length of the temperature in the transition region. The results have been reproduced in Figure 5. The mean free path of the rms speed particle near the top of the chromosphere (2090 km, $T = 1.4 \times 10^4$ K) is approximately 6×10^{-3} of the scale height of the temperature profile. (The mean free path usually evaluated is that function of temperature and density from Spitzer 1962 which really refers to the free path of the rms particle and *not* to the average free path over the distribution of speeds.) This value, combined with the estimate in the previous paragraph, illustrates that the initial free path of the particles communicating with the thermal populations at coronal altitudes is in excess of 10^3 times the length scale of the temperature profile! *The Chapman-Enskog premise is violated completely; free-streaming effects must be addressed in the first, not the second, approximation for the kinetic communication*! Above at least $H \sim 2093$ km (and possibly even lower) there is a problem with a localized perturbation expansion for the usual transport coefficients. The high

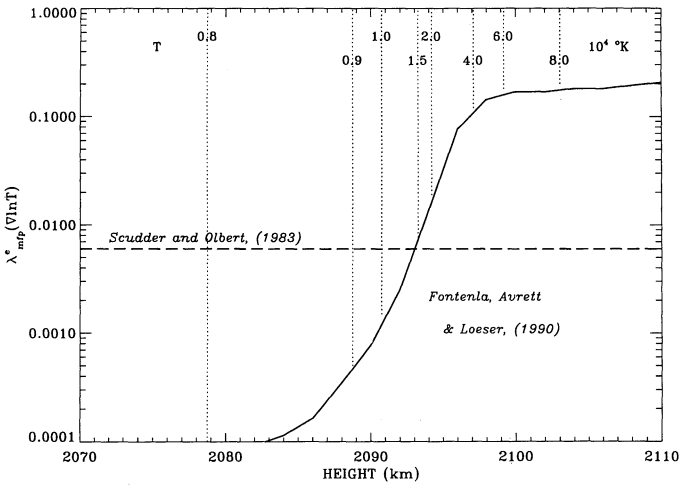

FIG. 5.—Electron Knudsen number. Ratio of the electron thermal *mean* free path to the temperature scale height; adapted from Fontenla, Avrett, & Loeser (1990).

chromosphere, the transition region and, in fact, the entire corona needs a different kinetic approach (cf. Scudder & Olbert 1979a, 1983; Schoub 1983) that does not involve a perturbation expansion à la Enskog. In this paper the possibilities of such a regime are explored further in the coronal context.

To illustrate that the unavoidable Coulomb collisions may be appropriately regarded as a perturbation for the filtration solutions presented here, an analysis is presented (§ 3) of the cumulative number of 90° collisions experienced between the base of the transition region and the height of the observations as a function of the observed particle's energy. In this way an a posteriori demonstration is provided that the unavoidable Coulomb collisions do not substantively modify the collisionless access of the "velocity filtration" type across the inhomogeneity of the transition region into the corona. This is shown to be true in § 3 in spite of the fact that at lower kinetic speeds (appropriate to the thermal particle at that altitude) the Coulomb collisions can simultaneously be significant.

1.5. *Inhomogeneity*

The photosphere is in a deep potential well formed by gravity which stratifies the extension of the atmosphere into space. The radically different gravitational attraction of electrons and ions requires another radially varying force in the form of the electric field to maintain quasi-neutrality. The radial form of this electric field is not known a priori. The electrons are attracted toward the Sun by a spatially dependent force that is almost solely determined by the electric field necessary to enforce local charge neutrality. Although the ions experience a stronger gravitational attraction ($\Phi_{G+} = -1869.9$ eV), the attraction is cut approximately in half by this same electric force reducing the net equivalent well for an ion to be approximately -984 eV (in "closed" magnetic structures). In this way electrons and ions at the base of the transition region are *both* in (slightly) different attractive potential wells that are of comparable depths and *significantly* larger than their chromospheric thermal energy of 0.5 eV. The TR is not even approximately encapsulated in an isothermal heat bath, so there is no a priori reason that a Maxwellian distribution is assured in this locale. The Enskog approach for transport coefficients collapses in the strong inhomogeneity of the transition region/low corona, since the Knudsen number perturbation parameter $\lambda(w)_{fp}/L_{scale}$, for the particles of speed w that energetically can gain access to the upper reaches of the transition region and low corona are invariably large compared with unity. Accordingly, the kinetic transport problem in these regimes is no longer "local" but "global" in the sense of Scudder & Olbert (1979a), and the Chapman-Enskog perturbation expansion is divergent. It is important in this connection to reiterate that CE can be mathematically consistent only if all its postulates are met in the physical system being studied; the divergence of CE and the need for something different stems from nature's capricious decision to not fulfill one or more of the interlocking prerequisites of the CE. Even without producing a completely self-consistent alternative to the CE results, it is definitely clear that the CE results cannot be appropriate when its premises have been violated.

1.6. *Thesis*

By observations and analysis the mechanical energy of the HCZ is dissipated principally in the chromosphere (cf. Narain & Ulmschneider 1990 for a review). In this paper it is assumed that the conversion from directed bulk mechanical energy flux

to random energy flux takes place in a way that is unlikely to inflate the random velocity distribution in a self-similar way. This implies that the velocity distribution at the virtual edge of the star where the plasma is nearly fully ionized will, because of the spatial inhomogeneity and the properties of the Coulomb cross section, contain an unassimilated "suprathermal" distribution of random energies moving upward along $\boldsymbol{B}$. This happens in much the same way as the radiation field becomes directional as the optical depth of the source region becomes less than unity; the analogy is not complete, but the equations of particle and radiation transport have many similarities. The principal differences are the fact that the collisional "opacity" has such a violent speed dependence, the additional requirement of charge neutrality, and the attendant particle coupling to the electric and gravitational fields. Because the outward fully ionized versus inward partially ionized column densities for this layer where the HCZ energy is deposited are so disparate, because of the strong speed dependence of the free path in a fully ionized plasma discussed in Paper I, and because of the strong phase-space density gradient in this region, it would require a "Maxwell demon" (or an isothermal enclosure) to ensure that the local distribution remained a Maxwellian. This is particularly important for those particles ($E \geq 48T_{\text{chromosphere}}$) that can gain energetic access from the levels ($H \sim 2090$ km) where $T_{\text{chromosphere}} \sim 2$ eV up into the low corona. Previously this strong speed dependence of the Coulomb cross section was used by Parker (1958b) to suggest that suprathermal distribution might be the by-products of Fermi interactions with the large-amplitude magnetized fluid motions in the 10^6 K corona; he proposed that this interaction with the large-amplitude waves in the 10^6 K corona was capable of replenishing the coronal gas and maintaining its temperature elevated. Although he established that this process might go on provided that adequate wave fields were present, he did not show that the actual temperature inversion of the transition region to corona would result from it. The present approach studies the consequence of a given nonthermal boundary condition, *without* any *in situ* sustaining energization mechanism above the lower transition region boundary. It is shown below that the presently postulated nonthermal boundary condition in the low transition region evolves self-consistently into the inverted temperature profile with the corona hotter than the high chromosphere and naturally explains the occurrence and steepness of the transition region.

The non-Maxwellian postulate can explain (§ 6) the range of observed solar wind speeds and (§ 5) the observed, omnipresent "nonthermal" or "turbulent speed" spectroscopic widths of ions which have been reported in the low corona (Cheng, Doschek, & Feldman 1979) and throughout the high chromosphere to coronal transition region (Nicolas et al. 1982; Dere 1989). Previously *in situ* evidence has been advanced (Fairfield & Scudder 1985; Baker et al. 1986; Riehl & Hardy 1986) to illustrate that the electron exobase spectrum of the corona is almost always nonthermal.

The "suprathermal tails" in the high chromosphere would imply that an *infinite* number of indices exist for how far the system is removed from statistical equilibrium: these are the infinity of velocity-weighted moments of the actual distribution function relative to those of an equivalent energy density Maxwellian. All these moments are required to reconstruct the information of a general nonthermal phase-space distribution. The next two moments above $\{n, V, T\}$ from the moment hierarchy are the heat flux tensor $m\langle www\rangle/2$ and the "hyper" pressure tensor, proportional to $\langle wwww\rangle$. Local collisional gas equilibrium (LCGE) presumes that these and *all* higher order moments are ignorably different from the corresponding moments of a Maxwellian of the same density and temperature. In particular, Spitzer & Härm (1953) and Braginskii (1965) transport relations are predicated on a perturbation expansion for the velocity distribution function which is only consistent when the heat flow makes a correction to adiabatic theory that is second-order small in the Knudsen number, and then only when the fluid expansion speed is suitably subsonic (cf. Scudder & Olbert 1983). *In the present paper the moment hierarchy truncation postulate is questioned at the base of the transition region and above the location where the HCZ energy deposition is complete, but where the plasma is again almost completely ionized; the collisionless Vlasov solutions (in the FIPH approximation developed in Paper I) presented below permits one to sidestep the approximation of truncation to assess the importance of all the higher order moments.*

At the height where the directed HCZ energy flux is converted to nondirected energy and where the dominant mass ion is at least ionized once, there is no assurance that the velocity probability distribution of electrons and ions can be represented sufficiently accurately by any finite truncation of moments. Since it cannot be a priori assured by the H theorem, a Maxwellian should *not* be presumed. In closed magnetic topologies (as in Fig. 6) the opposing "skews" from different footpoints make it plausible that nearly symmetrical, but nonthermal, boundary distributions are mathematically compatible footpoint boundary conditions (as in the velocity space insets of Fig. 6) and should be considered further; such distributions would have nonnegligible hyperpressure tensor moments as well as other higher even moments (cf. Fig. 6) that would be larger than their counterparts for a Maxwellian of equal density and temperature. For the open topologies of coronal holes, distributions with net flux, skew, and higher order odd moments will be important.

Detailed results for systems where suprathermals are important cannot be recovered by application of the usual truncations and closure approximations of the fluid density-momentum-energy moment equations; the usual fluid moment truncation at the energy equation is hostile to the accurate

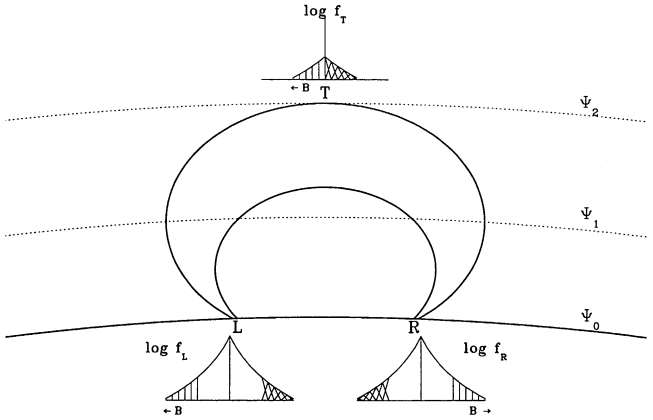

FIG. 6.—Appropriate and consistent nonthermal boundary conditions on closed loop. Shading indicates corresponding portions of the footpoint boundary conditions required for Vlasov compatibility. Unshaded portions at the L and R footpoints are "filtered out" en route to the apex because of inadequate kinetic energy in the equivalent attractive potential ψ.

description of what is kinetically possible in systems with significant, spatially varying suprathermal populations. Finally, there remain to be determined the detailed consequences of collisions, which are corrections beyond the "ballistic" FIPH effects considered here.

The purposes of this paper are (1) to develop the velocity filtration idea further for the solar case with a full three-dimensional velocity space that acknowledges the possibility of magnetic intensity variations along the tube of force; (2) to produce quasi-neutral solutions for low-lying closed isomagnetic flux-tube geometries which demonstrate that transition region to coronal temperature profiles can be achieved; (3) to outline the manner in which this filtration model explains the known morphology of the observed variations of temperature in and below the corona as organized by height of loop structure, magnetic field direction, and intensity; (4) to outline the observable consequences of the thesis, including its prediction for the scaling of "nonthermal" Doppler widths with formation temperature and flow velocity; and (5) to look at solar wind and other astrophysical implications of the process. The minor difference between the open and closed topologies will be examined; the "filtration" mechanism can, in addition to explaining the heating of closed loops, produce inverted temperature profiles over coronal holes as well as the distended maximum inferred at 2–5 $R_\odot$ (Munro & Jackson 1977; Withbroe et al. 1985; Lallement et al. 1986).

2. AMBIPOLAR SOLUTIONS: CLOSED LOOPS

In general the magnetic intensity will vary along a coronal tube of force which forms a loop. The observational constraints on the magnitude of this variation remain sketchy and model-dependent. From a deconvolution of VLA microwave measurements of a resolved coronal loop using a "submerged dipole" flux-tube model, Holman & Brosius (1986) inferred footpoint-to-apex variations of a factor of 3–5. Limited, high chromospheric transition region measurements by Henze et al. (1982) have suggested a mean variation of B through the transition region of 0.5 G km^{-1}, which represents less than a 20% variation of the usually quoted photospheric field strengths of 1 kG. Many models for coronal loops and their resonant properties treat them as if they are isomagnetic with length.

For the present paper the theory of velocity filtration is developed for the spatially varying, but radially monotonically decreasing, magnetic field to show that the basic "velocity filtration" process of Paper I remains with its inclusion. After that demonstration, the discussion of the filtration effect in the remainder of the present paper is, however, restricted *for the sake of clarity* to low-lying isomagnetic loops. By restricting the focus to closed loops, symmetric distributions are viable first-order descriptions for the FIPH problem as illustrated in Figure 6.

2.1. *Formulation*

Local charge neutrality implicitly determines the electrostatic potential function, $\Phi_E(s(x))$, which together with the gravitational potential energy for the jth species, Φ_{Gj}, determines the species-dependent effective potential $\psi_j(x)$ for all x along a given magnetic tube of force of locus $s(x)$ under consideration:

$$\psi_j(x) = Z_j e\Phi_E(x) + \Phi_{Gj}(x) , \tag{7}$$

$$n_-[\psi_-(m, M_*, x)] = \sum_j Z_j n_j[\psi_j(Z_j, M_j, M_*, x)] , \tag{8}$$

where M_*, M_j, and m are the mass of the star, the jth ion, and the electron, respectively.

Using the method of characteristics, the three-dimensional velocity space generalization of the density equation (eq. [29] of Paper I) has the form

$$N_i(x', \psi_i, \epsilon = -1) = N_i(x)(1 + \eta_i)(1 + \xi_i)^{-\kappa_i + 1/2} \quad \text{(3D)} , \tag{9a}$$

where

$$\xi_i \equiv \frac{2\Delta\psi_i}{(2\kappa_i - 3)k_B T_i} = \frac{v_{\Psi_i}^2}{\kappa_i w_{c_i}^2} , \tag{9b}$$

and $v_{\Psi_i}^2$ is the speed equivalent for the ith species of the energy lost progressing up the attractive potential between x and x'. The κ_i and w_{c_i} values are shape parameters of the ith species that control the suprathermal tail strength and most probable speed, respectively, of the modeled three-dimensional generalization of the nonthermal kappa distribution used in Paper I. The function η_i contains the corrections to the density for the magnetic field intensity variations along the loop for the ith species and is given by the expression

$$\eta_i \equiv -\delta^{1/2}\left[\frac{\delta(1 + \xi_i)}{\delta + \xi_i}\right]^{\kappa_i - 1/2} , \tag{9c}$$

where the field strength variation is controlled by

$$\delta \equiv \frac{B_1(x) - B_2(x')}{B_1(x)} , \quad 0 \le \delta < 1 . \tag{9d}$$

The correction to the density for inhomogeneous field strength along the loop reduces the density below the isomagnetic result; this reduction goes as $-\delta^\kappa$ as the field contrast disappears ($\delta \downarrow 0$) and $(1 + \eta) \to (\delta - 1)(\frac{1}{2} + \kappa\xi)/(1 + \xi)$ as the most extreme field intensity variation possible ($\delta \uparrow 1$).

Since all moments of the Vlasov solution are known, the temperature profile can also be determined once Φ_E is known. The three-dimensional phase-space analog of the pressure evolution (eq. [27] of Paper I) is

$$P_i(x', \psi_i, \epsilon = -1) = P_i(x)(1 + \Pi_i)(1 + \xi_i)^{-\kappa_i + 3/2} \quad \text{(3D)} , \tag{10a}$$

where the function Π_i contains the effects of the varying field strength along the tube of force and is given by

$$\Pi_i \equiv \delta^{1/2}\frac{2}{3}\left(\kappa_i - \frac{3}{2}\right)\left[\frac{\delta(1 + \xi_i)}{\delta + \xi_i}\right]^{\kappa_i - 1/2} - \kappa_i\delta^{1/2}\frac{2}{3}\left[\frac{\delta(1 + \xi_i)}{\delta + \xi_i}\right]^{\kappa_i - 3/2} . \tag{10b}$$

The implied dependence of the temperature on the effective potential profile has the same structure in the three-dimensional phase space as in the one-dimensional one, viz.,

$$T_i(x', \psi_i, \epsilon = -1) = T_i(x)(1 + \Upsilon_i)(1 + \xi_i) \quad \text{(3D)} , \tag{11a}$$

where Υ_i contains the contributions for the variations of the magnetic field along the flux tube given in equation (11b) below.

Equation (11a) shows the modified, but linear, scaling of the inversion temperature with the change in potential energy parameter, ξ_i of equation (9b). This equation is the analog of a similar relation derived in Paper I (eq. [30a]). To recover the polytrope law with $\gamma < 1$, the potential parameter must be eliminated by using equations (9a) and (11a), while simultaneously assuming that Υ, which is proportional to the field contrast along the tube of force, vanishes.

The function Υ is given by the expression

$$\Upsilon_i \equiv \frac{2\kappa\delta^{\kappa_i-1}}{3}\frac{(\delta-1)\xi_i}{\delta+\xi_i}\left(\frac{1+\xi_i}{\delta+\xi_i}\right)^{\kappa_i-3/2} \times\left\{1-\delta^{1/2}\left[\frac{\delta(1+\xi_i)}{\delta+\xi_i}\right]^{\kappa_i-1/2}\right\}^{-1}. \quad (11b)$$

Two interesting limits for Υ occur for the isomagnetic limit when $\delta\downarrow 0$ and the strongly inhomogeneous regime $\delta\uparrow 1$. For weak-field variations where $\delta\downarrow 0$, Υ vanishes rather rapidly, as $\delta^{\kappa-1}$. In the opposite limit of vanishing field at x', when $\delta\uparrow 1$, and as the potential increases, $\kappa\xi\uparrow\infty$, the correction to unity in the filtration heating asymptotically approaches $\Upsilon=-\frac{2}{3}$. For completeness the full limiting expression as $\delta\uparrow 1$ for Υ is

$$\Upsilon_i(\delta\uparrow 1)\simeq\frac{-2\kappa\xi}{3\kappa\xi+1}. \quad (11c)$$

Because $\kappa\xi$ is large even in the transition region, strong magnetic field variations will only cause $T(x')$ to be reduced by no more than a factor of 3 below the simple isomagnetic prediction of velocity filtration, where $T(x')$ grows as $(1+\xi)$.

Equations (11b) and (11c) together with (11a) demonstrate that the velocity filtration effect is the dominant and persistent effect even in the presence of strong monotonic field variations.

Since the primary interest of this paper is to study the unforeseen implications of velocity filtration for changing the temperature, and the magnetic intensity does not vary strongly across the rapidly increasing TR, only isomagnetic flux tubes are considered in the remainder of the present paper. Clearly, however, the pressure and the density separately will have more significant effects than their ratio, which determines the temperature.

2.2. *Electron-Proton Plasma*

Using equation (9a), under the simplifying assumption that the protons are the only ion, the general ambipolar balance of equation (8) may be instructively simplified, viz.,

$$\xi_+\simeq\left(\frac{1+\eta_+}{1+\eta_-}\right)^{\kappa_+-1/2}(1+\xi_-)^{(2\kappa_--1)/(2\kappa_+-1)}-1. \quad (12)$$

The speed equivalents of the effective potential energy changes for electrons and ions are defined by the relations

$$v_{\Psi_+}^2=v_{\rm esc}^2\frac{r-R_*}{r}-v_{\phi_+}^2, \quad (13a)$$

$$v_{\Psi_-}^2=v_{\rm esc}^2\frac{r-R_*}{r}+v_{\phi_-}^2, \quad (13b)$$

where $v_{\rm esc}^2=2GM_*/R_*$; $v_{\phi j}^2$ is the speed equivalent for the jth species of the absolute value of the change of the electrostatic potential, $\Phi_E(r)-\Phi_E(R_*)$, which we desire to determine, defined by the relations

$$v_{\phi_+}^2=\frac{2|e\Phi_E(r)-e\Phi_E(R_*)|}{M}, \quad (14a)$$

$$v_{\phi_-}^2=\frac{2|-e\Phi_E(r)+e\Phi_E(R_*)|}{m}, \quad (14b)$$

where m and M are the electron and proton masses, respectively.

2.2.1. *Analytic Behavior: $\kappa_+=\kappa_-$*

2.2.1.1. *Potential*

Making the isomagnetic approximations, assuming common suprathermal tail parameters ($\kappa_-=\kappa_+$) and that the boundary electron and ion temperatures are equal, equation (12) is solvable for the change in the electrostatic potential energy. Under these approximations the electrostatic potential, Φ_E, is approximately one-half the size of, opposite in sign, but *strictly proportional to*, the ion gravitational potential Φ_{G+}. The proportionality constant, ζ, has the same form as that derived by Pannekeok (1922) and independently by Rosseland (1924) for Maxwellian boundary condition isothermal fluids:

$$|e|\Delta\Phi_E(r)\equiv-\Delta\Phi_{G+}(r)\zeta(\kappa_-=\kappa_+), \quad (15a)$$

where

$$\zeta(\kappa_-=\kappa_+,\ \text{all } r)=\frac{1}{2}\left(1-\frac{m}{M}\right)\equiv\zeta_{\rm PR}(\kappa=\infty). \quad (15b)$$

Equations (15a) and (15b) determine the effective potential, $\psi_\pm$, with which electrons and ions interact, given by the expression

$$\begin{aligned}\Delta\psi_\pm&=\pm|e|\Delta\Phi_E+\frac{m_\pm}{M}\Delta\Phi_{G+}\\&=\left[\pm(-1)\frac{1}{2}\left(1-\frac{m}{M}\right)+\frac{m_\pm}{M}\right]\Delta\Phi_{G+}\\&=\frac{1}{2}\left(1+\frac{m}{M}\right)\Delta\Phi_{G+}\\&=\Xi(\kappa_e=\kappa_i)\Delta\Phi_{G+},\end{aligned} \quad (15c)$$

which yields

$$\frac{1}{2}m_\pm v_{\psi_\pm}^2(r,\kappa_+=\kappa_-)\equiv\frac{1}{2}Mv_{\rm esc}^2\frac{r-R_*}{r}\frac{1}{2}\left(1+\frac{m}{M}\right). \quad (15d)$$

The common Maxwellian limit ($\kappa_-=\kappa_+=\infty$) of Pannekeok and Rosseland is a special case of the regime $\kappa_-=\kappa_+$. *The present derivation shows for finite $\kappa_-=\kappa_+$ that the previously determined Pannekeok-Rosseland potential profile is unmodified.* Notice for future reference (Scudder 1992b) that the equivalent potential, $\Delta\psi_\pm$, in equation (15d) is strictly proportional to the gravitational potential, $\Delta\Phi_{G+}$ (eq. [15c]) and is thus uniformly attractive and monotonic for all radial distances.

Using the general form (11a) for the isomagnetic temperature profile, the analytic, indistinguishable electron and ion temperature profiles are explicitly given by the more general, present relation which depends on the size of the nonthermal tails in the boundary distribution $\propto\kappa^{-1}$, viz.,

$$T_\pm(x',\kappa_+=\kappa_-=\kappa,\epsilon=-1)=T_*(R_*)\left[1+\frac{1}{2\kappa-3}\frac{GM_*(M+m)}{k_{\rm B}T_*R_*}\frac{r-R_*}{r}\right]. \quad (16)$$

where T_* is the inner boundary temperature.

In striking contrast with the isothermal profile obtained by Rosseland and Pannekeok (cf. graphical discussion of these limits in § 2.2 and analytical discussion in § 4.2 of Paper I), *the nonthermal boundary condition modeled by finite κ in equation (16) admits a new "velocity filtration" effect which predicts that the quasi-neutral temperature profile of the plasma will be*

inverted as r increases (cf. § 2.3 of Paper I for a graphical discussion of how this mathematical result arises). *In the Maxwellian boundary condition limit* ($\kappa \to \infty$), *equation* (*16*) *reduces to the familiar isothermal exponential atmosphere result of Pannekeok and Rosseland.* The quantitative importance of this inversion depends on the depth of the potential well in units of kT_* at the bottom of the well. For ZAMS stars, with thin, tightly bound atmospheres, this ratio usually exceeds 10^3 (cf. § 6 for further discussion).

The temperature inversion of equation (16) is *not* predicated on the usual scenarios of depositing bulk mechanical (ρV^2) or magnetic energy ($B^2/8\pi$) throughout the vicinity where the temperature profile is needed to increase; the inversion profile is caused by the increasingly complete exclusion, or "filtration" with height, of the lowest kinetic energy portions of the nonthermal boundary velocity distribution function. Velocity filtration is the explicit consequence of conservation of energy in an attractive (here gravity and ambipolar electric) force field in the presence of a nonthermal boundary condition. *Velocity filtration provides a description of the "distribution" or transport of the information of the incomplete thermalization ("Maxwellization") of the HCZ energy deposited in the high chromosphere.* The present kinetic calculation nonlocally determines the temperature profile along the tube of force by reconciling the filtration of particle trajectories caused by the spatially varying equivalent potential required by charge quasi-neutrality, gravity, and the boundary conditions. At the moment level this description would require truncations and closure at some unknown level above the fourth level of the hyperpressure tensor.

The present velocity filtration model for coronal heating should be contrasted with the topological dissipation model of Parker (1990), in which the mechanical churning of the photospheric footpoints of magnetic flux tubes is suggested to braid the contents of the loops until their stresses can only be relieved by the formation of current sheets; these sheets, in turn, are dissipated by resistive losses along the entire length of the loops. A three-dimensional rendition of such a set of current sheets is indicated by the colored strands in the breakaway view of a coronal arch of Figure 7*a* (Plate 1) patterned after Parker's (1981a, b, 1983a, b, 1986, 1990) sketches of his ideas of topological dissipation as the source of the coronal heating. In this way a honeycomb-like labyrinth of currents is viewed as the source of the heating of the coronal loops. The topological model suggests that *local conversion* of the mechanical (field) energy takes place in these sheets *well up into the corona* along the entire interfaces of those reconnecting "flux tubes" which make up the macroscopic loop. This scenario is of the type alluded to in § 1 that places the (Joule) heat source ($\Delta B^2/8\pi$) in the midst of the plasma to be heated. The sketch of Figure 7*a* indicates that the heating might be most intense ("white"-hot) in the innermost regions of the arcade where the twist of adjoining field lines would be most severe, and lower (deeper red) as the outer circumference of the tube is approached.

By contrast, velocity filtration naturally produces a temperature increase within the arcade that is uniform in cross section in the plane parallel to the mean photospheric surface, and increasingly "hotter" (whiter) within each flux tube (and hence the entire horizontal coronal loop cross section) toward the apex of the loop (cf. Fig. 7*b*); this inversion is caused by a coherent, selective, but reversible, transfer of particle kinetic energy into potential energy just as discussed abstractly in Paper I. Unlike Paper I, the present solutions reconcile the different interactions of electrons and ions with their respective potentials to demonstrate plasma temperature inversions that are also quasi-neutral. The topological dissipation model would produce temperature modifications along the thin colored surface current sheets of the honeycomb (cf. Fig. 7*a*) which bound the otherwise unidirectional subarcade scale "flux tubes." The interiors of these twisted tubes remain at considerably cooler temperatures because of the inhibition of cross-field heat transport by the strong magnetic field. Thus a horizontal section of Parker's model of a magnetic arcade would be heated nonuniformly by this process (Fig. 7*a*). By contrast, the velocity filtration model (Fig. 7*b*) naturally maintains the gas uniformly at the same temperature for all parts of the arcade that are at the same elevation above the photosphere and places hotter material nearer the apex than at the footpoints *without a distributed wave or magnetic conversion source term in the internal energy equation within the loop.*

2.2.1.2. *Scale Height*

The logarithmic temperature scale height, L_τ, for solutions of equal κ is given by the expression

$$\frac{L_\tau}{r} = \left[1 + \frac{1}{2\kappa - 3}\frac{GM_*(M+m)}{k_B T_* R_*}\frac{r - R_*}{r}\right] \times \left[\frac{1}{2\kappa - 3}\frac{GM_*(M+m)}{k_B T_* R_*}\frac{R_*}{r}\right]^{-1} \simeq \frac{(2\kappa - 3)C_S^2(R_*)}{V_{esc}^2(R_*)} = \frac{(2\kappa - 3)L_D}{R_*} \quad (r \simeq R_*) . \quad (17a)$$

For $r \sim R_*$ this inversion scale height divided by the stellar radius is proportional to the photospheric density scale height, $L_D/R_* \equiv kT_* R_*/[GM_*(M+m)]$ with multiplicative scaling factor of $2\kappa - 3$. This expression may also be represented as proportional to the square of the ratio of the isothermal acoustic speed to the escape speed.

For prominent suprathermal tails (small κ) the suggested scale for the temperature increase can be quite short and is to be contrasted with the infinite thermal scale length (and κ) obtained for the original Maxwellian-based calculation of Pannekeok. Inserting the canonical numbers, the "velocity filtration" temperature scale length near the transition region ($T_0 \sim 5700$ K) can be estimated to be

$$L_\tau(\kappa_- = \kappa_+) \simeq R_\odot \frac{(2\kappa - 3)k_B T_0}{(GM_\odot M/R_\odot)\Xi} = 6.9 \times 10\ \text{km}^5 \times \frac{(2\kappa - 3) \times 1.38 \times 10^{-16} \times 5700 \times 6.9 \times 10^{10}}{\Xi \times 6.67 \times 10^{-8} \times 1.99 \times 10^{33} \times 1.67 \times 10^{-24}} = (2\kappa - 3) \times 344\ \text{km}\ (2\Xi) > 344(2\Xi)\ \text{km} = 4.9 \times 10^{-4}(2\Xi)R_\odot , \quad (17b)$$

where the inequality results from $\kappa > 2$ necessary to ensure that the base distribution has a finite energy flux as discussed above. Recall that estimates of Figure 4 above suggest $\kappa \sim 1.74$, not far from the value of 2 used in the last estimate in equation (17b); in § 5 we will determine κ_+ in this region from spectroscopic data to be $\kappa_+ = 2.1 \pm 0.6$; in § 1.1.2 κ_- was suggested to be in the range $2.49 \leq \kappa_- \leq 6.25$. Solutions in §§ 2.2.2–2.2.3 below show that $\Xi \leq \frac{1}{2}$. The value of κ is also estimated in § 6.4 to range between 2.44 and 7.1 and on rare occasions between 2 and 10 based on the observed variations

of the solar wind speed. The thin scale for the logarithmic derivative implied by equation (17b) is comparable to implied widths of the transition region as inferred from diagnostic lines reviewed by Cassinelli & MacGregor (1986).

So long as the potential remains monotonic, the large-r scale length L_τ rapidly grows as r^2, and the thermal profile becomes very flat. This asymptotic result is somewhat artificial, since the neglected decreasing magnetic field will ultimately modify this result. In addition, when there are any odd moments in the boundary distribution, this is the regime where bulk acceleration will be important as well, with further modifications of the thermal, electrical, and hence equivalent potential profiles. In this case ψ may not remain monotonic (cf. Jockers 1970), and the simple predictions of velocity filtration will be modified (cf. § 6 below).

Finally, since in this regime in the isomagnetic approximation the relation between pressure and density is polytropic (Paper I), the pressure scale height, L_P, is related simply to the density scale height as $L_P = L_D/\gamma$. As shown in Paper I, the polytrope index γ is determined by the boundary κ by the relation

$$\gamma = \frac{2\kappa - 3}{2\kappa - 1} < 1 \,. \tag{18}$$

Equation (18) implies that the pressure gradient scale height at $\kappa \simeq 1.7$ (motivated by the trend in Fig. 4) is 6 times larger than the density scale height. Perhaps this result explains the seeming success of models for the transition region which treat the thin transition layer *as if* it were approximately isobaric (cf. Gibson 1973 for a discussion).

2.2.2. *Analytic Behavior: $r \simeq R_*$, Arbitrary κ_-, κ_+*

2.2.2.1. *Potential*

Near the reference level, R_*, where v_Ψ^2 vanishes, the first term of the binomial series approximation to equation (12) above is sufficiently accurate to establish the relation between the electrical and gravitational potential energy change when the ion and electron boundary velocity distributions do not have the same suprathermal character:

$$|e|\,\Delta\Phi_E(r \simeq R_*) \equiv -\Delta\Phi_{G+}\,\zeta(\kappa_-, \kappa_+, r \sim R_*) \,, \tag{19a}$$

where the proportionality constant ζ is determined by the strength of the suprathermal tails at the reference level (at the base of the transition region) given by the expression

$$\zeta(\kappa_-, \kappa_+, r \sim R_*) = \frac{1}{2}\left[1 - \frac{m}{M}\frac{2\kappa - 1}{\kappa_+ + \kappa_- - 1} + \frac{\kappa_+ - \kappa_-}{\kappa_+ + \kappa_- - 1}\right]. \tag{19b}$$

This proportionality factor normalized by the analogous Pannekeok-Rosseland (PR) value, $\zeta(\kappa_-, \kappa_+, r \sim R_*)/\zeta_{\rm PR}$, is illustrated in Figure 8. The arrangement of the terms in equation (19b) for ζ is motivated by the Pannekeok-Rosseland results (eq. [15b]) and, more generally, the $\kappa_+ = \kappa_-$ value for ζ, which is precisely $\frac{1}{2}(1 - m/M)$; the correction terms demonstrate the effects of different $\kappa_\pm$ and show that these corrections vanish for the equal but finite κ regimes discussed earlier. In particular, *if the electrons are more nonthermal than the ions, $\kappa_- < \kappa_+$, the electrical potential well gets deeper than it would if the kappas were equal or had their relative sizes reversed.*

The kinetic energy equivalent of the effective potential in equation (15a) can be rewritten in terms of ζ to illustrate its effects and the impact of its size (which is only accurate for small r):

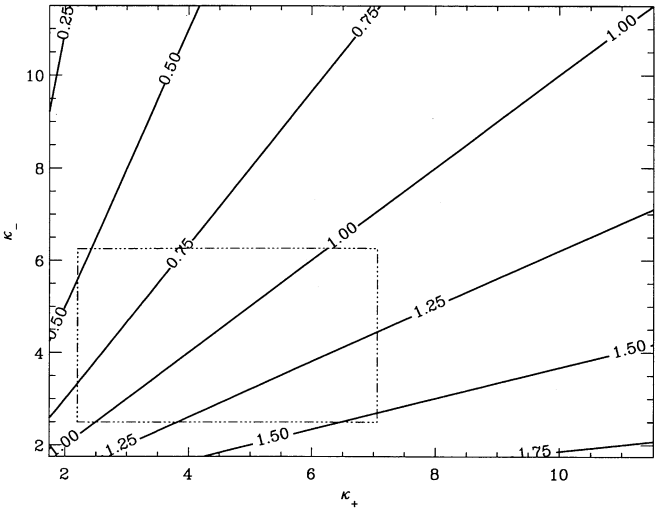

FIG. 8.—$\zeta(\kappa_-, \kappa_+, r \sim R_\odot)/\zeta_{\rm PR}$ as a function of κ_+ and κ_- in a closed magnetic geometry from eqs. (19a) and (19b). Dash-dot-dot-dot rectangle indicates likely intervals of κ_+, κ_- expected from other arguments summarized in Fig. 3.

$$\Delta\psi_+ \equiv \Delta\Phi_{G+}[1 - \zeta(r)] \to \Delta\Phi_{G+}[1 - \zeta(r \sim R_*)] \,, \tag{20a}$$

$$\Delta\psi_- \equiv \Delta\Phi_{G+}\left[\zeta(r) + \frac{m}{M}\right] \to \Delta\Phi_{G+}\left[\zeta(r \sim R_*) + \frac{m}{M}\right]. \tag{20b}$$

Using equation (19b), equations (20a) and (20b) may be reduced to the form

$$\Delta\psi_+ \simeq \Delta\Phi_{G+}\,\frac{1}{2}\left(1 + \frac{m}{M}\frac{2\kappa_- - 1}{\kappa_+ + \kappa_- - 1} - \frac{\kappa_+ - \kappa_-}{\kappa_+ + \kappa_- - 1}\right), \tag{21a}$$

$$\Delta\psi_- \simeq \Delta\Phi_{G+}\,\frac{1}{2}\left(1 + \frac{m}{M}\frac{2\kappa_+ - 1}{\kappa_+ + \kappa_- - 1} + \frac{\kappa_+ - \kappa_-}{\kappa_+ + \kappa_- - 1}\right). \tag{21b}$$

Equations (21a) and (21b) demonstrate that when the suprathermal tails of the boundary proton and electron distributions are not equally matched, the equivalent potentials in which the electrons and ions find themselves will be different: when the electrons are more nonthermal than the ions ($\kappa_- < \kappa_+$), the ions are more loosely bound than in the Pannekeok-Rosseland model; conversely, in the circumstance that the ions are more nonthermal than the electrons, they would be more tightly bound than the Pannekeok-Rosseland model would suggest.

2.2.2.2. *Scale Height*

Using the approximations of equations (20a) and (20b), instructive expressions for the small-r temperature profiles of the electrons and ions are obtained, analogous to equation (16), with the factor of $\frac{1}{2}(1 + m/M)$ replaced by ζ for the electrons and by $1 - \zeta$ for the proton:

$$T_+(x', \epsilon = -1) = T_*(R_*) \times \left[1 + \frac{2}{2\kappa_+ - 3}\frac{GM_*M}{k_B T_* R_*}(1 - \zeta)\frac{r - R_*}{r}\right], \tag{22a}$$

$$T_-(x', \epsilon = -1) = T_*(R_*) \times \left[1 + \frac{2}{2\kappa_- - 3}\frac{GM_*M}{k_B T_* R_*}\left(\zeta + \frac{m}{M}\right)\frac{r - R_*}{r}\right], \tag{22b}$$

from which it follows that the electron and ion scale heights, $L_{\tau_\pm}$, are given by expression (17a) with the factor of $\frac{1}{2}$ replaced by ζ in L_{τ_-} and by $1-\zeta$ in L_{τ_+}. Since nonthermal tails can easily double ζ, the shortest temperature scale length would be for the electrons in analogy to equation (17a) which would be $\simeq 170$ km, when the ion distribution was more thermally distributed than the electrons ($\kappa_+ > \kappa_-$).

2.2.3. *Numerical Profiles: General $r, \kappa_\pm$*

Radial profiles for arbitrary parameters not included in the above analysis require a numerical solution of equation (9a). An example of such a solution is shown in Figure 9, where $\kappa_+ = 3$ and $\kappa_- = 2.92$, and the solutions start at 2000 km with a common electron and ion temperature $T_* = 5520$ K. The rapid rise of the temperature profile is the reflection of (1) the nonthermal boundary conditions supposed at the base of the transition region, (2) the prescribed spatial dependence of the gravitational potential together with the implied, *self-consistently determined* electrical field necessary to enforce quasi-neutrality, and (3) the large absolute size of the dimensionless ratio ξ_i (eq. [9b]) of the effective potential energy well at the surface of the Sun scaled by TR base random energy, kT_*. The ratio in condition (3) may also be rewritten as the ratio of the stellar radius to the density scale height, L_D, viz.,

$$\xi_+ = \frac{R_*}{(2\kappa_+ - 3)L_D}(1-\zeta)\frac{r-R_*}{r},$$

$$\xi_- = \frac{R_*}{(2\kappa_- - 3)L_D}\left(\zeta + \frac{m}{M}\right)\frac{r-R_*}{r}.$$

R_*/L_D is well predicted by stellar structure theory, and is invariably large because the solar/stellar atmosphere is gravitationally bound in lowest approximation.

Figure 10 illustrates the attainable range of $T_{\rm corona}$ that such inversions from the solar chromosphere could support for different boundary combinations of (κ_-, κ_+) as determined by numerical solution of equation (9a) with $T_{-*} = T_{+*} = 5520$ K. $T_{\rm corona}$ is the average of T_- and T_+ at 3 $R_\odot$, well beyond where the multi–million-degree coronal (closed-loop) profiles have

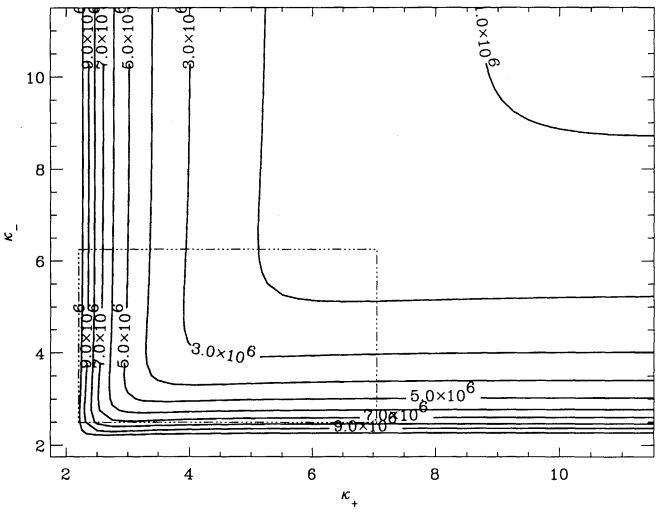

FIG. 10.—Contour of $T_{\rm corona} = (T_- + T_+)/2$ for solar case at $R = 3\ R_\odot$. Dash-dot-dot-dot rectangle indicates likely intervals of κ_+, κ_- expected from other arguments summarized in Fig. 3.

essentially saturated. The κ pair of Figure 9 is typical; many nearby and quite different pairs of choices can achieve the range of reported coronal temperatures. In addition, different electron and ion temperature profiles are possible by this process.

Figure 11 illustrates the numerically determined variation at 3 $R_\odot$ of the size of ζ, which is the electrostatic potential energy drop, $|e\Delta\Phi_E|$, in units of the gravitational potential drop, $\Delta\Phi_G$, viz.,

$$\zeta \equiv \frac{|e\Delta\Phi_E(3\ R_\odot)|}{|\Delta\Phi_G(3\ R_\odot)|},$$

scaled, in turn, by the Pannekeok-Rosseland value $\zeta_{\rm PR} = \frac{1}{2}(1 - m/M)$. The baseline value of $\zeta/\zeta_{\rm PR}$ is thus unity for equal κ's as derived in equation (15b) valid for all R. With the surface depicted in Figure 11, it is clear for large r that the unequal electron and ion suprathermal tail forms of the boundary distributions systematically modify the magnitude of the electric

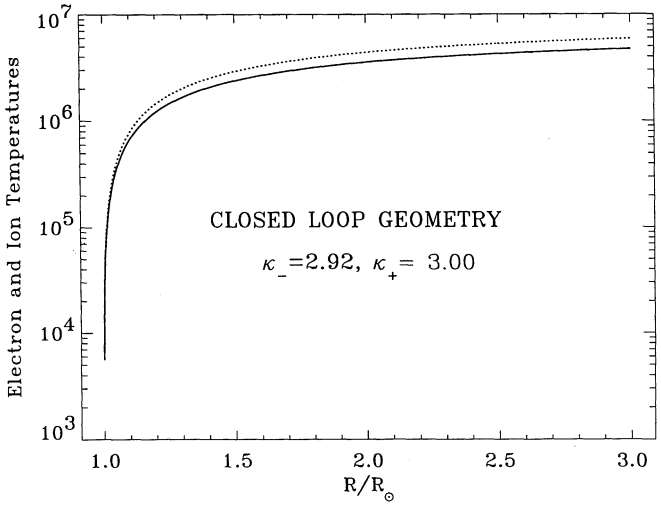

FIG. 9.—Velocity filtration ambipolar solution. Radial profile from numerical solution of the isomagnetic ambipolar equation (eq. [9a]). Dotted (solid) curves illustrate the electron (ion) temperature (τ) profiles assuming that ($\kappa_- = 2.92$, $\kappa_+ = 3$) characterize the inner boundary velocity distributions.

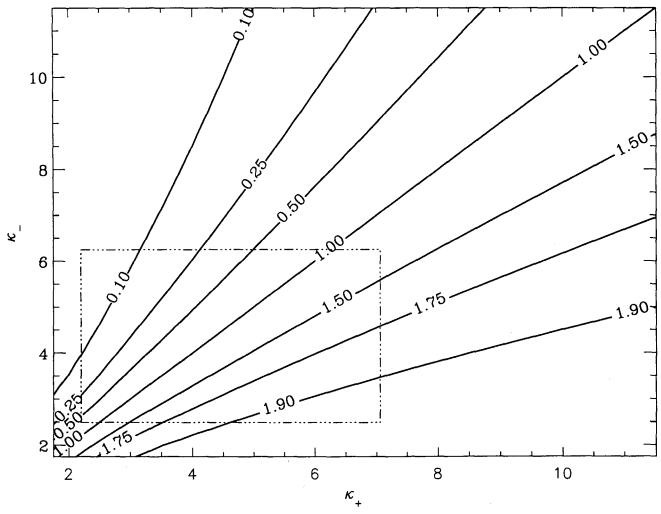

FIG. 11.—$|\Delta\Phi_E(3\ R_\odot)/\Delta\Phi_G(3\ R_\odot)|/\zeta_{\rm PR} \equiv \zeta(\kappa_-, \kappa_+, 3\ R_\odot)/\zeta_{\rm PR}$, ratio of electrical to gravitational potential normalized by the corresponding ratio from the theory of Rosseland and Pannekeok. Dash-dot-dot-dot rectangle indicates likely intervals of κ_+, κ_- expected from other arguments summarized in Fig. 3.

contribution to the effective potential well. As in the small-r, isomagnetic approach for ζ illustrated in Figure 8, the value of the electrical potential difference determined here *without approximation* is increased when $\kappa_- < \kappa_+$, and it is decreased when $\kappa_- > \kappa_+$. The results for ζ of these fully nonlinear solutions for the potential illustrate that the effect of the electric potential can almost be doubled relative to the Pannekeok-Rosseland values when $\kappa_- < \kappa_+$, and almost negated completely when $\kappa_- > \kappa_+$ in some extreme combinations. The usual fluid theories tacitly assume that $\zeta = \zeta_{PR}$ in the limit of slow flow. Significant theoretical differences from this limit do occur for the κ combinations where $[(\zeta/\zeta_{PR}) - 1]$ are largest. In these parameter regimes, interesting modifications for minor ion extraction and scale heights should be expected.

Figure 12 illustrates that electrons can be asymptotically hotter than the protons and vice versa; the organization is such that smaller κ_j boundary conditions favor higher T_j for larger r. This is traceable to the nature of the ζ/ζ_{PR} surface of Figure 11; the electrical potential is smaller for $\kappa_- > \kappa_+$ than it is for $\kappa_- = \kappa_+$, and is larger than this for $\kappa_+ > \kappa_-$. Figure 13 illustrates where the ions can be preferentially "heated" in this approach. The ion "heating" is proportional to the ψ_+ potential barrier traversed. When the electron boundary distribution has weaker suprathermal tails ($\kappa_- > \kappa_+$), the accelerating electric force is reduced, leaving the ions in a deeper effective potential well, causing a more drastic filtration and, thus, "heating."

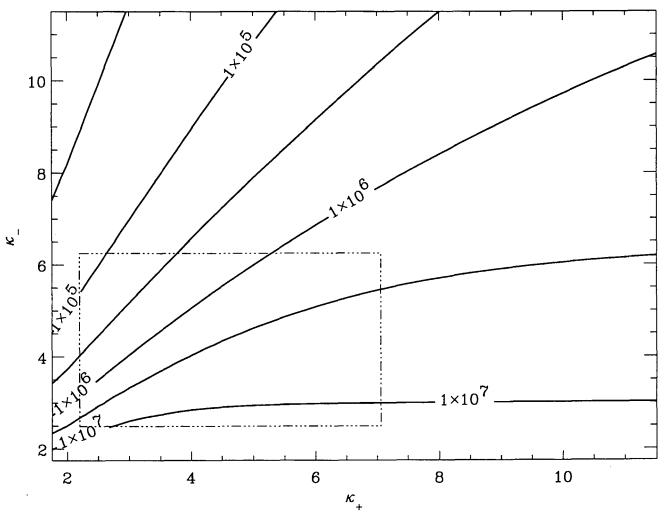

FIG. 12.—Contour of the electron inversion temperature, $T_-(\kappa_-, \kappa_+)$, at $R = 3\ R_\odot$. Dash-dot-dot-dot rectangle indicates likely intervals of κ_+, κ_- expected from other arguments summarized in Fig. 3.

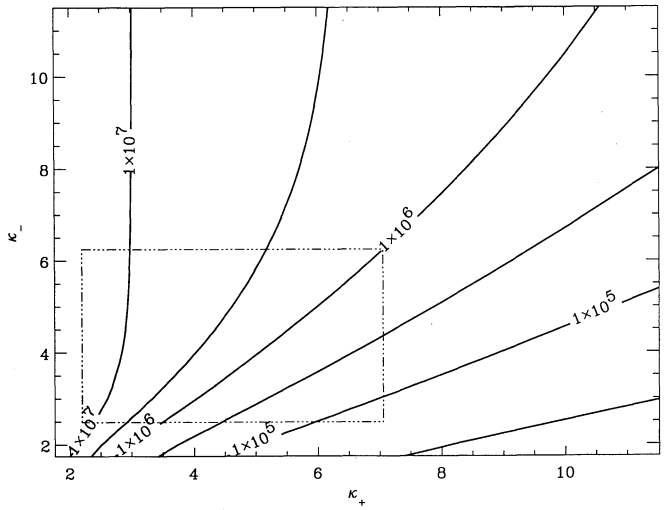

FIG. 13.—Contour of the proton inversion temperature, $T_+(\kappa_-, \kappa_+)$, at $R = 3\ R_\odot$. Dash-dot-dot-dot rectangle indicates likely intervals of κ_+, κ_- expected from other arguments summarized in Fig. 3.

2.3. *Electron-Proton, Minor Positive Ion*

When the plasma contains minor ions, the electrostatic potential is to first order unmodified, and the behavior of the minor ion temperature in the effective, but approximate, potential determined from the electron-proton electrical potential can be written down without further calculation. Consider a minor ion of mass $M_\mu = A_\mu M$, charge Z_μ, and suprathermal index κ_μ. Using the general form for the temperature profile of a nonthermal spectrum (eq. [11a]) we can arrive at the conclusion

$$T_\mu(x', \kappa_\mu, \epsilon = -1) = T_{\mu_*}\left\{1 + \underline{\frac{M_\mu v_{esc}^2 (r - R_*)}{(2\kappa_\mu - 3) k_B T_{\mu_*}\, r}\left[1 - \zeta(\kappa_-, \kappa_+, r)\frac{Z_\mu}{A_\mu}\right]}\right\}. \quad (23)$$

Since in equation (23) the underscored correction to unity is so large, this type of calculation would suggest that if the minor ion were supplied from a location near the inner boundary where all species had the same reference temperature, the minor ions (especially when in low stages of ionization such that $\zeta Z_\mu/A_\mu < 1$) would have temperatures $T_\mu(x')$ strongly correlated with, if not proportional to, their masses. This effect vanishes if the boundary minor ion velocity distributions are presumed to be Maxwellian ($\kappa_\mu \to \infty$). In fact, if Z/A is much less than unity, the temperatures of the minor ions will be proportional to the minor-ion mass, with a small correction for its actual charge state. To date there has been no satisfactory explanation of the solar wind minor ions possessing temperatures on the average that are proportional to their masses (Schmidt et al. 1980; Ogilvie et al 1980; Bochsler 1984). The typical solar wind ions used for these comparisons such as $^4He^{2+}$, $^{16}O^{6+,7+}$, $^{56}Fe^{10+,11+,12+}$ all have rather similar and small Z_j/A_j (=0.5, 0.375, 0.4375, 0.178, 0.196, 0.214). Long-term solar wind measurements (Bochsler 1984) yield temperature ratios $T(Fe):T(O^{7+}):T(O^{6+}):T(He^{2+}) = 14.1:4.9:4.5:1$. Performing the ratios indicated using equation (23) and $\zeta = \frac{1}{2}$, a match to the data can be achieved by adjusting the species κ_μ in the ratios of $\kappa_{Fe}:\kappa_0:\kappa_{He} = 1.34:0.97:1$. A search should be conducted for the presence of asymmetric suprathermal tails on the mass- and charge-resolved interplanetary ion distributions with the new generation time-of-flight instrumentation as recently described by Gloeckler (1990). (During the refereeing process of this paper, Gloeckler 1991 announced clear evidence for the routine occurrence in the solar wind of asymmetric suprathermal tails on mass-resolved spectra of H^+, He^{2+}, C^{4+}, and O^{6+}). The above effect and its related implications for the open topology case may play a role in the explanation of the preferential escape of minor ions with low first ionization potential (FIP) (cf. Meyer 1988 for a review); whenever $\zeta > \frac{1}{2}(\kappa_- < \kappa_+)$, there is the possibility of enhancing the extraction electric field relative to gravity in the presence of suprathermal electrons, which is not in any previous fluid theory. By enhancing the extraction electric field in the presence of the same structure gravitational force, the species with low FIP are assisted to gain further height in the transition region and

corona than if they had a higher FIP. Strictly speaking, this expectation is for species with comparable nuclear masses, so that the gravitational effects are of similar importance.

3. CAN COLLISIONS CURTAIL VELOCITY FILTRATION?

The traditional assessment of the importance of collisions in the transition region and low corona compares the *mean* free path for momentum transfer with the shortest macroscopic scales in the problem. If this number is small, the system is argued to be collision-dominated and a (magneto)hydrodynamical analysis proceeds. Figure 5 discussed earlier is an example of this type of analysis. For a fully ionized plasma there is *no* single free path that can be evaluated to ascertain that such a hydrodynamic truncation of the fluid equations will be valid. Because the free path in the plasma varies as the fourth power of the particle speed, the most frequently occurring speed particle's free path will be 100 times smaller than that for a particle of only 3.16 times its speed! By dimensional analysis, particles at and above this speed regime are those that are energetically permitted to get across the TR to the corona and determine the size and sign of the heat flow, which can strongly influence thermal profiles.

The calculations in § 2 have shown what can happen when no collisions are permitted, but, as discussed in Paper I, the fully ionized plasma hybrid (FIPH) approach actually "finesses" the role of collisions in lowest order. In this section an a posteriori inventory is made of the number of cumulative 90° collisions *ignored* by the approach taken in this paper; a determination is also made of the characteristics on which these significant corrections should be expected. The purpose is to show that the trajectories where Coulomb collisions are significant represent portions of the mapped distributions which are a subset of the turning orbits of Figure 8 in Paper I; these same orbits are already required by the method of characteristics to be symmetric in velocity space in a frame at rest with respect to the Sun. This symmetric distribution function of negative total energy orbits is by the FIPH choice of boundary conditions nearly a Maxwellian distribution already, so that the neglected collisions in these regions will not influence $f(v)$ much but will drive the low-energy distribution toward a local Maxwellian form in the frame where the ions are at rest: on the whole, the number and mean energy of these collisionally influenced particles are, by choice of the class of boundary distributions considered, not seriously misassigned by the present collisionless approximation.

Finally, it is shown quantitatively below that for the orbits modeled as free streaming, the unavoidable Coulomb collisions are relatively unimportant compared with the effects of free streaming. This last result is possible even in the presence of the high transition region densities because the kinetic energy of the particles which are the determinants of the distribution at 1.03 $R_\odot$ is well above kT in the low transition region; accordingly, although the number of scattering centers is very high, their collision cross section is so much lower than that of the most probably occurring particle at that altitude that they can traverse the high-density regimes almost unscathed. In the rapidly decreasing background density profile, these particles are subsequently most impeded by the energy requirements for climbing out of the equivalent potential well.

To address the effects of collisions on the free-streaming solution presented in this paper, an estimate has been made of the total number of 90° deflection "collisions" experienced by a particle between the base of the transition region en route to the local position in the transition region or corona. The assumed density and temperature of the "field" or scattering particles are consistent with charge neutrality as the velocity filtration process prescribes. The approach is to estimate the following path integral for particles that reach a given thermal speed, $w(r)$, at altitude r, after having expended 0.5 mv_Ψ^2 kinetic energy equivalent getting to r from the base of the transition region, R_*. Specifically, the following integral was evaluated using the Rosenbluth, Macdonald, & Judd (1957), collision frequency, $\nu_{\rm RMJ}$;

$$N(w(r)) = \int_0^{t(w(r))} \nu_{\rm RMJ}(w(r'), n(r'))dt(r') , \tag{24a}$$

$$N(w(r)) = \frac{R_*}{\lambda_{\rm mfp}(R_*)} \int_1^{r/R_*} \frac{n(\xi R_*)}{n(R_*)} \frac{I(w(\xi R_*), \xi R_*)}{I(w_c(R_*), R_*)} \times \frac{w_c^4(R_*)d\xi}{[w^2(r) + v_\Psi^2(r) - v_\Psi^2(\xi R_*)]^2} . \tag{24b}$$

Using the isomagnetic form of equation (9a) to replace the density ratio in the integrand of equation (24b) yields

$$N(w(r)) = \frac{R_*}{\lambda_{\rm mfp}(R_*)} \int_1^{r/R_*} \frac{\Lambda(w(\xi R_*), w_c(R_*))w_c^4(R_*)}{[w^2(r) + v_\Psi^2(r) - v_\Psi^2(\xi R_*)]^2} \times \left[\frac{\kappa w_c^2(R_*)}{\kappa w_c^2(R_*) + v_\Psi^2(\xi R_*)}\right]^{\kappa - 1/2} d\xi , \tag{24c}$$

where

$$\Lambda(\alpha(x), \beta(y)) = I(\alpha, x)/I(\beta, y),$$

$$I(w(x), x) = \Sigma(w(x)/w_{c+}(x)) + 0.5\ \Sigma(w(x)/w_{c-}(x)) ,$$

and where $\Sigma(\omega)$ is defined by the relation

$$\Sigma(\omega) = \text{erf}\ (\omega)[1 - 1/(2\omega^2)] + \exp\ (-\omega^2)/(\omega\pi^{1/2}) .$$

The velocity filtration solution has also been used to determine the background thermal spread of targets, $w_c(\xi r)$, necessary to evaluate $\nu(r)$ using the RMJ Fokker-Planck speed-dependent expression for $\nu_{90°}$.

The results for N are contoured in Figure 14 as a function of location in the *local* thermal speed distribution (x-axis) and a measure of the spatial location along the vertical axis. The convenient variable along the vertical axis is the change in the effective potential energy traversed in units of the most probable speed energy at the base of the transition region, viz., $\Delta e\psi(r)/[0.5mw_c(R_*)^2]$. At the base of the transition region for the solar corona $w_c^2(R_*)$ corresponds to approximately 0.5 eV, while the conventional base of the solar corona at 1.03 $R_\odot$ is located at $\sim$200 eV higher equivalent potential than the base of the transition region. The dotted contours are the loci of individual particles; those dotted contours which become horizontal are heliospherically bound particles which go through zero kinetic energy at some finite radial distance. The dotted curve tangent to the upper edge of the box is the total energy $E = 0$ trajectory.

The labeled solid curves correspond to the isocontours of the logarithm of the number N of *cumulative* 90° collisions since leaving R_*. This figure clearly shows that most of the distribution function at the base of the corona (1.03 $R_\odot$) is essentially ballistically related to the velocity distribution at the base of the transition region. Only below $w \sim 2w_c(1.03\ R_\odot)$

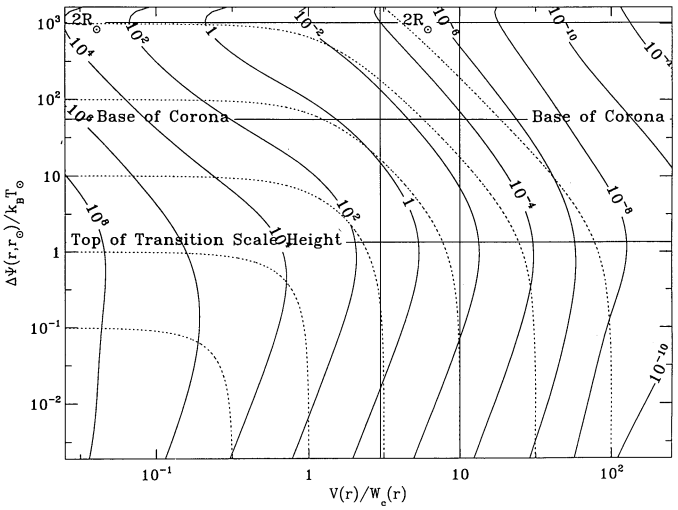

FIG. 14.—Cumulative number of 90° Coulomb scatterings en route from the transition region. Abscissa is the logarithm of the *local* kinetic speed in units of the local most probable speed particle appropriate to the spatial location of the ordinate. Ordinate increases with increasing radius and is the logarithm of the change in the equivalent potential, $\Delta\psi$, in units of kT_*, the high chromospheric reference temperature. Solid (dashed) contours are paths of constant integral number of Coulomb collisions (total energy). Proceeding along a dotted curve the solid isocontour curves traversed give an indication of the cumulative number of 90° collisions experienced since leaving the transition region. Dashed curves starting at $V(r_*)/w_c(r_*) \simeq 20$ are necessary to appear as a 1 thermal speed particle at the canonical coronal base of 1.03 $R_\odot$. The Coulomb cross section is so small at these speeds in the transition region where the density is so high that there is not much scattering. Conversely, at the same altitude the particle scattering is vigorous at $V(r_*)/w_c(r_*) \leq 1$. By referring to Table 1 the speed ranges of importance for various moments of the distribution have been tabulated as a function of κ, for density, momentum, pressure, and heat flux. To be sure that all moments of this type are adequately determined by the appropriate kinetic theory, the distribution function must be predicted well in the intervals indicated. The point should be clear that the phase space where these integrals are determined is overwhelmingly determined by particles that have "seen" very few collisions en route from the $H \simeq 2090$ km height in the transition region.

has there been the cumulative equivalent of one "collision" prior to particle arrival at this altitude. Above these speeds in the velocity space at 1.03 $R_\odot$ the entire heat-determining portion of the distribution is essentially dictated by free-streaming effects from below at the low transition region. Table 1 reveals that the quantitative value of the heat flux is strongly influenced by these free-streaming particles. Until the particle's kinetic energy is reduced by the coherent forces to be comparable to the local thermal spread, the number of collisions experienced is relatively innocuous. As the particle approaches the local thermal speed, copious collisions set in and the memory of the low transition region is lost. However, the particles above the local thermal speed are clearly seen to have a strong memory of the lower transition region conditions. *It is this nonlocality of this kinetic regime that permits the steady velocity filtration effects to take precedence in the transition region and low corona.*

On the basis of this type of calculation it is appropriate to consider the velocity filtration effects as the first-order effects and the consequences of the collisions as the perturbations. This is especially warranted when it is considered that the velocity filtration solutions require the lower energy portions of the phase space to be symmetric already, even before effects of collisions are assessed. The copious Coulomb collisions merely attempt to make this low-energy portion of the distribution into the Maxwellian form in a frame comoving with the ions. Both of these corrections represent small corrections to the distribution function, especially in the subsonic transition region. These modifications are more amenable to perturbative analysis than the unwieldy, if not impossible, attempts to attach suprathermal tails via a Spitzer-Braginskii perturbative correction to a Maxwellian lowest order distribution.

4. SUMMARY OF OBSERVATIONAL CONSTRAINTS ON A VIABLE HEATING MECHANISM

Clearly, a mechanism is of no value if it does not economically organize the known experimental morphology and,

TABLE 1

RANGE WHERE SPEED INTEGRANDS $f_\kappa(v)v^{2+l}$ ARE SIGNIFICANT[a]

	$l=0$ DENSITY			$l=1$ MOMENTUM			$l=2$ PRESSURE			$l=3$ HEAT FLUX		
κ	0.1 max	max	0.1 max	0.1 max	max	0.1 max	0.1 max	max	0.1 max	0.1 max	max	0.1 max
2.....	0.18	1.00	3.65	0.35	1.51	5.75	0.55	2.00	11.36	0.81	3.16	54.62
3.....	0.18	1.00	3.08	0.35	1.34	4.08	0.53	1.73	5.63	0.73	2.24	8.55
4.....	0.18	1.00	2.83	0.35	1.31	3.52	0.53	1.63	4.40	0.71	2.00	5.63
5.....	0.19	1.00	2.69	0.35	1.29	3.24	0.52	1.58	3.88	0.70	1.89	4.66
6.....	0.19	1.00	2.61	0.35	1.28	3.07	0.52	1.55	3.59	0.69	1.83	4.17
7.....	0.19	1.00	2.55	0.36	1.27	2.96	0.52	1.53	3.40	0.69	1.78	3.88
8.....	0.19	1.00	2.50	0.36	1.26	2.89	0.52	1.51	3.28	0.68	1.75	3.69
9.....	0.19	1.00	2.47	0.36	1.26	2.83	0.52	1.50	3.18	0.68	1.73	3.56
10.....	0.19	1.00	2.44	0.36	1.26	2.78	0.52	1.49	3.11	0.68	1.71	3.46
11.....	0.19	1.00	2.42	0.36	1.25	2.74	0.52	1.48	3.06	0.68	1.70	3.38
12.....	0.19	1.00	2.40	0.36	1.25	2.71	0.52	1.48	3.01	0.67	1.69	3.31
13.....	0.19	1.00	2.38	0.36	1.25	2.69	0.52	1.47	2.98	0.67	1.68	3.26
14.....	0.19	1.00	2.37	0.36	1.25	2.67	0.52	1.47	2.95	0.67	1.67	3.22
15.....	0.19	1.00	2.36	0.36	1.25	2.65	0.52	1.46	2.92	0.67	1.67	3.18
16.....	0.19	1.00	2.35	0.36	1.24	2.63	0.52	1.46	2.90	0.67	1.66	3.15
17.....	0.19	1.00	2.34	0.36	1.24	2.62	0.52	1.46	2.88	0.67	1.66	3.13
18.....	0.19	1.00	2.34	0.36	1.24	2.61	0.52	1.46	2.86	0.67	1.65	3.10
19.....	0.19	1.00	2.33	0.36	1.24	2.60	0.52	1.45	2.85	0.67	1.65	3.08
∞.....	0.20	1.00	2.21	0.36	1.22	2.42	0.52	1.41	2.59	0.66	1.58	2.75

[a] In units of w_c.

more importantly, predict new things which should be investigated as corollaries. A brief discussion follows of the observational constraints (Zirin 1988) as organized within the velocity filtration framework.

1. *A temperature increase, also known as "heating," is reported to take place over magnetically enhanced regions.*—Historically this correlation was one of the principal motivations for investigating the role of magnetic energy conversion to heat the corona. However, there remains the possibility, explored here, that the concentration of magnetic flux along the granule and supergranule boundaries causes a certain intensification of the underlying mechanical energy (as in a converging funnel), so that the magnetohydrodynamic energy, momentum, and mass flux from the HCZ that get up to the photospheric/chromospheric heights are concentrated in field-aligned flows before the ordered mechanical flux is attenuated by shocks or other mechanisms in the low chromosphere. Since the conservation of mass and energy equations for field-aligned fluid flow may be restated as

$$\text{Continuity:} \qquad \frac{\rho V_{\parallel}}{|\boldsymbol{B}|} = C_1 ,$$

$$\text{Energy flux:} \qquad \frac{\text{Parallel energy flux}}{|\boldsymbol{B}|} = C_2 ,$$

the intensification of $|\boldsymbol{B}|$ near the boundary of the cell causes the momentum flux in the upwelling flow to be intensified in the constricting cross section of the flux tube. In this picture the HCZ need not pick out locales to dump the heat, but the enhanced fields swept to the sides of the supergranular cells may themselves provide a channel for the energy density that the HCZ provides otherwise relatively uniformly to this height. For this mechanism to work, the field lines within the granulation boundary are only required not to be strictly vertical across the altitude of the granule. Since the bulk convection flow toward the network provides a contribution for dynamic confinement at the visible side of the cell, and the divergent flow on the bottom of the cell does not, only an especially contrived gas-pressure profile could prevent the mass, momentum, and energy flux intensification process outlined here.

The intensification of the underlying energy flux in strong $|\boldsymbol{B}|$ regions implies that the conversion of coherent mechanical energy along these tubes occurs at a lower height in the chromosphere and is enhanced in these regions; accordingly, the requirements for phase-space assimilation of this energy density is correspondingly enhanced. *It is thus suggested that the suprathermal tails should be enhanced above the intensified $|\boldsymbol{B}|$ locations in the network.* In the language of Paper I, intensified tails are associated with smaller κ indices, weaker polytrope γ's increasingly removed below unity, and hence stronger "heating" for the same density decrease with height above the network. From equation (31c) in Paper I it was concluded that $d \ln T / d \ln n = -2/(2\kappa - 1)$, so that smaller κ yields a stronger anticorrelation between T and n and could be the cause of reports of enhanced "heating" in these regions even though there is no entropy production in the higher temperature regime in this scenario.

2. *The "heating" is correlated with vertical magnetic field structures.*—Because the plasma is magnetized, as the magnetic field approaches the vertical direction the parallel motion of the particles, and hence the characteristic trajectories of the Vlasov solution, have the greatest range (limited only by the particle's total energy) to attain heights in the effective potential that have a larger potential energy difference relative to the reference location. In the simplest model the equivalent potential is stratified in the radial direction and $T(s(x'))$ should be a monotonically increasing function of arc length s along a given flux tube so long as it makes progress vertically from the surface (cf. Fig. 7*b*).

In lowest order the magnetic flux tube of the particles then determines to which altitudes a particle can gain access consistent with its total energy (cf. Fig. 6). The shading of the velocity space insets in Figure 6 depict the regions of phase space that are connected by particle trajectories. *The magnetic field energy plays no role in this repartition of potential and internal energy per particle in the gas.*

3. *Effect 2 slows the general cooling even directly above the photosphere.*—In the present model, this regime is still a place where the above effects of particle access are important but where the overall energy loss from the volume element is modified by the presence of partially ionized plasma and is still relatively well coupled to the radiation field, which controls the overall temperature profile; the above kinetic effect could play a role here but not be the dominant effect at altitudes between the photosphere and transition region.

4. *Horizontal fields are not "heated."*—As the corollary to the main explanation, field lines that are horizontal lie predominantly on an isocontour of the equivalent potential; since under the velocity filtration process the particle's access to the different levels in the effective potential ensures "heating" signatures, there will be only a minimal effect expected in this geometry, particularly when these structures can be shown to be at low altitudes. Clearly from point 2, the top of a closed loop has horizontal fields, but these are at a substantial height where considerable velocity filtration has already produced the temperature inversion effect as in Figure 7*b*.

5. *Every area of increased field is bright.*—Zirin (1988) suggests that this observational fact argues against episodic mechanisms like reconnection for the explanation of the brightness in these locales. The present suggestion of the way that enhanced field strength regions act as intensifiers to the transmitted charged particle energy fluxes presented to the network would serve here to reemphasize a similar explanation for these observations.

6. *Emerging flux and attendant reconnection are always sites of additional "heating."*—Zirin (1988) implies that this morphology is superposed on top of the baseline heating scenario, thus underscoring its time-dependent role in the heating story.

7. *Except in reconnection regions, heating is proportional to $|\boldsymbol{B}|$.*—This is not really different from effect 1.

8. *"If non-thermal energy were present in the photosphere it might somehow be focussed on the tiny amount of material above so as to crack the whip" (Zirin 1988).*—The present calculations and those of Paper I illustrate how the nonthermal energy in the form of a departure from a Maxwellian form at the base of the transition region can, by the process of velocity filtration, strongly influence τ, the height variation of the mean random energy of the particles. The velocity filtration in the reversible potential serves to raise the mean energy of the particles that can gain energetic and topological access to the higher altitudes in the given tube of force.

9. *The Biermann-Schatzmann-Schwarzschild theory of acoustic noise (Biermann 1948; Schatzmann 1949; Schwarzschild 1948) predicts, according to Zirin, uniform heating except possibly in ultrastrong-field regimes.*—Zirin claims that this by

itself cannot explain the morphology of the observed coronal heating. The recent review by Narain & Ulmschneider (1990) also summarizes that the power remaining in acoustic noise in the transition region and low corona is off by several orders of magnitude for maintaining the corona by a local conversion of residual mechanical energy at these altitudes.

10. *The Osterbrock theory of MHD cannot get the dissipatible wave energy density above the temperature minimum, and therefore it is difficult to heat the corona at higher heights (cf. Parker 1990).*—The termination of the mechanical energy at or near the temperature minimum implies (by the continuity of energy flux) that it must be repartitioned into some other form, particularly along the strong-field regimes where the field cannot be bent out of the radial. Narain & Ulmschneider (1990) summarize the overwhelming evidence that suggests that the highest conceivable point where the acoustic and slow branches could damp would be in the upper reaches of the chromosphere. These authors also suggest that the Alfvénic power will not damp in the transition regions or above, having easy access into the solar wind; however, if Alfvén waves supply the momentum to the coronal holes, why are they not more plentiful in interplanetary space (cf. Roberts 1989)? How can this mode heat the open corona as summarized by Heyvaerts and Priest (1983) if it hardly interacts with it?

11. *X-ray loops are hottest at their highest point.*—The ambipolar solutions presented in § 2 clearly illustrate (cf. Fig. 7*b*) that high, X-ray–producing temperature plasmas are possible by this effect, and the highest temperatures and lowest densities along any given tube of force are expected at the highest point in the loop. Figures 7*b* and 9 also show that above the TR heights the temperature profile along the top of a loop would grossly be described as "isothermal" with a high temperature. The Rosner-Tucker-Vaiana (1978) relation suggests that T is proportional to $L^{1/3}$ of the magnetic loop which is correlated with its height above the photosphere. While the present model was not introduced to explain the observed correlation with loop height, it is a natural feature of the sensitivity of the heating to the number of equivalent potential surfaces traversed (cf. Fig. 6). This is a trivial consequence of the basic idea of velocity space filtration in a radially organized attractive equivalent potential.

12. "*One way or another, the high temperature of the Sun's atmosphere must be a consequence of i) the rapid fall off in density from its surface, coupled with ii) magnetic elements playing the role of the whip in tying subsurface to atmospheric regions*" (*Zirin 1988*).—The possibility of the relevance of the FIPH style closure developed here and in Paper I is clearly the result of the strong inhomogeneity in the Sun's density profile: (1) the reduction of scattering centers; (2) the radial asymmetry of the scattering centers, with respect to the outward direction; (3) the Coulomb cross section's speed dependence, which permits such a nonthermal boundary condition in the low levels of the transition region to produce the temperature inversion in the transition region into the corona; while (4) the magnetic field plays the role of a conduit in connecting the regions where the particles and hence the characteristics have access. While essential to organizing solar morphology, the role of the magnetic field in this view is "passive" in that it only facilitates striations in the temperature structure but does not contribute to the structure by *locally* converting $B^2/8\pi$ into heat as in the picture of the topological dissipation model of Parker (cf. Fig. 7*a*). *Gravity and its attendant, inhomogeneity, are the essential ingredients of the velocity filtration mechanism, not the magnetic field.*

13. *Observationally, the coronal hole plasma temperature exceeds that of the photosphere, but not by as large a factor as the closed loop regions of the corona.*—The calculations of Paper I show similar effects, with a flowing gas as opposed to a nonflowing one. The present model does not collapse with a change of the magnetic topology from closed to open. The basic filtration mechanism has new possible outcomes that are allowed by the closed-field to open-field topology change; the filtration cause of $T_{\rm corona}$ is not compromised. Because coronal holes are open, there are additional freedoms not available in the closed configurations that allow energy to be transformed not only between potential and random energy but also between bulk flow and heat flux reservoirs. Other things being equal, such as similar boundary pressure, density, and suprathermal tail strength, the additional exit channels would drain some energy per particle which in the closed topology could only go into temperature. This drain becomes serious near the transonic point, but at lower altitudes *the change of magnetic topology does not disrupt the velocity filtration process; this topological robustness is in marked contrast to the fragility of the resonant absorption or topological dissipation models for getting the corona hot; these mechanisms are rendered ineffective in the open magnetic geometry by the removal of the cavity in the one case or the loss of dual footpoint "line tying" in the other.*

From this overview of the observations it should be clear that much of what is known about solar coronal "heating" morphology can follow simply from the velocity filtration process.

5. LINE PROFILE IMPLICATIONS

The proposed nonthermal distribution of emitters and scatterers that underlies the subsequent filtration scenario for the temperature inversion of the stellar envelope/corona should have some observable consequences in the line emission and absorption profiles. In this section the Hjerting, or Voigt, line profile is generalized to reflect a kappa prototype nonthermal distribution of absorbers/emitters. *Below, the wings and half-widths of the lines are demonstrated to be sensitive to the ion nonthermal random speed distribution of the gas and are shown to be capable of mimicking the effects widely attributed by spectroscopists to "turbulent," but spatially unresolved, bulk speeds.*

The distribution, F, of particle velocities along a given Cartesian axis of a kappa distribution at rest is given by the expression

$$F_\kappa\, dv_x = \frac{A_\kappa\, dv_x}{\kappa^{1/2} w_c [1 + (v_x/w_c)^2/\kappa]^\kappa}, \tag{25}$$

where A_κ is the normalization constant for the three-dimensional kappa distribution, $A_\kappa = \Gamma(\kappa + 1)/\Gamma(\kappa - \frac{1}{2})/\kappa^{3/2}$. Using the formula for the wavelength shift, scaled by the line-center wavelength, λ_0, for a nucleus moving with speed $v_x(\Delta\lambda/\lambda_0 = -v_x/c)$, the distribution of wavelength shifts caused by a kappa distribution of emitters is given by

$$F(\Delta\lambda)d(\Delta\lambda) = \frac{d(\Delta\lambda)}{\Delta\lambda_{\rm D}^c}\frac{A_\kappa}{2}\left[1 + \left(\frac{\lambda}{\Delta\lambda_{\rm D}^c}\right)^2 \frac{1}{\kappa}\right]^{-\kappa}, \tag{26}$$

where $\Delta\lambda_{\rm D}^c = \lambda_0\, w_c/c$ is the Doppler width associated with the most probable speed particle. Convolving the atomic absorption coefficient

$$a_\lambda(\lambda + \Delta\lambda) = \pi r_e\, \lambda_0^2 f \frac{\Delta\lambda_N}{4\pi^2(\lambda + \Delta\lambda - \lambda_0)^2 + (\Delta\lambda_N/2)^2} \tag{27}$$

with equation (26), where r_e is the classical electron radius, $\Delta\lambda_N$ is the intrinsic nuclear line width, and f is the oscillator strength, yields the nuclear Doppler (ND) convolved line profile in the form

$$a_\lambda^{\rm ND}(a, w, \kappa) = a_{\lambda_0}^{\rm D} S(a, w, \kappa) , \quad (28)$$

where $a_{\lambda_0}^{\rm D} = \pi^{1/2} r_e \lambda_0^2 f/\Delta\lambda_{\rm D}^c$. $S(a, w, \kappa)$ is the generalization of the Voigt-Hjerting function, which now depends on the nonthermal tail index, κ, and is given by the expression

$$S(a, w, \kappa) = \frac{aA_\kappa}{\pi^{1/2}} \int_{-\infty}^{+\infty} \frac{d\xi}{(1 + \xi^2/\kappa)^\kappa [(w - \xi)^2 + a^2]} . \quad (29)$$

Analytically, the $\lim_{\kappa\to\infty} S(a, w, \kappa)$ is $H(a, w)$, the customary Voigt-Hjerting profile. Here, as in the notation of Voigt profiles, a is inversely proportional to the thermal speed of the gas, being proportional to the ratio of nuclear to most probable speed Doppler line widths, viz.,

$$a \equiv \frac{\Delta\lambda_N}{4\pi\Delta\lambda_{\rm D}^c} = \frac{\Delta\lambda_N}{\lambda_0} \frac{c}{4\pi w_c} . \quad (30)$$

Examples of the influence of suprathermal tails (finite κ) on the line profile functions $S(a, w, \kappa)$ are illustrated in Figures 15*a* and 15*b*. All nuclear and most probable speed Doppler parameters are held fixed for these illustrations of the influence of different strength suprathermal tails on the line profile. The Voigt profile (based on a Maxwellian gas distribution) is reproduced for reference as the solid curve in both Figures 15*a* and 15*b*. For the modest departures from Maxwellian behavior ($\kappa = 11.9$) depicted with the segmented curve in Figure 15*a*, the line width and depth at line center relative to the continuum are increased and decreased, respectively, while strongly nonthermal particle distributions (Fig. 15*b*) can significantly enhance the wing of the line and at the same time further broaden the line core and reduce the line-center amplitude.

In the classical Voigt-Hjerting profiles a smaller a parameter corresponds to producing enhanced wings of the line. Smaller

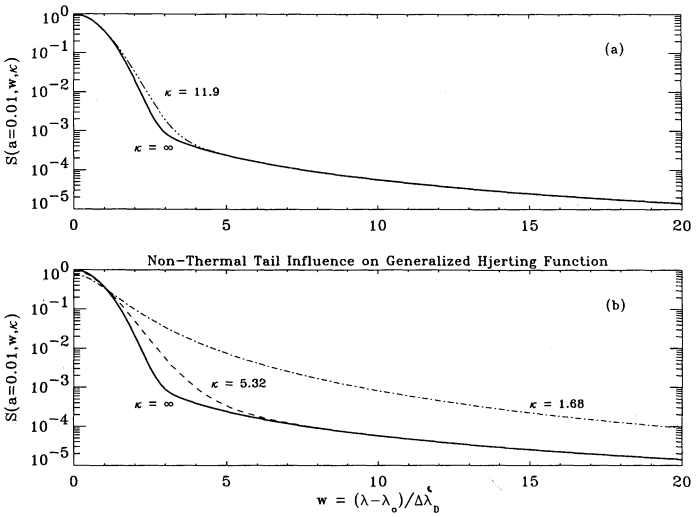

FIG. 15.—Generalized Voigt profile modifications with nonthermal distributions. The solid trace is the Voigt profile; the dashed curve illustrates the influence of the suprathermals. (*a*) Near-Maxwellian nonthermal influence: comparison for a weakly suprathermal population with $\kappa = 11.9$. (*b*) Nonthermal tail influence on generalized Hjerting function: a similar comparison, but with strongly nonthermal distributions: $\kappa = 5.32$ (*dashed curve*) and $\kappa = 1.68$ (*dash-dot curve*).

a corresponds to larger $\Delta\lambda_{\rm D}^c$, which in turn is proportional to the thermal velocity of the gas (eq. [30]). In recent years it has become customary to include also in the Doppler width the effects of postulated "turbulent or nonthermal" bulk velocities, assumed to have Gaussian distributions with e-folding width of size $V_{\rm NT}$, yet postulated to be temporally and spatially unresolved (cf. Gibson 1973 for a "derivation"). Augmenting the effective Doppler width by this ad hoc procedure lowers the quantity a and presumably gives a better fit to the data by significantly enhancing the half-width and wing of the line.

Because the physical conclusions from line profile measurements represent a significant model inversion with attendant nonuniqueness, *it is possible that some of the signatures* (illustrated in Figs. 15*a* and 15*b*) *attributed to unresolved "turbulent or nonthermal" velocities could be suprathermal* (*i.e., nonthermal distribution*) *tail signatures in disguise.* To provide an overview of the types of line profile variations that the generalized S function provides, Figure 16 illustrates isocontours of the ratio of S line profiles for finite κ to those of infinite κ (i.e., Voigt profiles without any postulated "turbulent" contributions) as a function of distance, w, from line center along the abscissa and strength of nonthermal tails along the ordinate. Maxwellian behavior is approached at small ordinate values, extremely nonthermal distributions at large ordinate values. The line profiles beyond $w = 1$ are generally enhanced, ranging from 3 to 30 times, especially for w in the interval (2, 7), although significant wing enhancements out to $w = 20$ can clearly occur. Below $w = 1$, slight depressions ($<20\%$–30%) at the line center (cf. Fig. 15*b*) are the general modifications when κ is finite.

It must remain for future work to test the relative merit of these two approaches to the line inversion problem. An important clue in this connection is the already reported association of enhanced "turbulent velocities" with magnetic intensity (Nicolas et al. 1982). If this signature really reflected enhanced suprathermal tails, this association would support the earlier arguments (§ 3) of how "heating" observations are organized with $|\boldsymbol{B}|$. Nicolas and coworkers also reported that the "turbulent" or "nonthermal" speeds were also positively correlated with temperature; the data suggest $V_{\rm NT} \propto T^{1/2}$. Nicolas and coworkers further showed that $V_{\rm NT}$ was episodically, but poorly, "correlated" with the bulk Doppler speed (which is known to be correlated with vertical and strong B); however, $V_{\rm NT}$ *always* possessed a nonzero threshold size even when the Doppler shift was unmeasurably small. Fluid turbulent velocities would presumably disappear with the DC flow speed, but that is not the reported morphology of the $V_{\rm NT}$ observations! Finally, Dere (1989) has reported on direct measurements of the Doppler velocity indicated by the displacement of line centers and the simultaneous, but indirect, inferences of the unresolved "turbulent" velocities from the anomalous Doppler widths; he concludes that the observed k-spectrum of the spatially resolved Doppler flows is flatter than that of the inertial range of a turbulent fluid. Dere concluded that the driving source of energy for $V_{\rm NT}$ could *not* be a cascade from the energetically dominant, observed, long-wavelength bulk velocity fluctuations into the unresolved, but inferred, short-wavelength k regime of $V_{\rm NT}$. *In short, the canonical, but ad hoc,* "bulk speed turbulence" *explanation for these line profiles appears open for serious revision.*

The measurements of Nicolas and coworkers of nonthermal speeds and their correlation with temperature is simply explained with the present description of the evolution of the

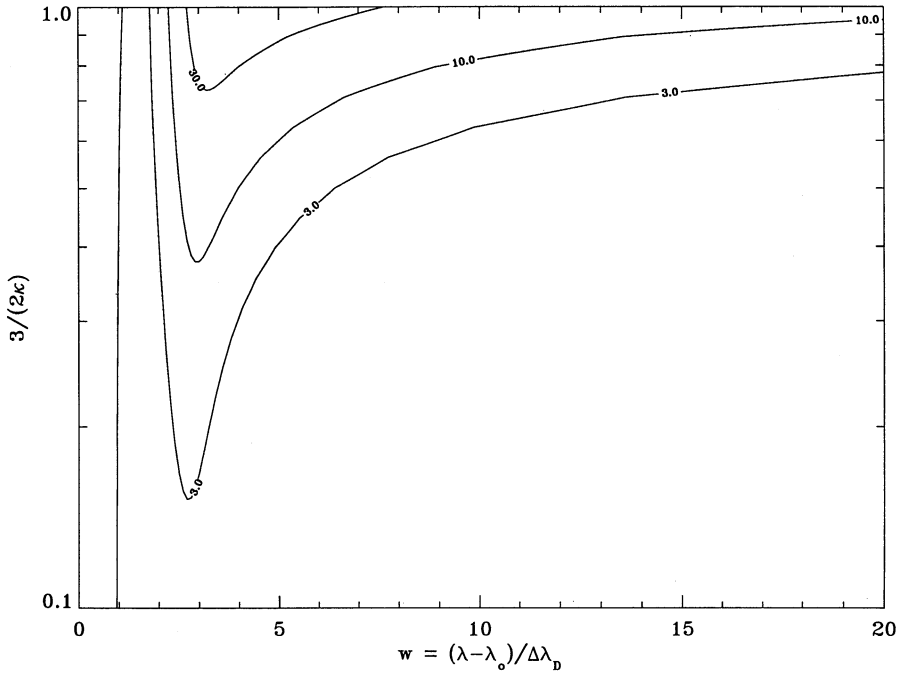

FIG. 16.—$S(a = 0.01, w, \kappa)/S(a = 0.01, w, \kappa = \infty)$. Overview of generalized Voigt function relative to that for an exact Maxwellian. The abscissa is standard notation for displacement from line center. The plotted ordinate is the quantity $3/(2\kappa)$ which lies in the range [0, 1]; κ lies in the range $[\infty, 3/2]$. In this way the most nonthermal comparison is at the top edge, and the Maxwellian is approached at the lower edge. The contoured quantity is the ratio of the line profile at the wavelength and κ to the corresponding value for the Voigt-Hjerting profile. For finite κ the line center is slightly depressed, but it is generally enhanced in the e-folding and wing regions.

distribution function under velocity filtration. Consider a kappa distribution as a nonthermal model. The equivalent width, $V_{\rm width}$, for a kappa distribution is principally determined by the relation

$$V^2_{\rm width}(x) = \frac{2\kappa}{2\kappa - 3} w_c^2 , \tag{31}$$

where w_c is the speed of the most probably occurring particle in the distribution at x. The spectroscopic characterization of the half-width of the line determines $V_{\rm width}$. The source region temperature assignment, $T_{\rm rad}$, is determined by the statistical mechanics of ionization and recombination using a Maxwellian model for rates. For lines sensitive to recombination, which in turn depends most strongly on the mean energy of that portion of the velocity distribution below which the particle density is determined, the effective $T_{\rm rad}$ could reasonably be associated with the speed equivalent of the most probably occurring particle in the distribution (cf. Table 1). This occurs at w_c for any value of κ. This implies that $k_{\rm B} T_{\rm rad} \equiv AMw_c^2/2$. The excess Doppler width reported as a "bulk speed turbulence" or "nonthermal" contribution to the apparent line width would take the form

$$V^2_{\rm NT}(x) \equiv V^2_{\rm width}(x) - \frac{2k_{\rm B} T_{\rm rad}(x)}{AM} \tag{32a}$$

$$= \frac{3}{2\kappa - 3} w_c^2 , \tag{32b}$$

or

$$V_{\rm NT}(x) = \left[\frac{6k_{\rm B} T_{\rm rad}(x)}{(2\kappa - 3)(AM)}\right]^{1/2} , \tag{33}$$

predicting a square-root dependence of the "nonthermal" speed, $V_{\rm NT}$, on the ambient temperature variation. It is easy to show that the square of the width of the kappa distribution (eq. [31]) is amplified by the factor $(1 + \xi)$ when moving to a new location, x', up the potential and that the square of the speed of the most probably occurring particle in the new location also grows as $(1 + \xi)$, so that equation (33) is structurally correct as the temperature varies for all x along the same tube of force where the potential is monotonic and attractive. The square-root dependence of the excess Doppler width on the source region temperature (called $V_{\rm NT}$ by Nicolas et al. 1982) is clearly predicted by equation (33); an interpretation of the proportionality constant in terms of the suprathermal tail constant κ and species mass is also suggested.

The reported measurements of Nicolas et al (1982) are replotted in the left-hand panel of Figure 17 [multiplied by $(A/16)^{1/2}$ to remove the mass dependence of eq. (33)] versus the source region temperature, $T_{\rm rad}$, reported by these authors for UV transition region lines. Superposed on these data is the best-fit log-log linear regression line and confidence bands for all mass normalized data taken together. The fit slope value of 0.53 is indistinguishable from the velocity filtration prediction (eq. [33]) of 0.5. The fit for the four oxygen lines which would not require the mass internormalization yielded an overdetermined least-squares slope of 0.53. The intercept of the slope in log-log coordinates for all the data determines the optimal value of $< \kappa_+ >_{\rm fit} \sim 2.1 \pm 0.6$ for these ions. Using all the mesurements separately in the expected interrelationship (eq. [33]) yielded a mean value of $\langle \kappa_+ \rangle = 2.1 \pm 0.7$. *These inferences for κ_+ from the Doppler lines are consistent with that inferred from Figure 4 in § 1, where a value of $\kappa \sim 1.7$ was suggested from the density and temperature profiles across the transition region into the low corona. This value of κ_+ is also*

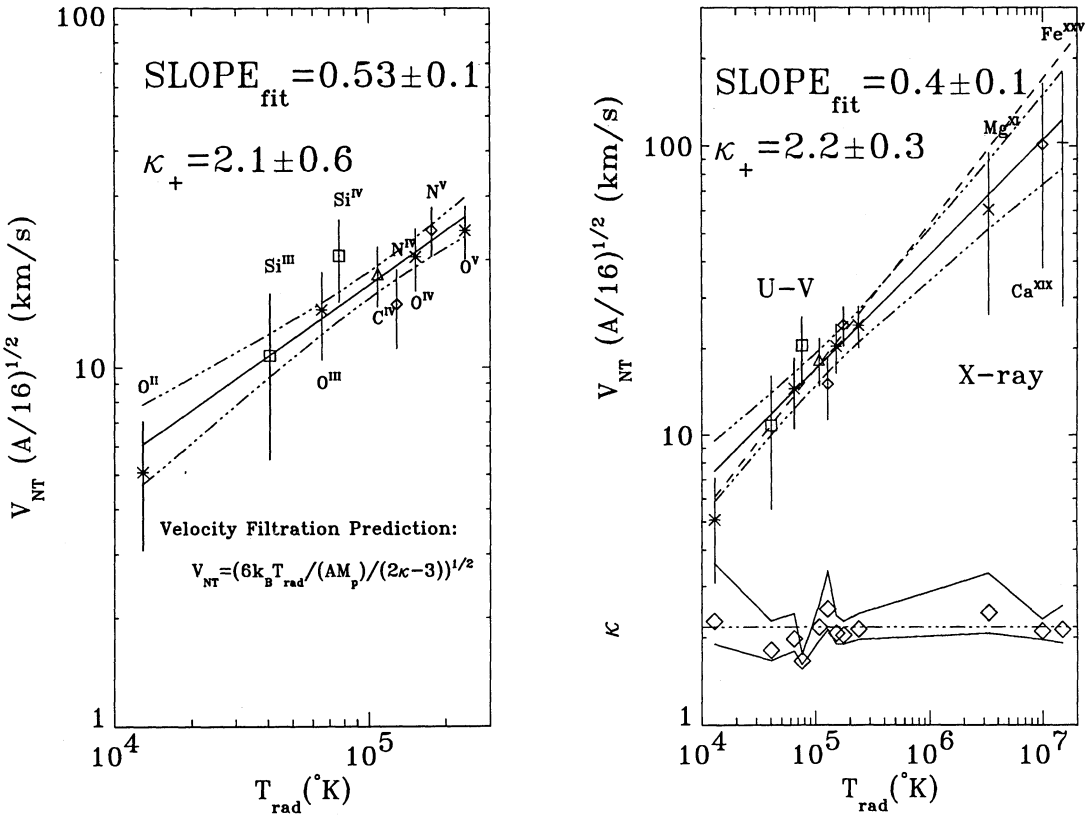

FIG. 17.—"Turbulent" speeds as suprathermal tails. (*Left*) Correlation of V_{NT} from UV lines and T_{rad} in the transition region; data adapted from Nicolas et al. (1982), Fig. 5. (*Right*) Composite of UV and X-ray estimates of V_{NT} vs. T_{rad}, illustrating compatibility with $T^{1/2}$ over three decades of dynamic range. The dashed line is the best-fit from the left-hand panel from UV lines only, but extrapolated up to X-ray temperatures. Diamonds illustrate estimates of κ_+ required from each V_{NT} observation assuming that $T^{1/2}$ scaling is correct. Horizontal dash-dot-dot-dot line indicates the arithmetic mean of these estimates of $\langle\kappa_+\rangle \simeq 2.2$ for $10^4 < T_{rad} < 2 \times 10^7$ K.

within the range of κ_- suggested as necessary in Figure 3 for the replenishment of the coronal losses.

Rather than interpreting the UV excess Doppler widths as "turbulent" bulk speeds, the velocity filtration model would assign this excess width to "nonthermal" aspects of the *random* probability distribution. In so doing, Dere's (1989) dilemma about the observable speed power spectrum being "unable" to feed the unresolved "turbulent" velocities via a turbulent cascade process can be obviated; the *reportedly omnipresent "nonthermal" velocities can now be understood by appealing to the gravitationally induced ubiquity of suprathermal distributions whether the medium is flowing or not.* Finally, the disconcerting prospect of supersonic turbulent bulk velocities that have been reported by Brueckner & Bartoe (1983) could be viewed as unusual, suprathermal tail enhancements involving a relatively small portion of the ambient density, but not involving any coherent bulk motion. This reinterpretation is all the more urgent given Dere's (1989) analysis, which does *not* support a turbulent cascade's ability to feed the inferred short-scale bulk speed activity associated with the traditional interpretation of V_{NT}; the markedly reduced energy requirement to inflate the wings of a nonthermal distribution, as opposed to moving the entire mass density back and forth at these supersonic velocities, would appear to be a step in the correct direction. *Most important, the present organization of the detailed solar findings of the nonthermal fit parameters places the nonthermal velocity distribution postulate for the circumstellar inversion discussed in this paper on a firm experimental basis at a depth where the question is most pressing: in the transition region itself.*

The right-hand panel of Figure 17 illustrates that recently reported X-ray V_{NT} measurements (e.g., Saba & Strong 1991) are also compatible with the $T^{1/2}$ scaling suggested by equation (33) from velocity filtration and the UV data in the left-hand panel. Although the UV and X-ray data have different sources of measurement error, together they suggest a $T^{0.4\pm0.1}$ dependence, organizing three decades of formation temperature with a single concept. This scaling is consistent with the $T^{0.53}$ inferred from the UV lines. Assuming the $T^{1/2}$ scaling, each observation and dispersion of V_{NT} can be used to estimate a value of κ_+ that will reconcile the observations and equation (33). These estimates of κ_+ are plotted as diamonds in the right-hand panel. There upper and lower excursions have been connected to form an error band, while a horizontal line has been drawn to reflect the average κ_+ inferred to be $\langle\kappa_+\rangle \simeq 2.2$.

6. ASTROPHYSICAL IMPLICATIONS

6.1. *Stellar Corona Temperature Predictions*

Since no special circumstances have been invoked to produce temperature inversions at our star, it would seem reasonable to see what astrophysical consequences can be suggested from equation (16) and different star types. The spatial form of

the "inversion" temperature becomes

$$T(r) = O(1)T_*(R_*)\left(1 + \frac{R_*}{L_D}\frac{2\zeta}{2\kappa - 3}\frac{r - R_*}{r}\right), \quad (34a)$$

where the effects of the magnetic field discussed in equations (9*a*) and (9*b*) are retained in the $O(1)$ coefficient. Because the explicit correction to unity in equation (34a) is so large for most stars, this expression may be simplified at $2R_*$ to be

$$T_{\rm inversion} \equiv T(2R_*) \simeq O(1)T_*\left(\frac{2\zeta}{4\kappa - 6}\frac{R_*}{L_D}\right). \quad (34b)$$

Apart from the value of κ and $\zeta \sim \frac{1}{2}$, the quantity in equation (34b) which shapes the relative size of $T_{\rm inversion}$ versus T_* is the ratio of the stellar radius, R_*, to the photospheric density scale height, L_D; this ratio is invariably large because the photosphere is essentially bound. *By equation (34b) any bound atmosphere that has a nonthermal distribution in the regime analogous to the base of the transition region should have a circumstellar thermal inversion zone. The magnitude of the temperature contrast is determined by the prominence of the suprathermals* ($\propto \kappa^{-1}$) *in the boundary spectrum and, ironically, the tightness by which the atmosphere is gravitationally bound,* $(R_*/L_D) \gg 1$.

Tabular data for stars on the ZAMS, giants and supergiants were obtained from Bowers & Deeming (1984) to determine the values of $T_{\rm inversion}$ using equation (34a) assuming a strongly nonthermal (but solar-like) distribution at the top of the stellar atmosphere ($\kappa_\pm = 2$) and $\zeta = \zeta_{\rm PR} = \frac{1}{2}$. Four patterns are immediately obvious in Figure 18, even presupposing that all classes of stars have the same nearly maximal suprathermal tail boundary condition: (1) the separate stellar groups retain their identities in their predicted inversion temperature; (2) all the ZAMS stars in this ad hoc sample yield inversion temperatures in excess of (2–3 × 10^6 K, which qualifies them to have "coronae" in the sense of having sufficiently energetic gases to produce the traditional "coronal" lines; (3) the giant stars have significantly cooler "inversion temperatures," well removed from 10^6 K, implying that at best they might have

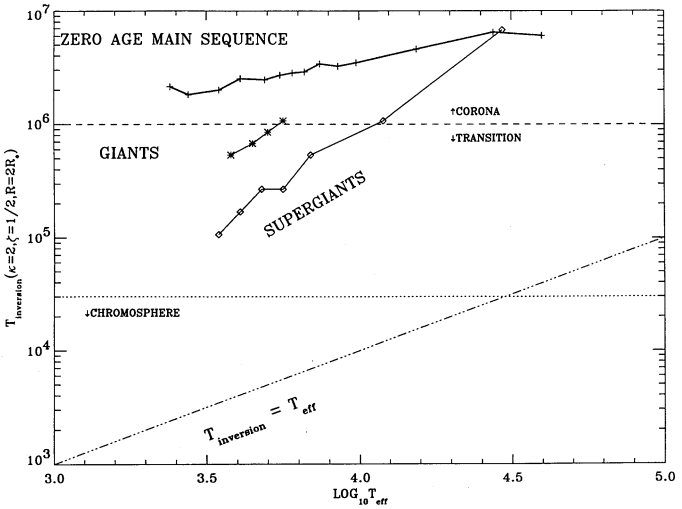

FIG. 18.—Velocity filtration predictions. Stellar "inversion" temperatures suggested by the present paper at $2R_*$ assuming $\kappa = 2$ and $\zeta = \frac{1}{2}$ for sample stars with properties tabulated by Bowers & Deeming (1984). Corona regime refers to $T \geq 10^6$ K, which is adequate for thermal X-ray production. See text, § 6.1, for discussion of implications.

chromospheric lines but never "coronal" ones; (4) the circumstellar envelopes of the supergiants as a group appear even cooler than the other two groups of stars of the same spectral type, except the hottest supergiants, which would appear to have inversion temperatures which might qualify for the adjective "coronal."

Cassinelli & MacGregor (1986) have recently reviewed the stellar-solar problem, and their summary is particularly relevant in light of the preceding calculations:

> Main sequence stars possess chromospheres, transition regions, and coronae whose structure and energy balance (but not always the level of activity) are probably quite similar to those of the analogous regions in the solar atmosphere. Like the Sun, these stars undergo mass loss in the form of hot, tenuous, and fairly high velocity stellar winds. As one proceeds from the main sequence towards the Giant and Supergiant branches in the cool portion of the H-R diagram, both the thermal and dynamical structure of the atmospheres under consideration change. Gas temperatures in the outer atmospheres of the coolest and most luminous Supergiants never exceed values characteristic of the solar chromosphere or do so over very limited regions of limited spatial extent. These stars possess cool, massive winds with terminal velocities well below the gravitational escape speed of the stellar surface. Intermediate between the main sequence and the supergiants are the so-called hybrid stars. The atmospheres of these stars contain gas at transition region temperatures and observations of blue shifted Mg II absorption features imply the existence of relatively high velocity winds with mass loss substantially in excess of those appropriate to main sequence stars [pp. 83–84].

From this independent review of the literature the velocity filtration approach with $\kappa \simeq 2$ is quantitatively in line with the magnitudes of the inversion temperatures of other ZAMS stars and with the recent surveys (Rosner et al. 1985) that show that they invariably have X-ray–emitting coronae, but not in numerical accord with the reported envelope temperatures of the giants and supergiants. The velocity filtration estimates of Figure 18 are practical upper bounds, provided that the post-photospheric regions of all stars possess significant nonthermal distributions like that of our Sun. By choosing the suprathermal tail parameter κ to be larger than the illustrative value of 2 in Figure 18, the envelope of "inversion" temperature of the star can be *any* number between the effective surface/transition region base temperature indicated by the diagonal dashed line and the number suggested by the extreme velocity filtration calculation depicted in Figure 18. The typical κ parameters at the envelope bases of the giants and supergiants might be higher, possibly because they are absorbing less HCZ–like power or possess more inelastic scatterers (from dust or incomplete ionization); if so, the inversion temperatures of the giants and supergiants can be adjusted to peak out under the filtration process at no higher than "chromospheric"-like temperatures. Below it is shown that this assumption helps with organizing the asymptotic wind properties for these stars as well.

6.2. *On the Existence of Critical Points in Stellar Coronae*

If the ratio of the escape speed to the thermal speed (surface gravity to temperature) in an expanding atmosphere exceeds a critical value, a transonic transition may occur where the

expansion continues to accelerate to supersonic speeds (Parker 1958a). Prior observations of the solar corona had clearly suggested that this ratio of Parker's work was greater than unity; the observed coronal temperature placed the numerical critical point of Parker's theory *above* the solar surface, making supersonic winds an interesting theoretical possibility subsequently confirmed by *in situ* measurements. However, the general existence and location of a critical point in the atmosphere of *any* star depended on an unestablished "heating" mechanism and an unknown temperature profile at an implicitly defined location; this ambiguity left considerable doubt whether many stellar atmospheres would arrange themselves as had the Sun so as to "realize" a supersonic expansion.

It is now shown that the ion and electron thermal speeds and the local escape speed at all points inside the monotonic attractive well are indeed functionally rather generally linked under the velocity filtration mechanism so that critical point locations can be rather generally shown to be above the stellar surface. Rewriting equation (34a) in terms of the local gravitational escape speed, $V_{esc}(r)$, and the electron and ion thermal speed, $w_{\pm}(r)$, yields

$$w_{\pm}^2(r) - w^2(R_*) = V_{esc}^2(r)\left(\frac{r - R_*}{R_*}\right)\frac{2\zeta(r, \kappa)}{(2\kappa - 3)\alpha(U_{\parallel}(r))}, \quad (34c)$$

where $\alpha(r) = 1$ for field lines with no mass flux but increases from 1 toward 2 at the critical point r_*, if there is an initial mass flux. The function $\alpha(r)$ phenomenologically accounts for the diversion of kinetic energy per particle into flow energy that will occur when mass flux is allowed at the coronal base. The function $\alpha(r)$ approaches 2, since, at the critical point, $w^2(r_*, U \neq 0) = U^2(r_*)$, and thus roughly half of the available energy as temperature on closed field lines ($\alpha \equiv 1$) is diverted into flow energy if a critical point is achieved.

In Figure 19 solutions from equation (34a) above are contrasted with the approximate profiles of equation (34c) that allow for mass flux and a critical point to form. The dash-dot curves are the closed-field temperature profiles of equation (34a), while the solid curves reflect the assumed form of

$$\alpha^{-1}(r) = \left[1 - \frac{1}{2}\left(\frac{r - R_*}{r_* - R_*}\right)^{\epsilon}\right], \quad \epsilon > 0, \quad (34d)$$

in equation (34c). Any function $\alpha(r)$ that goes smoothly from 1 to 2, with a positive derivative at r_*, would suffice; equation (34d) represents a simple function that suffices to allow a preliminary estimate of the impact of velocity filtration on critical point location. When the dynamical equations are fully solved, $\alpha(r)$ can be replaced by a diagnostic that reflects the actual radial expansion of the flow.

Using equations (34c) and (34d), an estimate can be made of the *possible* locations of a critical point under velocity filtration closure within the framework of the modeled conversion of thermal to flow energy in equation (34d). From the conserva-

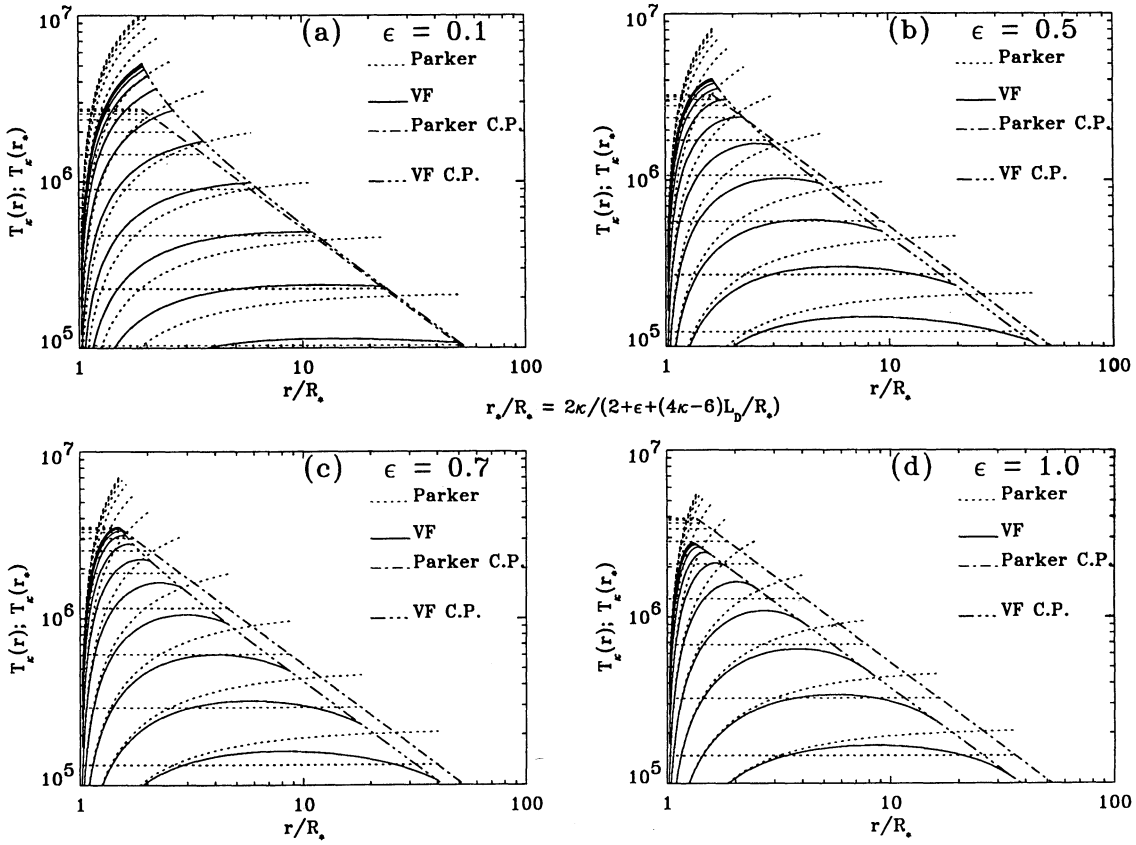

FIG. 19.—Temperature profiles inside critical point. Velocity filtration profiles for different κ's and acceleration assumptions across the subsonic regions (ϵ). Horizontal dotted lines are the corresponding Parker isothermal solution within the corresponding velocity filtration critical point. The dotted *curve* is the nonflowing velocity filtration solution. The different sets of curves on each panel correspond to different values of κ (2.012, 2.014, 2.02, 2.03, 2.07, 2.14, 2.33, 2.76, 3.78, 6.14, 11.67, 24.58), with smaller κ's giving higher temperature profiles. Different values of κ yield different temperature slopes at the critical point: small κ's lead to positive slopes for small ϵ, while larger κ's lead to negative slopes approaching the limiting possible for a critical point of -1 as $\kappa \to \infty$.

tion equations a *necessary* condition (cf. Holzer 1988, for example) for a critical point at r_* is that the following equation be satisfied:

$$\frac{2w_{\rm th}^2(r_*)}{r_*} - \left.\frac{dw_{\rm th}^2}{dr}\right|_{r_*} - \frac{GM_\odot}{r_*^2} = 0 . \tag{35a}$$

The potential critical point in stellar radii can be found with equation (34c) and

$$\alpha(r_*) \simeq 2 \tag{35b}$$

and $\kappa_+ = \kappa_-$ to be located at

$$\frac{r_*^{\rm VF}(\kappa, \epsilon)}{R_*} = \frac{2\kappa}{2 + \epsilon + (4\kappa - 6)L_D/R_*} \simeq \frac{\kappa}{1 + \epsilon/2} \tag{36a}$$

and is, under the velocity filtration hypothesis, determined by the strength of the suprathermal tails via κ (with a slight correction for the actual expansion gradient at the critical point and an even weaker sensitivity to the ratio of the scale height to stellar radius). For κ between 2.5 and 6.25, with $\epsilon \simeq \frac{1}{2}$ and $\zeta = \frac{1}{2}$, r_* would range between $2.0R_*$ and $4.9R_*$. *As the inner boundary distribution functions become more thermal* and κ increases, *the critical point radius increases directly as* κ.

Since κ must be greater than 2 for there to be a finite energy flux, there is a minimum critical point radius:

$$r_*^{\rm VF} > R_{\rm min} \equiv \frac{2}{1 + \epsilon_{\rm max}/2} R_* \simeq \frac{4}{3} R_* , \tag{36b}$$

where $\epsilon_{\rm max} = 1$ is the largest tolerable value consistent with existence of a critical point as shown below in § 6.3. Thus Parker's critical point existence arguments translate into a *lower* bound on the possible value of the critical radius. *Equation (36b) demonstrates that with velocity filtration as the model of the temperature profile, any critical point will occur outside the coronal base*; this should be contrasted with the possibility in Parker's early modeling that if the coronal temperature *were* to exceed 5.25×10^6 K, the critical point would not materialize in the flow, since the mathematical critical point would be below the solar surface!

At the critical point given by equation (36a), the relationship of the thermal speed and the escape velocity becomes

$$w_{\rm th}^2(r_*^{\rm VF}) \simeq w_{\rm th}^2(R_*) + \frac{1 + (\epsilon - 1)/(2\kappa - 3)}{4 + 2\epsilon} V_{\rm esc}^2(r_*^{\rm VF}) \tag{37a}$$

and should be contrasted with Parker's (1958a) result for an assumed isothermal solar wind expansion of

$$w_{\rm th}^2(r_*) = \tfrac{1}{4} V_{\rm esc}^2(r_*) . \tag{37b}$$

For small $w_{\rm th}^2(R_*)$ and increasing, but still finite, values of κ, equations (37a) and (37b) are essentially indistinguishable. These dash-dot-dash and dash-dot-dot-dot loci are shown to be nearly synonymous in Figure 19, where they delineate the outer radial boundary of the (solid) subsonic radial thermal profiles under the different assumptions.

6.3. *Temperature Variations at Possible Critical Points*

According to filtration, the temperature at the critical point (using eqs. [34], [36], and $\alpha = 2$) would be

$$T_\kappa(r_*(\kappa)) \simeq 5500 + 5.5 \times 10^6 \frac{2\kappa - (2 + \epsilon)}{\kappa(2\kappa - 3)} \text{ K} \quad \text{(filtration)} , \tag{38a}$$

which ranges ($\epsilon \simeq \frac{1}{2}$) between 2.9×10^6 and 1.3×10^6 K for κ between 2.4 and 4.5, respectively. If Parker's critical point occurred at the radial locations required by velocity filtration above, the isothermal temperature required to allow a critical point given by equation (36a) would be

$$T(r_*(\kappa)) \equiv \frac{MV_{\rm esc}^2(r_*)}{8k_{\rm B}} \simeq 5.25 \times 10^6 \frac{2 + \epsilon}{2\kappa} \text{ K} \quad \text{(isothermal Parker)} , \tag{38b}$$

which ranges between 2.7×10^6 and 8.8×10^5 K for κ between 2.4 and 6.25, respectively. The isothermal values required by equation (38b) are indicated by the horizontal dotted lines in Figure 19. *Velocity filtration provides a temperature at the critical point, $T(r_*)$, not dissimilar to that isothermal value above* $1.03\ R_\odot$ *presupposed by Parker*; comparable Parker–VF curves are those which end at the same dimensionless radius which is the critical point of the solution. The curved dotted lines are the VF profiles inside the possible critical point assuming no bulk flow.

However, *unlike* Parker's isothermal temperature profile, the velocity filtration solutions (1) yield a TR–like profile *below* $1.03\ R_*$ (cf. Figs. 9 and 19) and a solar temperature profile that easily achieves values greater than 10^6 K for a wide variety of nonthermal parameters; (2) suggest a theoretical critical point in the flow at ($R \simeq 0.8\kappa\ R_\odot$); *and* (3) produce temperature gradients at the critical point that are still rising (cf. Fig. 19) as in profiles with a temperature maximum outside the critical point consistent with the empirical inferences of Munro & Jackson (1977) for some choices of the rate of conversion of thermal to bulk energy.

The power-law exponent β of the temperature at the critical point is given by the relation

$$\beta \equiv \left.\frac{d\ln T}{d\ln r}\right|_{r_*} = \frac{1 + \epsilon(\frac{1}{2} - \kappa)}{\kappa - 1 - \epsilon/2} . \tag{38c}$$

Parker's original work (1958a) exploited conservation laws to show that temperature gradients of either sign were possible at the critical point as long as the power-law exponent is between -1 and 2. Limiting values of the temperature power-law exponent β at the critical point under velocity filtration are consistent with Parker's limitations, viz.,

$$\lim_{\kappa \to \infty} \beta = -\epsilon < 0 , \qquad \lim_{\kappa \to 2} \beta \simeq 1 - \epsilon > 0 . \tag{38d}$$

The small-κ regime yields critical point positive temperature gradients, while large-κ boundary conditions lead to negative slopes at the critical point. As κ grows, $\epsilon < 1$ gives expansions consistent with Parker's steepest gradients with a critical point and $\epsilon > 0$ is required for a model where positive acceleration occurs at the critical point. Thus β according to VF occurs within the range of $-1 < \beta < 1$, consistent with Parker's overall requirements. For $0 < \epsilon < 1$ this modeling is consistent with Parker's conditions from conservation laws.

From condition (36b) several interesting consequences proceed, as illustrated in Figure 20. A critical point may be *realized* (1) *if* the boundary distribution function's nonthermal properties (κ) are suitable; (2) *provided* that a mass flux exists at the inner boundary condition; and (3) in the circumstances

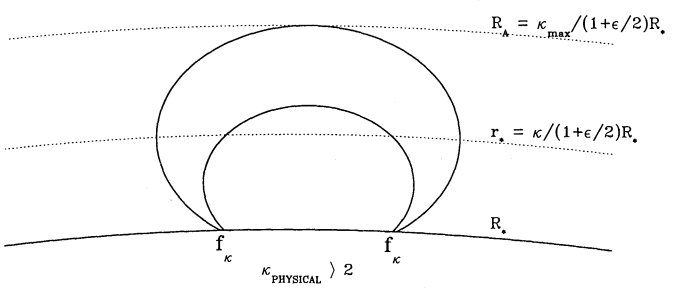

FIG. 20.—Impact of the existence of minimum distance for critical point formation in relation to the apex height of the originating magnetic loop. Depending on certain inequalities, a loop may not be able to sustain a supersonic expansion along its locus. Loops with $R_A < 2/(1+\epsilon/2)R_*$ can possess no critical point; loops with $\kappa > \kappa_{max}$ cannot either; critical points require $2 < \kappa < \kappa_{max}$. This figure points to a rationale for the magnetic flux that is susceptible to solar wind expansion and the existence of flux loops on which any mass flux will come back down at the other footpoint of the loop.

that the magnetic topology does not prevent particle access to this height, $r_* = 2\kappa/(2+\epsilon)R_*$. If the magnetic tubes of force reenter the lower TR before extending beyond R_{min} of equation (36b), *no* possible critical point can occur, regardless of the value of κ at the inner boundary. To achieve supersonic flow, the boundary condition must possess a mass flux, so that the transonic condition can be realized. Mass flux from a boundary distribution characterized by κ_* on a magnetic arcade with its apex, R_A, *inside* of $\kappa_* R_*$ *cannot* achieve a supersonic expansion; such a boundary condition might be a candidate for a spicule which returns most of their upwelling mass flux back to lower altitudes on the returning flux of the arcade. Conversely, the steady supersonic wind should come from boundary f_κ's with a mass flux on magnetic tubes of force with loci $r(s)$ that extend beyond $r(s_*) = (4/3)R_*$. Pneumann & Orrall (1986) have summarized that the wind appears to control the magnetic field and its directions completely by 2 $R_\odot$. This suggestion is also consistent with the findings of Bugoslavskaya (1949) reviewed by Newkirk (1967), where the *mean* apex height of closed arches from all eclipses (1887–1945) was 1.6 $R_\odot$. A value of $\epsilon \simeq \frac{1}{2}$ in equation (36b) would be consistent with this average finding. The profiles of Figure 19*c* corresponding to $\epsilon = \frac{1}{2}$ yield temperature profiles more like those suggested by Munro & Jackson (1977). "Source surface" models such as those of Schatten (1972), Levine & Altschuler (1974, and Levine (1976) have made this or similar assumptions for the radius where the solar magnetic flux is modeled to be drawn out by the solar wind flow. Modeling of *U* radio bursts have come up with similar dimensions. A recent study by Stewart & Vorphal (1977) gives evidence that such looplike structures probably only extend from 1.1 to 2.0 $R_\odot$.

6.4. *Parker-Style Asymptotic Winds for Stellar Coronae*

Under velocity filtration (eq. [36a]) all stars would be capable of Parker-type winds, *provided* that the boundary distributions have reasonably small κ's and suitable magnetic configurations in the sense of equation (36b). For larger than minimal κ's, i.e., less pronounced tails, the location of the critical point grows linearly with κ and inversely with ζ. If the boundary magnetic field topology does not extend to this distance, supersonic distension of the arcade is unlikely. A Maxwellian electron and proton boundary distribution, for example, puts the critical point at practically an infinite distance. The dependence of the critical point location on the suprathermal tail strength is really the signature of the inversion temperature itself (eq. [38a]); as κ goes to infinity, the velocity filtration effect, while present, does not cause the temperature to go up if both species are Maxwellians (eq. [11a], since $\xi = 0$). In this extreme situation we are faced with driving the solar wind with a photospheric (5500 K) temperature rather than with a 10^6 K one, a situation Parker (1965) demonstrated would not produce a wind.

On this basis, an estimate can be made of the asymptotic wind speeds for stars in the H-R diagram as determined by the thermal speed of the proton at the temperature corresponding to the inversion temperature estimated above. Using equation (38a) above, together with the asymptotic form of Parker's (1963) isothermal solution $U_\infty \simeq [4k_B T_{corona}/\mu M \ln (r/R_\odot)]^{1/2}$, an estimate of the variation of asymptotic wind speed in terms of escape velocity can be made, viz.,

$$\frac{U_\infty}{V_{esc}} \simeq \left\{\left[\frac{2\zeta(\kappa-1)}{\kappa(2\kappa-3)} + \frac{L_D}{R_*}\right]\ln\left(\frac{r}{R_*}\right)\right\}^{1/2}. \quad (39)$$

Using the velocity filtration to produce the coronal inversion, equation (39) shows that the practical upper limit from this type of wind expansion is several times $V_{esc} \simeq 617$ km s^{-1}, depending on how far out the isothermal solution can be maintained. Using solar values, equation (39) is illustrated in Figure 21 for an assumed value of r/R_* of 20. The horizontal dashed lines indicate the nominal interval and typical value for the solar wind speed. The vertical abscissae, corresponding to these ordinate values, suggest the corresponding values of $\kappa_- = \kappa_+$ that return in equation (39) this value of the speed.

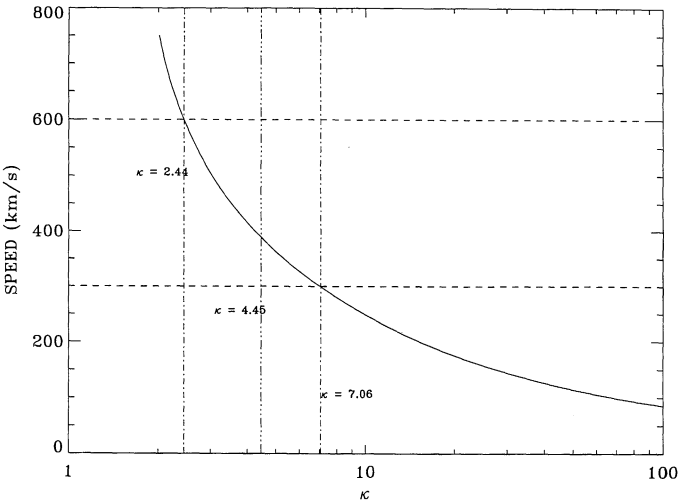

FIG. 21.—Implied variation of the asymptotic solar wind speed as a function of the assumed κ of the boundary conditions. The upper and lower horizontal lines correspond to the most frequently occurring solar wind speed range between 300 and 600 km s^{-1}. The middle horizontal line corresponds to the more typical 390 km s^{-1} usually reported. According to eq. (39), this range corresponds to a range of κ's in the range [7.06, 2.44], with the smaller κ and stronger nonthermal tails accompanying higher asymptotic wind speeds. The typical solar wind speed of 390 km s^{-1} corresponds to $\kappa \simeq 4.45$. Higher speeds correspond to even lower κ's and/or $\xi > \frac{1}{2}$. The extraordinary situations with solar wind speeds below 200 km s^{-1} correspond to $\kappa \geq 10$. The observed variation of solar wind speeds at the orbit of Earth could be ascribed to a restricted range of κ-values as the appropriate boundary conditions.

The typical solar wind speed of 390 km s^{-1} corresponds to $\kappa = 4.46$, while the typical range 300–600 km s^{-1} of the wind speed corresponds to an interval of $7.06 > \kappa > 2.44$. Clearly, faster winds can be achieved with $\kappa < 2.44$.

Depending on how nonthermal the base velocity distribution function is below the temperature inversion and how well the expansion is supported by keeping its temperature elevated, there is a substantial range of possible asymptotic wind speeds that may be achieved. If, for example, the star's atmosphere does not have a mechanism like the HCZ bringing mechanical energy to the photospheric layers, it could have a more nearly Maxwellian ($\kappa \gg 10$), but still nonthermal, post-photospheric distribution; in that circumstance the inversion temperature might only achieve chromospheric value if κ became large enough; these larger κ's would be adequate for the task of absorbing reduced levels of mechanical energy deposited near the stellar surface relative to those stellar atmospheres with active convection zones and more bulk conversion near the surface. By equation (39) higher κ stars would have lower *scaled* U_∞ than ZAMS stars with their vigorous convection zone layers and smaller κ's. In particular, there is a broad group of stars (namely, the cool giants and supergiants) reviewed by Cassinelli & MacGregor (1986) which have very sluggish *scaled* winds with $U_\infty/V_{esc} \ll 1$ that could be explained as having more nearly "Maxwellian" (κ large) surface layers due to the stage of their stellar evolution. Even though sluggish in the dimensionless sense here, these winds could still be vigorous in an absolute sense, because of the larger escape velocities for these stars.

Figure 18 was constructed under the nearly optimal $\kappa = 2$ scenario for a high inversion temperature. If weaker suprathermal tails (higher κ's) are the explanations for some stars' sluggish winds, the velocity filtration inversion temperature will be adjusted down accordingly. It is consistent with Figure 18 and Cassinelli & MacGregor's summary that these same stars have chromospheres at best, whereas $T_{inversion}(\kappa = 2)$ is clearly in excess of what would be termed chromospheric by an observer. Accordingly, from Figure 18, κ_{giants} should range from 20 to 60 and $\kappa_{supergiants}$ should range from 10 to 20 in order for their inversion temperatures to be "chromospheric" rather than TR–like in character. These numbers in turn imply $U_\infty/V_{esc} < O(0.1)$, for both classes, with the giants having the slower scaled winds. By distinguishing atmospheres at the same temperature, such as those on the main sequence, and giant/supergiants with possibly different outer layers, different scaled asymptotic wind speeds could be understood, even though their photospheric temperatures were identical.

The massive winds observed around hot, young stars have estimated asymptotic speeds that are of the order of the gravitational escape speed which is possible, even in the original Parker models. Although these winds are not as highly ionized as the solar wind, the role of suprathermal filtration in keeping their extended atmospheres hot and driving such winds deserves further, careful evaluation. The arguments and consequences of velocity filtration *and* possible radiative acceleration must be evaluated simultaneously.

7. DISCUSSION

A new, omnipresent, *coherent* velocity space filtration process has been shown to be a viable, time-independent process for understanding a stellar envelope as being hotter than its underlying layers. The filtration scenario relies on the theoretically motivated and experimentally determined non-Maxwellian velocity distributions of ions and /or electrons in other sampled astrophysical plasmas *and* the transition region. These distributions owe their existence to most, if not all, of the following: (1) the abruptly disrupted acoustic power brought to that level by the convection zone; (2) the speed dependence of the Coulomb cross section; (3) the radical inhomogeneities found at the edge of a star; and, ultimately, (4) gravity. The velocity filtration mechanism has an experimental basis: it has been documented with *in situ* plasma detectors across the Earth's magnetopause and quantitatively explains the electron mean energy ($\propto T_e$) and differential spectra in the polar rain (cf. Fairfield & Scudder 1985; Baker et al. 1986; Scudder 1989) and may be responsible for the anticorrelation of T_i and n_i in the Earth's plasma sheet reported by Huang et al. (1989). The temperature dependence of the excess ion Doppler width of transition region lines is predicted by velocity filtration in § 5; this is consistent with the presence of nonthermal ion distributions in the transition region.

The high chromosphere, transition region, and corona are locations of inhomogeneous, ultra-subsonic, increasingly fully ionized plasma in an attractive monotonic potential. *On the basis of Paper I, electrons and ions on linked tubes of magnetic flux are generally expected to have anticorrelated density and temperature profiles in such regions.*

Applying this calculation to the solar transition region, free-streaming effects in the conservative electrical and gravitational potentials can increase the chromospheric gas from its 5500 K mean energy; the solution profiles (cf. Figs. 9, and 19) have a scale height of approximately 350 km, yielding a sparser, lower pressure gas at higher altitudes of several million degrees equivalent temperature τ. Even allowing for radiative losses, it is clear that the filtration effect can easily balance such neglected losses en route to high altitude.

The temperatures of *both* electrons and ions have been shown to rise as the density falls; however, the temperature profile can be different for electrons and ions. Solutions to the ambipolar equations have been presented (Figs. 9, 10, 12, 13, and 19) to show that solar coronal and even flare electron or proton temperatures of 10^7 K can easily be achieved, and that a transition region of scale length $H \sim 350$ km is a natural by-produce of gravity, the different electron and ion mass, and the assumed nonthermal distribution in the high chromosphere and/or low transition region. This is a "direct drive" of the coronal temperature inversion and provides a robust channeling of the HCZ energy remnant to the stellar envelope that does not rely on a specific magnetic geometry to be effective. *With this explanation there is no need for a volumetric deposition of magnetic field or wave amplitude energy density above the chromosphere.*

However, the general occurrence of supersonic wind expansions would appear to have a geometric dependence on the magnetic structures above the TR per se. Although velocity filtration can produce a temperature inversion over either open or closed geometries, arguments have been presented to illustrate that several conditions must be met for a boundary plasma as heated by velocity filtration to feed a supersonic expansion: these conditions involve simultaneously the suprathermal tail characteristics of the boundary distribution function, the apex distance of the magnetic structure above the boundary under consideration, and the existence of a mass flux at the boundary condition (cf. Fig. 20).

When the electrons and ions have different suprathermal

behavior, the size of the ambipolar electrical potential in terms of the local gravitational potential is significantly modified relative to traditional theory. The kinetic energy assist from the electrical potential can be approximately doubled when boundary distributions have electron tails more prominent than those of the ions. The implied increase in the efficiency of electric relative to gravitational force in the presence of suprathermally dominant electrons may provide a clue for explaining the first ionization potential effect, whereby species with low FIP are preferentially enhanced in the corona relative to their density in the photosphere (cf. Meyer 1988). The velocity filtration description provides a first rationale for why minor solar wind ion distributions possess temperatures essentially proportional to their mass (§ 2.3).

Vertical magnetic field orientations are observationally preferred sites of coronal "heating"; this same $\boldsymbol{B}$ orientation is also favored by the present "velocity filtration" mechanism for producing temperature inversions by cumulative filtration to higher altitudes. In this geometry the larger potential drop along $\boldsymbol{B}$ permits more filtration and an increase in mean random energy. "Heating" reported by observers is also correlated with $|\boldsymbol{B}|$; in terms of the velocity filtration model the mechanical noise from the HCZ [which ultimately supplies the initial heating at the temperature minimum and modifies $f(v)$] does so by forcing energy and mass flux along threading magnetic flux which links the subphotosphere with the corona. If $\boldsymbol{B}$ provides the channel of this flux, $\rho v_{\|}/B$ would be conserved, leading to the steepening of waveforms at lower altitudes in these locales and preferential deposition there of energy in the form of shocks or other nonlinear transfers to the random as opposed to coherent part of the velocity space. Because of the speed dependence of the Coulomb cross section and the precipitous gradients in this region, the velocity filtration process is presented with a more nonthermal phase space in this locale, as a result of this channeling of the energy in strong magnetic fields, than on tubes of force which are considerably weaker. The model infers that the suprathermal tail of what has been called the inner boundary velocity distribution in this paper would be enhanced ($\kappa \downarrow$) in association with increased B, varying inversely with magnetic intensity, which is a measure of the flow-tube cross section. *According to the present interpretation, the nonthermal contribution to the Doppler width would also be enhanced in the strong-field region, not because of turbulent bulk motions but because of the enhanced suprathermal tails on the random distribution with κ reduced.* Lowering κ_{boundary} makes the value of γ even smaller than unity, which in turn implies that the magnitude of the logarithmic derivative of temperature relative to density increases further. Strong tails in these locales would explain the reported "turbulent" contributions to the Doppler width being correlated with B, as well as their square-root dependence on source region temperature.

The magnetic organization of the solar corona, while important for organizing theories and observational data, is *not* essential to the velocity filtration process, which could occur in totally nonmagnetic stars if they exist. If present, the strong magnetic field introduces further geometrical constraints on the particle's characteristic trajectories which permit further temperature striations in different flux tubes. Were the field not present, a more translationally uniform stratification with height would be expected, but the basic velocity inversion would remain because of gravity, the speed dependence of the Coulomb cross section, and the disparate electron and ion masses.

For a closed coronal loop, under most circumstances the "top" of the loop will also be the farthest point from the photosphere. Particles within the loop that can reach this highest point will have traversed the largest potential barrier of all and should comprise the sparsest and hottest (τ) portions of the loop (cf. Figs. 6 and 7*b*). A quiescent closed isomagnetic coronal loop is the most appropriate geometry for the mathematical predictions of polytrope behavior with $\gamma < 1$ to apply. *The basic anticorrelation between n and T, whether describable as a polytrope or not, has been shown to be expected even when the field strength varies significantly along the tube of force.*

The velocity filtration mechanism works equally well for open or closed (reentrant) magnetic topologies. The velocity filtration "heating" mechanism will be less efficient for open topologies, since they admit new energy "exit channels": bulk flow and heat flow. When the bulk flow is transonic, there is a significant drain on energy per particle otherwise stored as temperature. The basic filtration process continues, but with more varied consequences, among them the ability to accelerate the initial bulk fluid motion and the somewhat less strenuous contortions to keep the plasma neutral, since now the flow of the ions helps to neutralize the electron flux trying to escape the surface. With the advent of flow and acceleration of the plasma, the topology of the equivalent potential will be modified (cf. Jockers 1970).

Observationally, the plasma in the coronal hole is nearly as hot as the closed loops, and much hotter than the photosphere; this circumstance demands a mechanism of comparable efficiency in the different magnetic field geometries. *The viability of the premises of velocity filtration in open and closed topologies should be contrasted with those of the resonant heating and topological dissipation scenarios for closed topologies which have almost no chance of being operative in the magnetically "open" coronal hole topology (Parker 1990).*

The velocity filtration location r_*/R_* of possible critical points in the solar atmosphere has been shown to be essentially proportional to the suprathermal tail parameter κ; κ is inversely proportional to the overpopulation of suprathermal particles in the boundary velocity distribution. Critical point temperatures comparable to the isothermal values assumed by Parker have been recovered for small values of κ. The logarithmic temperature gradient at the critical point (cf. Fig. 19) can be positive for small κ, flat for intermediate values, and asymptotically approach the critical point with logarithmic derivative -1 as $\kappa \rightarrow \infty$. This behavior is consistent with the limits on this behavior derived by Parker (1958a) based on conservation laws. The positive gradients at the critical point suggest ways that the nonmonotonic temperature profiles over coronal holes may also be understood with the velocity filtration framework.

In the suprathermal family modeling undertaken, $\kappa > 2$ is a requirement for the boundary distribution to possess a finite energy flux. This translates into a minimum critical point location of approximately $1.3R_*$–$1.6R_*$. If magnetic arcades do not allow particles to this altitude, the supersonic wind transition is precluded. If the boundary distribution function is too thermal (κ too large) for a given magnetic arcade, a wind may not be possible either, providing a spectrum of possibilities that may determine which parts of the coronal base contribute to the distant solar wind expansion (cf. Fig. 20).

Generalized Doppler/nuclear line profiles of the Voigt-Hjerting type have been constructed on the basis of the nonthermal prototype distribution used for calculations in this

paper. It has been quantitatively demonstrated that the inflation of UV and X-ray line width and wing elevation can result from a nonthermal velocity distribution function of absorbers/emitters in a way that is competitive in qualitative effect with the inferred, but unresolved, "turbulent" and sometimes supersonic bulk velocities reported in the literature (Nicolas et al. 1982; Brueckner & Bartoe 1983). Because of the degeneracies in the mathematical inversion of the line profile, an open question remains whether the excess Doppler width and enhanced line wings attributed to "turbulent" velocities might not be the presently sought-after signatures of the nonthermal distributions that are the central idea of the velocity filtration explanations for the coronal temperature inversion advocated here. In this connection, the most recent report (Dere 1989) of these unresolved "turbulent" bulk motions argues that they are *inconsistent* with being the high-wavenumber recipient of a cascade of low-wavenumber bulk speed velocity turbulence which was simultaneously measured. Finally, the velocity filtration process advocated here can successfully predict the observed $T^{1/2}$ scaling of the excess Doppler speed attributed to "turbulent" speed, but assigns this excess width to the enhanced dispersion of the velocity distribution in the suprathermal regime. Application of the velocity filtration theory also has extracted a best-fit estimate of $\kappa_{\text{ions}} \sim 2.2 \pm 0.6$ for ions in the transition region, thereby suggesting for the first time based on observational data that nonthermal ion distributions are present in the transition zone.

Bound or quasi-bound atmospheres as they become ionized at least once (as at the top of the chromosphere!) will increasingly reflect the influence of the collisionless tendency for density and temperature to be anticorrelated and initially increase their temperature as the density decreases. The theory developed here illustrates that the enhancement at the peak of the temperature inversion scaled by the temperature at the photosphere is controlled by and nearly equal to the ratio of the stellar radius to the photospheric density scale height: $GM_* M/(2R_* k_B T_*)$, where T_* is the photospheric/chromospheric temperature of the star. Because the bulk of the atmosphere of a star is gravitationally bound, this controlling ratio of the temperature inversion is large, and a temperature inversion is a property of any star except the singular limit when the ionized plasma at the edge of the stellar atmosphere is assumed to be strictly Maxwellian. A previously published sampling of ZAMS stars was used to calculate $T_{\text{inversion}}$ according to the velocity filtration approach of this paper, and all of the stars were determined to have an inversion temperature in excess of 10^6 K (cf. Fig. 18), and would be thought capable of forming "coronal" lines as has recently been documented with *IUE*, *Copernicus*, and the *Einstein* spacecraft (Rosner et al. 1985). In this way the velocity filtration description provides a natural explanation of why the ZAMS stars have $T_{\text{envelopes}} \sim (200\text{–}300) \times T_{\text{photosphere}}$, which is one of the basic puzzles of X-ray astronomy summarized by Parker (1990).

The asymptotic winds are also shown to be controlled under the velocity filtration approach described in this paper by the prominence of the suprathermal tails at the inner boundary. Prominent tails precipitate winds at or slightly in excess of gravitational escape speeds, under the isothermal model for the temperature equation. Under the same model slower and slower asymptotic winds are predicted as the suprathermal tail is made less pronounced. In the limit of a purely Maxwellian distribution above the photosphere, the asymptotic wind speed becomes very small. In concert with empirical surveys, giant and supergiant stars would appear to have more nearly thermal distributions above their respective photospheres than ZAMS stars; they thus do not achieve the maximal inversion temperatures illustrated in Figure 18, but just "chromospheric" ones. Being more thermal implies that the asymptotic winds are a smaller fraction of the escape velocity consistent with the previously surveyed morphology of these stars as a class (Cassinelli & MacGregor 1986).

Exospheric theory starting from a Maxwellian boundary condition ($\kappa = \infty$) could not recover the present effects shown by equation (34a), because of the degenerate way that an attractive potential deforms the Maxwellian distribution function (cf. Fig. 3 of Paper I). In addition, the earlier exospheric modelers failed to realize the applicability of exospheric concepts at the base of the transition region for those particles that ultimately dominate the low coronal phase space, mistakenly arguing that free-streaming effects are only important above some inner boundary that was usually taken outside of 2.5 $R_\odot$ (Jockers 1970) or 1.03 $R_\odot$ (Brandt & Cassinelli 1966) on the basis of the density and *mean* free path. The present calculations show that a more realistic, but nevertheless straightforward, exospheric style calculation in the FIPH can provide a viable first-order description for the rearrangement of internal energy of the gas, including the coronal temperature inversion itself.

These ideas and explanations of the coronal temperature inversion have been shown to be consistent with, but extensions of, traditional statistical mechanics. These extensions, however, invalidate the *form* of the usual thermodynamic summaries of the statistical mechanical behavior of weak gradient systems, including that of the second law of thermodynamics. Therefore, it is incorrect to claim that "these results contradict the Second Law," because it is not presently known what *form* this law may take in open astrophysical systems, with their strong gradients and pervasive nonthermal distribution functions (cf. deGroot & Mazur 1984).

Truncated fluid theories will not be successful at understanding and predicting astrophysical observables until the closure approximations are demonstrated to be consistent with the microphysics of the problem at hand. The velocity space calculations of this paper and Paper I retain all fluid moments without the truncation of the moment equations that leads to the customary fluid equations for density, momentum, and energy. From the point of view of this paper and Paper I, a macroscopic theory that borrows closure approximations from neutral gasdynamics could never have understood the temperature inversion above the photosphere. Polytropic closure approximations with $1 \leq \gamma \leq 5/3$ would always be looking for heat sources to "fire" the temperature inversion, since all such schemes yield $dT/dn \geq 0$, a closure approximation that is orthogonal to the kinetic behavior of the free-streaming part of the velocity space described here. To retrieve the kinetic behavior described in this paper within the hierarchy of linked fluid moment equations would surely involve considerably more levels in the moment hierarchy beyond the usual three of density, momentum, and energy. In addition, for such an approach to be tractable, a closure approximation at some even more esoteric moment level than the heat flux would still be required. Surely, if the skills to close the moment equations at the semi-intuitive heat equation level have not been forthcoming in the last 30 years, it would appear unlikely that there now exists adequate intuition to close an augmented hierarchy of equations at a higher, more abstract level, as would be

required "at" and above the edge of a star. With this paper such a program for understanding the enigmatic temperature inversion has been replaced with a rather straightforward calculation that follows essentially from conservation of energy; this new approach carefully sidesteps the ambiguities of truncation and closure of the hierarchy, and does correctly predict the size and scale of the temperature inversion represented by the solar corona above the chromosphere as well as the omnipresence of nonthermally broadened lines and of X-ray–producing circumstellar shells about all stars on the ZAMS.

The present explanation replaces the enigma of the coronal temperature inversion with the new question: "Can formation of a suprathermal tail on the velocity distribution of electrons and ions be preempted in the high chromosphere/low transition region where the HCZ power is dissipated or reflected and the plasma is nearly fully ionized?" The preliminary answer given in this paper is that since the H theorem cannot be brought to bear in this regime, the non-Maxwellian distribution implied by the suprathermal tail is more likely than not. The subsequent velocity filtration of this distribution as a boundary condition for the fully ionized evolution of the overlying layers is then a natural explanation of the coronal temperature inversion.

Useful discussions were held with L. Burlaga, P. Cargill, D. Deming, E. N. Parker, D. Spicer, E. Whipple, and H. Zirin during the course of developing the ideas for this paper. Useful comments on an earlier version of this manuscript were made by S. Olbert of MIT. Data points for Figure 4 were kindly supplied by G. Withbroe.

REFERENCES

Alfvén, H. 1947, MNRAS, 107, 211
Baker, D. N., et al. 1986, J. Geophys. Res., 91, 5637
Biermann, L. 1948, Z. Astrophys., 25, 161
Bochsler, P. 1984, Ph.D. thesis, Univ. of Bern
Bowen, I. S., & Edlen, B. 1939, Nature, 143, 374
Bowers, R., & Deeming, T. 1984, Astrophysics. I. Stars (Boston: Jones & Bartlett)
Braginskii, S. 1965, Rev. Plasma Phys., 1, 205
Brandt, J. C., & Cassinelli, J. P. 1966, Icarus, 5, 47
Brueckner, G. E., & Bartoe, J.-D. F. 1983, ApJ, 272, 329
Bugoslavskaya, E. Y. 1949, Publ. Sternberg Inst., 19, 1
Cassinelli, J. P., & MacGregor, K. B. 1986, in Physics of the Sun. III, ed. P. A. Sturrock (Dordrecht: Reidel), 47
Chapman, S. 1916, Proc. R. Soc. Lond., A, 216, 279
Cheng, C. C., Doschek, G. A., & Feldman, U. 1979, ApJ, 227, 1037
Davila, J. M. 1986, in Coronal and Prominence Plasmas, ed. A. I. Poland (NASA CP-2442), 448
deGroot, S. R., & Mazur, P. 1984, Non-equilibrium Thermodynamics (New York: Dover),
Dere, K. P. 1989, ApJ, 340, 599
Dreicer, H. 1959, Phys. Rev. A, 115, 238
Enskog, D. 1917, Ph.D. thesis, Uppsala Univ.
Fairfield, D. H., & Scudder, J. D. 1985, J. Geophys. Res., 90, 4055
Fermi, E. 1936, Thermodynamics (New York: Dover)
Fontenla, J. M., Avrett, E. H., & Loeser, R. 1990, ApJ, 355, 700 (FAL)
Gibson, E. G. 1973, The Quiet Sun (NASA SP-303)
Gloeckler, G. 1990, Rev. Sci. Instr., 61, 3613
———. 1991, presentation at Solar Wind 7, Goslar, Germany
Grotrian, W. 1931a, Z. Astrophys., 2, 106
———. 1931b, Z. Astrophys., 3, 199
———. 1939, Naturwissenschaften, 27, 214
Henze, W., et al. 1982, Sol. Phys., 81, 231
Heyvaerts, J., & Priest, E. R. 1983, A&A, 117, 220
Hollweg, J. V. 1984, ApJ, 277, 392
———. 1986, J. Geophy. Res., 91, 4111
Holman, G., & Brosius, J. 1986, in Coronal and Prominence Plasmas, ed. A. I. Poland (NASA CP-2442), 297
Holzer, T. E. 1988, in Proc. Sixth Int. Solar Wind Conf., ed. V. Pizzo, T. E. Holzer, & D. G. Sime (NCAR/TN-306), 3
Huang, C. Y., Goertz, C. K., Frank, L. A., & Rostoker, G. 1989, Geophys. Res. Lett., 16, 563
Ionson, J. 1982, ApJ, 254, 318
Jockers, K. 1970, A&A, 6, 219
Lallement, R., Holzer, T. E., & Munro, R. H. 1986, J. Geophys. Res., 91, 751
Landau, L. D., & Lifshitz, E. M. 1960, Fluid Mechanics (New York: Pergamon)
Levine, R. H. 1976, Sol. Phys., 46, 159
Levine, R. H., & Altschuler, M. D. 1974, Sol. Phys., 36, 345
Ljepojevic, N. N., & MacNeice, P. 1988, Sol. Phys., 117, 123
———. 1989, Phys. Rev. A, 40, 981
Meyer, J.-P. 1988, ApJS, 57, 173
Montgomery, M. D. 1972, in Cosmic Plasmas, ed. K. Schindler (New York: Plenum), 61
Munro, R. H., & Jackson, B. V. 1977, ApJ, 213, 874
Narain, U., & Ulmschneider, P. 1990, Space Sci. Rev., 54, 377
Newkirk, G. 1967, ARA&A, 5, 213
Nicolas, K. R., Kjeldseth-Moe, O., Bartoe, J. D. F., & Brueckner, G. E. 1982, Sol. Phys., 81, 253
Ogilvie, K. W., Bochsler, P., Coplan, M. A., & Geiss, J. 1980, J. Geophys. Res., 85, 6069
Olbert, S. 1983, in Solar Wind 5, ed. M. Neugebauer (NASA CP-2280), 149
Onsager, L. 1931a, Phys. Rev., 37, 405
———. 1931b, Phys. Rev., 38, 2265
Osterbrock, D. E. 1960, ApJ, 134, 347
Pannekeok, A. 1922, Bull. Astron. Inst. Netherlands, 1, 107
Parker, E. N. 1958a, ApJ, 128, 664
———. 1958b, ApJ, 128, 677
———. 1963, Interplanetary Dynamical Properties (New York: Interscience)
———. 1965, Space Sci. Rev., 4, 666
———. 1972, ApJ, 174, 499
———. 1981a, ApJ, 244, 631
———. 1981b, ApJ, 244, 649
———. 1983a, ApJ, 264, 635
———. 1983b, ApJ, 264, 642
———. 1986, in Coronal and Prominence Plasmas, ed. A. I. Poland (NASA CP-2442), 2
———. 1990, Adv. Space Res., 10 (No. 9), 17
Pneumann, G. W., & Orrall, F. Q. 1986, in Physics of the Sun. II, ed. P. A. Sturrock, T. E. Holzer, D. M. Mihalas, & R. K. Ulrich (Dordrecht: Reidel), 95
Riehl, K. B., & Hardy, D. A. 1986, J. Geophys. Res., 91, 1557
Roberts, D. A. 1989, J. Geophys. Res., 94, 6899
Rosenbluth, M., Macdonald, W. M., & Judd, D. L. 1957, Phys. Rev., 107, 1
Rosner, R., Golub, L., & Vaiana, G. S. 1985, ARA&A, 23, 413
Rosner, R., Tucker, W. H., & Vaiana, G. S. 1978, ApJ, 643
Rosseland, S. 1924, MNRAS, 84, 720
Rossi, B., & Olbert, S. 1970, Introduction to the Physics of Space (New York: McGraw-Hill)
Roussel-Dupré, R. 1980, Sol. Phys., 68, 243
Saba, J. L. R., & Strong, K. T. 1991, ApJ, 375, 789
Schatten, K. 1972, in Solar Wind 2, ed. P. J. Coleman, C. P. Sonnett, & J. M. Wilcox, (NASA SP-308), 44
Schatzmann, E. 1949, Ann. d'Astrophys., 12, 203
Schmidt, W. K. H., Rosenbauer, H., Shelley, E. G., Sharp, R. D., & Johnson, R. G. 1980, Geophys. Res. Lett., 7, 697
Schwarzschild, M. 1948, ApJ, 107, 1
Scudder, J. D. 1989, Trans. AGU, 70, 432
———. 1992a, ApJ, 398, 299 (Paper I)
———. 1992b, J. Geophys. Res., submitted
Scudder, J. D., & Olbert, S. 1979a, J. Geophys. Res., 84, 2755
———. 1979b, J. Geophys. Res., 84, 6603
———. 1983, in Solar Wind 5, ed. M. Neugebauer (NASA CP-2280), 163
Shoub, E. C. 1982, Stanford. Inst. Plasma Phys. Rep., No. 46
———. 1983, ApJ, 226, 339
———. 1989, in Proc. Sixth Int. Solar Wind Conf. I, ed. V. Pizzo, T. E. Holzer, & D. Sime (Boulder: NCAR/TN-306), 59
Spitzer, L. 1962, Physics of Fully Ionized Gases (New York: Wiley Interscience)
Spitzer, L., & Härm, R. 1953, ApJ, 80, 977
Stewart, A., & Vorphal, M. 1977, Sol. Phys., 55, 11
Tidman, D. A., Guernsey, R. L., & Montgomery, D. C. 1964, Phys. Fluids, 7, 1089
Ulmschneider, P., Rosner, R., & Priest, E. 1991, Mechanisms of Chromospheric and Coronal Heating (Heidelberg: Springer-Verlag)
Waldemeier, M. 1945, Astron. Mitt. Zurich, No. 146
Withbroe, G. L. 1988, ApJ, 325, 442
Withbroe, G. L., Kohl, J. L., Weiser, H., Noci, G., & Munro, R. H. 1985, ApJ, 297, 324
Zirin, H. 1988, Astrophysics of the Sun (Cambridge: Cambridge Univ. Press)

1992ApJ...398..319S

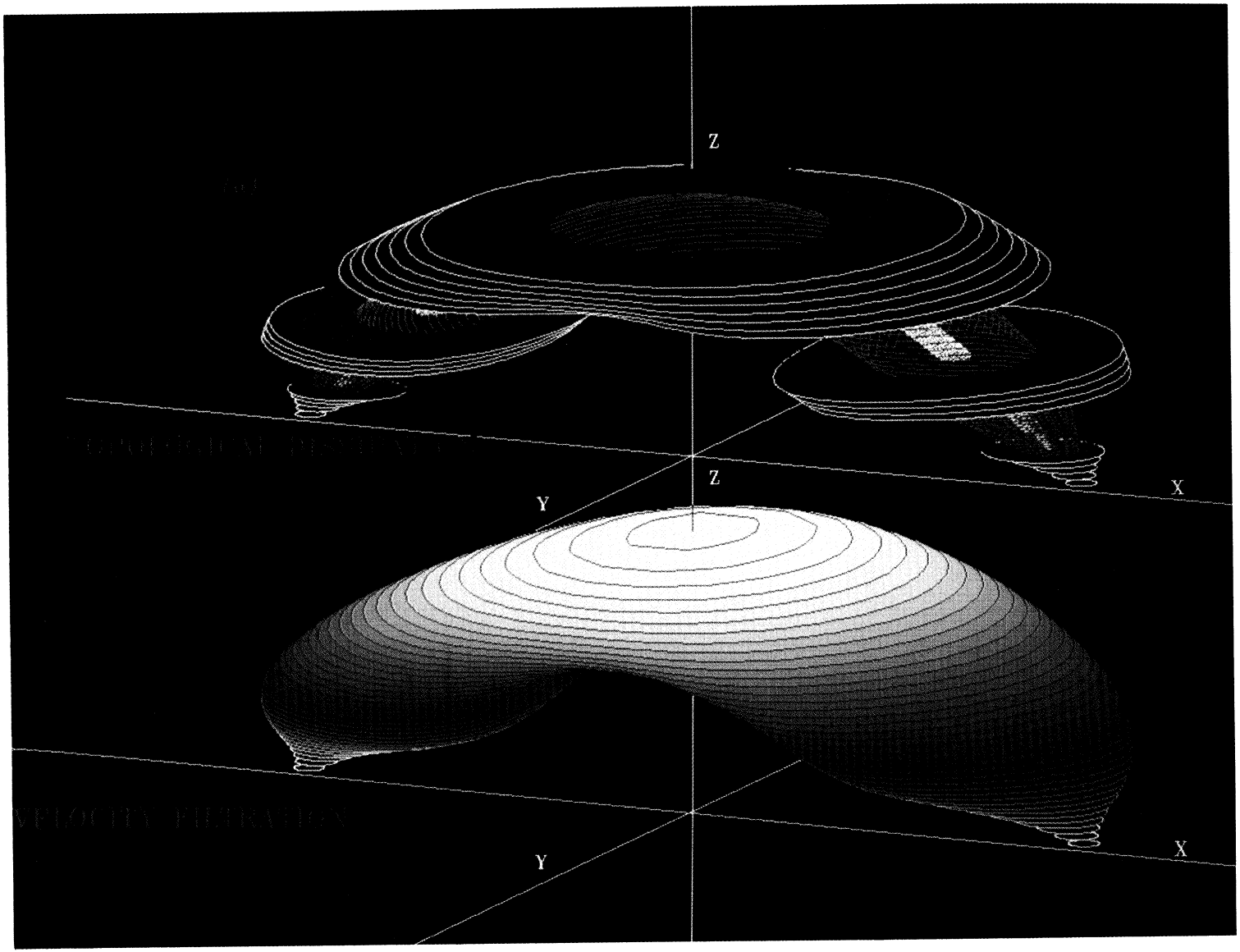

FIG. 7.—Expected heating in closed arcade and open flux tubes under (*a*) Parker's topological dissipation model and (*b*) the present velocity filtration model. In (*a*) is shown in breakaway section a subset of the heated labyrinth of *reconnection lines* argued by Parker to represent the minimum energy state of the twisted reconnecting tubes of force that make up the macro-arcade. As modeled, the shear and the heating are largest (whitest) near the center of the loop cross section and reduce (through the red spectrum to a dull red) as the perimeter of the loop is reached. The dissipation is localized in this model to this labyrinth of reconnection lines that are sparsely distributed through the arch cross section. The intervening material remains cool because of the magnetic inhibition of conduction across the strong magnetic field. The velocity filtration arcade has the same geometry as that depicted in breakaway section in (*a*). The velocity filtration model produces an arcade with a temperature (1) increasing with height in the z-direction and (2) independent of (x, y) for a fixed height z. In this way the white-hot regions are depicted at the top and the cooler darker red layers near the footpoint. Slight variations of the temperature in the (x, y, z_0)-plane section of the drawing (not shown) will occur in the generalized velocity filtration model (not shown), which would include the magnetic intensity variation along each tube of flux within the arcade.

SCUDDER (see 398, 331)

PLATE 1